JSCSEN 76(11)1455–1595(2011)

International Year of
CHEMISTRY
2011

Journal of the Serbian Chemical Society

VOLUME 76
No 11
BELGRADE 2011

Available on line at
www.shd.org.rs/JSCS/

Journal of the Serbian Chemical Society
eVersion electronic
JSCS-info@shd.org.rs • www.shd.org.rs/JSCS

J. Serb. Chem. Soc. Vol. 76, No. 11 (2011)

CONTENTS

Organic Chemistry

Biochemistry and Biotechnology

Inorganic Chemistry

Theoretical Chemistry

Physical Chemistry

Electrochemistry

Analytical Chemistry

Materials

Chemical Engineering

Environmental

Published by the Serbian Chemical Society
Karnegijeva 4/III, 11000 Belgrade, Serbia
Printed by the Faculty of Technology and Metallurgy
Karnegijeva 4, P.O. Box 35-03, 11120 Belgrade, Serbia

Journal of the Serbian Chemical Society
JSCS-info@shd.org.rs • www.shd.org.rs/JSCS
J. Serb. Chem. Soc. 76 (11) 1455–1463 (2011) UDC 547.587.11:54–145.2+547.262:54–723.4
JSCS–4219 *Original scientific paper*

Deprotonation of salicylic acid and 5-nitrosalicylic acid in aqueous solutions of ethanol

MOHAMMAD FARAJI[1]*, ALI FARAJTABAR[2], FARROKH GHARIB[3]
and HASSAN GHASEMNEJAD-BORSA[1]

[1]Department of Chemistry, Islamic Azad University, Babol Branch, Babol, [2]Department of Chemistry, Islamic Azad University, Jouybar Branch, Jouybar and [3]Chemistry Department, Faculty of Sciences, Shahid Beheshti University, Tehran, Evin, Iran

(Received 6 May, revised 21 June 2011)

Abstract: The protonation constant values of two hydroxybenzoic acids (salicylic and 5-nitrosalicylic acid) were studied in some water–ethanol solutions using spectrophotometric and potentiometric methods at 25 °C and in an ionic strength of 0.1 M sodium perchlorate. The results indicated that the pK_a values increase with increasing proportion of ethanol in mixed solvent. The dependence of the protonation constants on the variation of the solvent were correlated by the dielectric constants of the media. Furthermore, for a better understanding of the solvent influence, the obtained results were explained in terms of the Kamlet–Taft parameters α (hydrogen-bond donor acidity), π^* (dipolarity/polarizability) and β (hydrogen-bond acceptor basicity) by means of linear solvation energy relationships. The multiple linear regression analysis indicated that the pK_a values of salicylic acid were strongly dependent on the non-specific electrostatic solvent–solute interactions, whereas specific hydrogen bonding interactions controlled the protonation of nitrosalicylic acid in water–ethanol binary mixtures.

Keywords: pK_a; hydroxybenzoic acids; binary mixtures; solvent effects.

INTRODUCTION

The value of the protonation constant of compounds, pK_a, is a key parameter for predicting the extent of ionization of their functional groups with respect to the proton concentration of a medium. This parameter is essential in a wide range of research areas, such as chemistry, biochemistry and pharmacology. The fundamental physicochemical properties of drugs such as solubility and permeability are influenced by pH. Thus these properties for a diverse set of acidic or basic drug are directly related to their pK_a values.[1] It has been shown that the activity of enzymes and acid–base homeostasis of living organisms are prominently dependent on the protonation constants of the compounds present in the cell and in

---

* Corresponding author. E-mail: faraji@baboliau.ac.ir

doi: 10.2298/JSC100506129F

the body.[2] Hence, knowledge of pK_a values is necessary for the quantitative understanding and stability constant determination of the interactions between acidic or basic ligands and metal ions in complexes.[3–7]

Solvent mixtures, especially binary solutions of water and organic solvents, are widely used in a variety of chemical fields, such as solvent extraction, chemical synthesis and liquid chromatography. Furthermore, a pure solvent can frequently be mixed with others in order to obtain solutions with a variety of physical properties. Systematic investigations of solvent effects on thermodynamic and kinetic functions are interesting both from experimental and theoretical perspectives in chemical and biochemical analysis. The study of solvent effects in binary solvent mixtures is more complicated than in pure solvents because the solute–solvent and solvent–solvent interactions can create new solvent properties leading to preferential solvation. Preferential solvation occurs when solutes interact stronger with one of the components of the mixture and then this difference in the interactions is reflected in the composition of solute microenvironment.[8,9]

The use of empirical scales obtained from solvatochromic compounds is a suitable method for explaining solute–solvent interactions at a microscopic level. Some of the most extensively used parameters are the solvatochromic parameters which take into account all possible specific and non-specific interactions between solute and solvent molecules. Kamlet and Taft scaled their solvatochromic solvent parameters by introducing a developed solvatochromic comparison method.[10–14] The parameters α, β and π^* are a measure of the hydrogen bond donor acidity, hydrogen bond acceptor basicity and dipolarity–polarizability of the solvent, respectively. The sum of these solvent properties can be used to treat molecular solvent effects with the framework of the concept of linear solvation energy relationships.[15,16]

In continuation of previous studies,[17–21] in this study, the protonation constants of salicylic and 5-nitrosalicylic acid were determined in various mixtures of water–ethanol solvents to examine the solvent dependence of their acid–base equilibria properties. Salicylic and 5-nitrosalicylic acid are organic phenolic compounds which are widely used in organic drug synthesis. Their chemical structures are presented in Fig. 1.

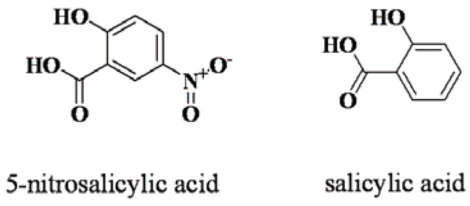

5-nitrosalicylic acid

salicylic acid

Fig. 1. Chemical structure of salicylic and 5-nitrosalicylic acid.

EXPERIMENTAL

Salicylic and 5-nitrosalicylic acid were obtained from Sigma–Aldrich. Ethanol was of the highest available purity (Merck) and was used without further purification. Stock solutions of NaOH and HCl were prepared from titrisol solutions (Merck). The water used was double-distilled water with a conductivity of 1.3±0.1 $\mu\Omega^{-1}$ cm^{-1}. Sodium perchlorate was supplied by Merck as an analytical reagent grade material and was used without further purification.

Potentiometric measurements were performed in a double-walled electrochemical cell thermostated at 25 °C. The ionic strength of the mixtures was maintained to 0.1 M with sodium perchlorate. A Jenway Research potentiometer, model 3520, with a combination of glass and reference electrode was used for the measurement of the electromotive force (*emf*) in potentiometric titrations of acidic solution mixtures.

Spectrophotometric measurements were performed on a UV–Vis Shimadzu 2100 spectrophotometer with a Pentium 4 computer using thermostated matched 10 mm quartz cells. A flow type measurement cell was used. A peristaltic pump allowed for the circulation of the solution under study from the electrochemical cell to the spectrophotometric cell; thus, the absorbance and the *emf* of the solution could be measured simultaneously. To exclude carbon dioxide from the system, a stream of purified nitrogen was passed through a sodium hydroxide solution and then bubbled slowly through the reaction solution.

Prior to each spectrophotometric titration, the electrochemical cell was calibrated to obtain the formal electrode potential *emf* °.[22,23] Approximately 20 ml of solutions of HCl in water–ethanol systems were titrated by the stepwise addition of NaOH solution. The equilibrium *emf* ° values of the cell were recorded after allowing potential stabilization. The *emf* values in each of binary mixtures were computed from the Nernst equation knowing the exact concentration of H^+ at each titration point and the reference electrode potential. In the next step, 25 mL of an acidic solution of hydroxybenzoic acid was titrated with a sodium hydroxide solution (0.1 mol dm^{-3}). The absorbance data were recorded in the interval of 200–400 nm after reading the *emf* values of the electrochemical cell. Then, the spectroscopic titration data were introduced to the Star program[24] to calculate the pK_a values of the two investigated compounds.

RESULTS AND DISCUSSION

Calibration of the electrochemical cell in water–ethanol mixtures

According to the Nernst equation, the potential of a glass electrode can be presented as:

$$emf = emf^\circ + k\log [H^+] + k\log \gamma_{H^+} + E_{LJ} \tag{1}$$

where E_{LJ} is the liquid junction potential, $k = 2.303RT/F$ in which R, T and F have their usual meanings and γ_{H^+} is the activity coefficient of the hydrogen ions. Difficulties in computing the activity coefficients of hydrogen ion in various aqueous mixtures of organic solvents lead to measuring *emf vs*. the H^+ concentration in solution. As the ionic strength of the solution was kept constant, the activity coefficient of the hydrogen ion was also constant. The non-ideality of the solutions is then included in k_a (the specific constant of a glass electrode in the acidic region), and thus:

$$emf = k_a + k\log [H^+] \tag{2}$$

with k_a being $emf^\circ + k\log \gamma_{H^+} + E_{LJ}$. The use of a glass electrode (with an aqueous inner solution) in non-aqueous media introduces a deviation from ideality. However, it was shown that the deviation is negligible and that a glass electrode is always usable in such media to measure H^+ concentration with a linear relation of E_{cell} *vs*. log $[H^+]$.[25]

Thus, the hydrogen ion concentration can be easily calculated by:

$$[H^+] = (M_{HCl}V_0 - M_{NaOH}V_1)/(V_0 + V_1) \tag{3}$$

where M_{HCl} and M_{NaOH} are the molarities of the acid and base, V_0 and V_1 are the initial volume of acid and the added volume of sodium hydroxide solution, respectively. The k_a values were calculated from measured *emf* and the known concentration of solvated proton at every titration point by linear regression analysis. The derived linear equations are reported in Table I.

TABLE I. The calibration equation of the electrochemical cell in different water–ethanol mixtures at 25 °C

Ethanol content, % (v/v)	Cell calibration equation
0	$emf = 365.20 + 59.11\log [H^+]$
10	$emf = 362.15 + 58.53\log [H^+]$
20	$emf = 360.34 + 59.21\log [H^+]$
30	$emf = 359.33 + 59.27\log [H^+]$
40	$emf = 358.48 + 59.22\log [H^+]$
50	$emf = 354.31 + 59.87\log [H^+]$

For all the binary mixtures, the slopes obtained from the least squares analysis were close to the theoretical Nernst value (59.167 mV at 25 °C) with correlation coefficients of nearly $r^2 = 0.99$. Therefore the pH values of the binary mixtures can be properly measured according to:

$$p_cH = (k_a - emf)/k \tag{4}$$

Computing protonation constants

The absorption spectra for salicylic acid and 5-nitrosalicylic acid at varying pH values in 50 % (v/v) ethanol are shown in Figs. 2 and 3, respectively.

For each binary solvent, the spectral absorbance in different pH values were used to construct a matrix **R** of size $m\times n$, where m is the number of different pH values in which the absorbance was determined at n wavelengths at 0.5 nm intervals. According to the Beer law, a least squares analysis was performed in the Star program environment to decompose the data matrix **R** into a matrix of pure concentration, **C**, and a matrix of pure spectral profiles, **S**, with the optimal residual error matrix **E**.

$$\mathbf{R} = \mathbf{CS} + \mathbf{E} \tag{5}$$

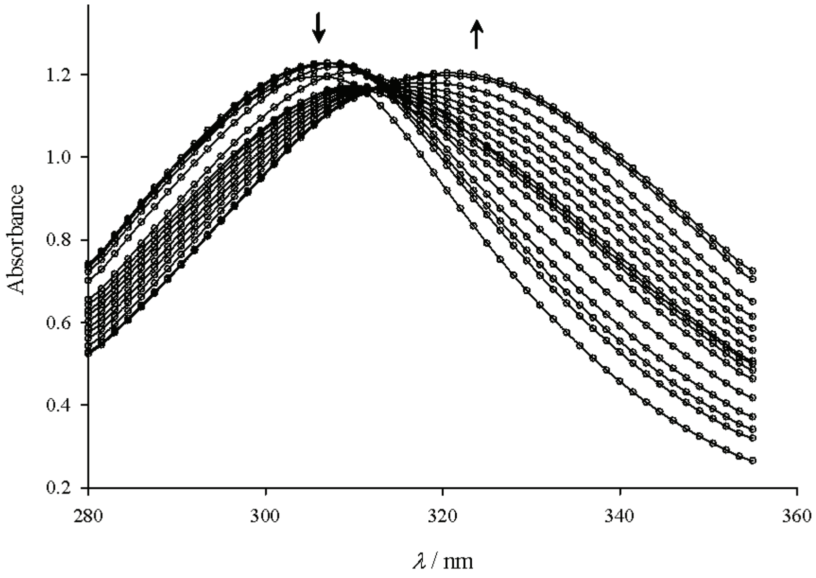

Fig. 2. Spectral change of salicylic acid (2.2×10^{-4} mol dm^{-3}) with decreasing pH in 50 % (v/v) ethanol.

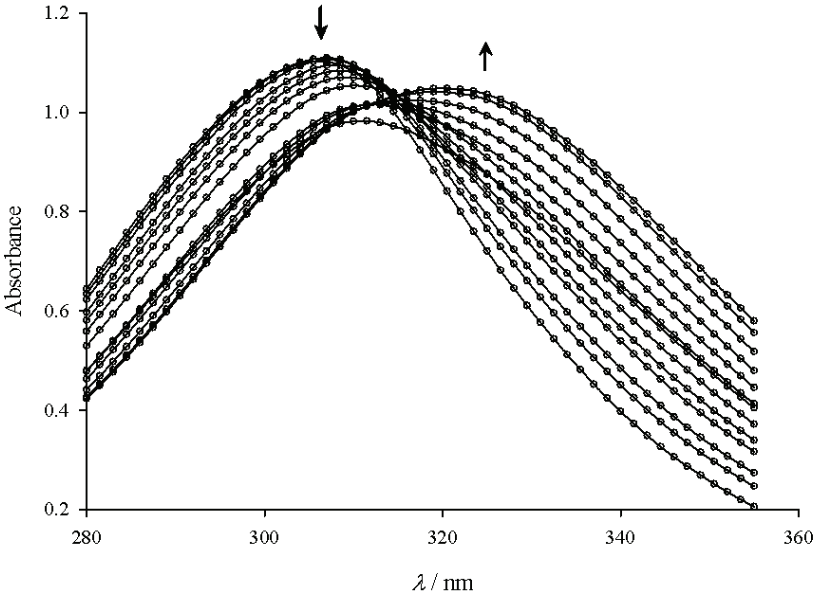

Fig. 3. Spectral change of 5-nitrosalicylic acid (8.5×10^{-5} mol dm^{-3}) with decreasing pH in 50 % (v/v) ethanol.

In iterative cycles, the matrices **C** and **S** were determined which best represent the original matrix **R**. These procedures were realized for a known number of components and using the initial estimation of the two **C** and **S** matrices. The matrix of pure concentration profiles is related to the protonation constant and the total concentration of the compounds. Under suitable constraints, the nonlinear least-squares fitting continues until the best set of parameters (pK_a and molar absorptivities of the species) is obtained that result in a minimum of **E**.

The protonation constants determined by the Star program are listed in Table II with the solvent parameters, dielectric constant (ε_r) and KAT parameters in various water–ethanol solvents mixtures.[26,27]

TABLE II. Protonation constants of salicylic acid and 5-nitrosalicylic acid with the KAT parameters and dielectric constants of different water–ethanol mixtures at 25 °C and constant ionic strength (0.1 mol dm^{-3} $NaClO_4$); the KAT solvatochromic parameters and the dielectric constants were taken from refs. 27 and 26, respectively

Ethanol content, % (v/v)	pK_a		α	β	π^*	ε
	Salicylic acid	5-Nitrosalicylic acid				
0	2.916±0.072	2.017±0.010	1.17	0.47	1.09	78.56
10	2.873±0.011	2.093±0.009	1.11	0.38	1.13	73.95
20	2.927±0.009	2.189±0.009	1.04	0.40	1.15	69.05
30	3.052±0.009	2.250±0.010	1.01	0.48	1.14	63.85
40	3.252±0.007	2.262±0.012	0.98	0.54	1.12	58.36
50	3.465±0.009	2.320±0.014	0.98	0.59	1.08	52.62

Effect of the solvent

As shown in Table II, the pK_a values of salicylic acid and 5-nitrosalicylic acid increase with increasing volume percentage of ethanol. The electron withdrawing nitro functional group in 5-nitrosalicylic acid leads to lower pK_a values in comparison to salicylic acid. The deprotonation equilibrium of the two hydroxybenzoic acids can be represented by $HA \leftrightarrows H^+ + A^-$. It is expected that because of solute–solvent electrostatic interactions, the neutral species (HA) are thermodynamically more stable than the ionic species (H^+ and A^-) in media with higher percentages of ethanol in which the dielectric constants are lower. In order to explore the possibility of this hypothesis, the pK_a values of substances were correlated to the reciprocal of the dielectric constants of the binary mixtures and their dependence interpreted according to the Born equation.[28] In the absence of the specific solute–solvent interactions, a plot of pK_a values *vs*. the reciprocal dielectric constant of the media, ε, should be linear:

$$\mathrm{p}K_a = (121.6n/r)(1/\varepsilon - 0.0128) \quad (6)$$

where r is the common radius of the ions and n is the square summation of the charges involved in the protonation equilibrium. In this work, a linear regression analysis was performed between pK_a and $1/\varepsilon$ values in different water–ethanol mixtures by using the Linest function in the Microsoft Excel program.[29] The following expressions were obtained in accordance with the Born equation, where the quantities shown in brackets are the standard deviation of the corresponding coefficients:

$$\mathrm{p}K_\mathrm{a}(\text{salicylic acid})=1.60(0.20) + 59.97(12.72)1/\varepsilon \qquad r^2 = 0.93 \qquad (7)$$

$$\mathrm{p}K_\mathrm{a}(\text{5-nitrosalicylic acid})=1.53(0.19) + 43.46(12.04)1/\varepsilon \qquad r^2 = 0.77 \qquad (8)$$

The squared correlation coefficient, r^2, measures the goodness-of-fit of the experimental data to the theoretical equation. These results indicate that the protonation constants of salicylic acid depend on the electrostatic forces and can be explained based on the Born equation, whereas the pK_a values of 5-nitrosalicylic acid do not follow the same order, indicating the existence of additional factors that influence the solute–solvent interactions. This observation is consistent with a previous study on the behavior of salicylic acid in water–DMSO mixtures.[19]

For a better evaluation of the solute–solvent interactions at the molecular level, the most significant KAT parameters were used. A multi-parametric equation was proposed to evaluate specific and nonspecific interactions within the framework of the linear solvation energy relationships (LSER) concept. The number of parameters in the equation depends on the significance of the solute–solvent interactions.[30,31] However, the general equation for LSER is usually expressed as:

$$\mathrm{p}K_\mathrm{a} = A_0 + a\alpha + b\beta + p\pi^* \qquad (9)$$

where A_0, a, b and p are independent coefficients characteristic of the process which indicate their sensitivity to the accompanying solvent properties. In order to explain the obtained pK_a values through the KAT solvent parameters, the protonation constants were correlated with solvent properties by means of multiple linear regressions in the Microsoft Excel program.[29] The fitted single, dual and multiparameteric equations are tabulated together with their regression statistics (r^2, standard deviations and F-statistic) in Table III for each substance.

TABLE III. The linear regression analysis of the KAT equation for the values of the protonation constant of salicylic acid and 5-nitrosalicylic acid in water-ethanol mixtures

LSER correlation equation	r^2	F-statistic
Salicylic acid		
$\mathrm{p}K_\mathrm{a} = 20.37(14.29) – 2.64(2.72)\alpha – 8.54(5.51)\pi^* – 9.18(9.56)\beta$	0.99	52.25
$\mathrm{p}K_\mathrm{a} = 6.66(0.36) – 0.04(0.22)\alpha – 3.28(0.49)\pi^*$	0.98	79.99
$\mathrm{p}K_\mathrm{a} = –1.74(1.16) + 5.59(1.05)\beta + 1.52(0.55)\alpha$	0.97	52.53
$\mathrm{p}K_\mathrm{a} = 6.58(1.43) + 0.07(0.79)\beta – 3.27(0.91)\pi^*$	0.98	79.43
$\mathrm{p}K_\mathrm{a} = 4.39(0.42) – 1.29(0.41)\alpha$	0.71	9.84
$\mathrm{p}K_\mathrm{a} = 1.45(0.27) + 2.79(0.46)\beta$	0.90	36.57
$\mathrm{p}K_\mathrm{a} = 6.70(0.25) – 3.35(0.23)\pi^*$	0.98	211.28
5-Nitrosalicylic acid		
$\mathrm{p}K_\mathrm{a} = –5.14(9.17) + 0.83(1.74)\alpha + 3.05(3.53)\pi^* + 5.44(6.14)\beta$	0.98	30.09
$\mathrm{p}K_\mathrm{a} = 2.98(0.23) – 0.71(0.14)\alpha – 0.07(0.31)\pi^*$	0.97	48.18
$\mathrm{p}K_\mathrm{a} = 2.76(0.59) + 0.16(0.53)\beta – 0.66(0.28)\alpha$	0.97	48.90

TABLE III. Continued

LSER correlation equation	r^2	F-statistic
5-Nitrosalicylic acid		
$pK_a = –0.80(0.80) + 2.53(0.44)\beta + 1.40(0.51)\pi^*$	0.98	60.68
$pK_a = 2.94(0.07) – 0.74(0.07)\alpha$	0.97	126.39
$pK_a = 1.38(0.12) + 1.37(0.21)\beta$	0.92	43.07
$pK_a = 3.69(0.48) – 1.39(0.44)\pi^*$	0.71	9.81

The F-statistic values were used to assess which of the LSER equations is statistically the optimum model. The best predictive mathematical equations in the fitted models were those that have highest F-statistic values and small standard deviation (Table III). In the case of salicylic acid, the non specific dipolarity–polarizability interactions have the most important effect on the pK_a values, whereas the deprotonation of 5-nitrosalicylic acid is extensively sensitive to specific hydrogen bonding interactions. The π^* scale for salicylic acid in the correlated model has a negative effect which means a decrease in the polarity of the media increases the pK_a values. The coefficient of the α term for 5-nitrosalicylic acid in the LSER equation is also negative, meaning a lower deprotonation of compound with decreasing solvent hydrogen bond acidity. These results are in complete agreement with the above assumption derived from the Born equation.

CONCLUSIONS

The protonation constants of salicylic acid and 5-nitrosalicylic acid were successfully determined in water and water–ethanol mixtures of 0–50 % ethanol (v/v) by spectrophotometric and potentiometric methods at 25 °C and at an ionic strength of 0.1 M sodium perchlorate. Generally, it was observed that the pK_a values of substances increase with increasing volume fraction of ethanol. The high correlation coefficients between the pK_a values and solvatochromic parameters of the binary mixtures (α and π^*) demonstrate the existence of a linear relationship between these magnitudes in these media.

Acknowledgement. The authors gratefully acknowledge the financial support from the Research Council of Islamic Azad University, Babol Branch.

ИЗВОД

ДЕПРОТОНОВАЊЕ САЛИЦИЛНЕ И 5-НИТРОСАЛИЦИЛНЕ КИСЕЛИНЕ У РАСТВОРИМА У СМЕШИ ВОДА–ЕТАНОЛ

MOHAMMAD FARAJI[1], ALI FARAJTABAR[2], FARROKH GHARIB[3] и HASSAN GHASEMNEJAD-BORSA[1]

[1]*Department of Chemistry, Islamic Azad University, Babol Branch, Babol,* [2]*Department of Chemistry, Islamic Azad University, Jouybar branch, Jouybar и* [3]*Chemistry Department, Faculty of Sciences, Shahid Beheshti University, Tehran, Evin, Iran*

Испитиване су вредности констате протоновања две хидроксибензове киселине (салицилна и 5-нитросалицилна) у различитим растворима у смеши вода–етанол, потенциометријски на 25 °C у раствору 0,1 М натријум-перхлората. Добијени резултати указују на то да pK_a вредности расту повећањем удела етанола у смеши растварача. Зависност константе протоновања од састава растварача корелисана је са диелектричном константом средине. У циљу бољег разумевања утицаја растварача, добијени резултати објашњени су линеарном зависношћу Камлет–Тафтових параметара α (киселост донора водоничне везе), π^* (диполарност/поларизабилност) и β (базност акцептора водоничне везе) и енергије солватације. Вишеструка линеарна регресиона анализа указује да pK_a вредности салицилне киселине значајно зависе од неспецифичних електростатичких интеракција растварач–растворена супстанца, док специфичне интеракције водоничних веза утичу на протоновање нитросалицилне киселине у бинарним смешама вода–етанол.

(Примљено 6. маја, ревидирано 21. јуна 2011)

REFERENCES

1. H. V. D. Waterbeemd, B. Testa, *Drug bioavailability: estimation of solubility, permeability, absorption and bioavailability*, Wiley-VCH, Weinheim, Germany, 2008
2. O. Holmes, *Human acid-base physiology*: *a student text*, Chapman & Hall Medical, London, UK, 1993
3. A. E. Martell, R. M. Smith, *Critical stability constants*, Plenum, New York, USA, 1974
4. S. K. Sahoo, B. K. Kanungo, M. Baral, *Monatsh. Chem*. **140** (2009) 139
5. A. Farajtabar, F. Gharib, P. Jamaat, N. Safari, *J. Chem. Eng. Data* **53** (2008) 350
6. F. Gharib, M. Jabbari, A. Farajtabar, *J. Mol. Liq*. **144** (2009) 5
7. F. Gharib, A. Farajtabar, *Rev. Inorg. Chem*. **29** (2009) 37
8. A. Habibi-Yangjeh, *Bull. Korean Chem. Soc*. **25** (2004) 1165
9. P. M. Mancini, L. R. Vottero, *J. Phys. Org. Chem.* **19** (2006) 34
10. M. J. Kamlet, R. W. Taft, *J. Am. Chem. Soc.* **98** (1976) 377
11. R. W. Taft, M. J. Kamlet, *J. Am. Chem. Soc.* **98** (1976) 2886
12. M. J. Kamlet, J. L. M. Abboud, R. W. Taft, *J. Am. Chem. Soc.* **99** (1977) 6027
13. G. S. Ušćumlić, J. B. Nikolić, *J. Serb. Chem. Soc.* **74** (2009) 1335
14. J. B. Nikolić, G. S. Ušćumlić, *J. Serb. Chem. Soc*. **72** (2007) 1217
15. C. Reichardt, *Solvents and Solvent Effects in Organic Chemistry*, Wiley-VCH, Weinheim, Germany, 2004
16. O. A. El-Seoud, *Pure Appl. Chem*. **81** (2009) 697
17. F. Gharib, M. Jabbari, A. Farajtabar, A. Shamel, *J. Chem. Eng. Data* **53** (2008) 1772
18. F. Gharib, A. Shamel, *J. Chem. Eng. Data* **54** (2009) 993
19. A. Farajtabar, F. Gharib, *Monatsh. Chem*. **141** (2010) 381
20. A. Farjtabar, F. Gharib, *J. Solution Chem*. **39** (2010) 231
21. F. Gharib, A. Farajtabar, A. M. Farahani, F. Bahmani, *J. Chem. Eng. Data* **55** (2010) 327
22. G. Gran, *Acta Chem. Scand*. **4** (1950) 559
23. G. Gran, *Analyst* **77** (1952) 661
24. J. L. Beltran, R. Codony, M. D. Prat, *Anal. Chim. Acta* **276** (1993) 441
25. J. S. J. Ferrer, E. Couallier, M. Rakib, G. Durand, *Electrochim. Acta* **52** (2007) 5773
26. F. Hernandez-Luis, M. V. Vazquez, M. A. Esteso, *J. Mol. Liq*. **108** (2003) 283
27. U. Buhvestov, F. Rived, C. Rafols, E. Bosch, M. Roses, *J. Phys. Org. Chem*. **11** (2003) 185
28. J. Barbosa, D. Barron, J. L. Beltran, S. Buti, *Talanta* **45** (1998) 817
29. E. J. Billo, *Excel for Chemists: A Comprehensive Guide*, Wiley-VCH, Weinheim, Germany, 2001
30. S. Z. Drmanić, A. D. Marinković, B. Ž. Jovanović, *J. Serb. Chem. Soc*. **74** (2009) 1359
31. N. D. Divjak, N. R. Banjac, N. V. Valentić, G. S. Ušćumlić, *J. Serb. Chem. Soc*. **74** (2009) 1195.

Journal of the Serbian Chemical Society
JSCS-info@shd.org.rs • www.shd.org.rs/JSCS

J. Serb. Chem. Soc. 76 (11) 1465–1470 (2011) UDC 634.722:581.19:581.48:633.879.6
JSCS–4220 *Original scientific paper*

Chemical composition of white currant seed extract

DEJAN GOĐEVAC[1]*, VLATKA VAJS[1], SLOBODAN MILOSAVLJEVIĆ[2],
BOBAN ĐORĐEVIĆ[3], GORDANA ZDUNIĆ[4] and VELE TEŠEVIĆ[2]

[1]*Institute of Chemistry, Technology and Metallurgy, University of Belgrade, Njegoševa 12, Belgrade,* [2]*Faculty of Chemistry, University of Belgrade, Studentski trg 16, Belgrade,* [3]*Faculty of Agriculture, University of Belgrade, Nemanjina 6, Zemun and* [4]*Institute for Medicinal Plants Research Dr Josif Pančić, Tadeuša Košćuška 1, Belgrade, Serbia*

(Received 17 June 2011)

Abstract: From the seeds of white currant (*Ribes rubrum*, cv. White Champagne), a new sesquiterpenoid glycoside **1** was isolated, along with two known compounds: dihydrophaseic acid 3'-*O*-β-D-glucopyranoside (**2**), and 3-carboxymethyl-indole-1-*N*-β-D-glucopyranoside (**3**). The structure of the new compound was identified as dihydrophaseic acid 3'-*O*-β-gentiobioside, based on extensive NMR and MS spectral studies.

Keywords: white currant; seeds; sesquiterpenoid glucoside; dihydrophaseic acid derivative; indole derivative; 2D NMR.

INTRODUCTION

The genus *Ribes* is native to the Northern Hemisphere, and several species have been cultivated as a food crop since the early 1500s in Europe, and were taken to North America with the colonists in the 1700s. This genus contains about 150 species, grouped into categories including red and white currants, black currants, ornamental currants, golden currants, and gooseberries.

Despite the low content of dominant berry phenolics such as ellagic acid, anthocyanins and other flavonoids, it was shown that white currants are effective in preventing cancer initiation and progression in the Min mouse.[1] It was also found that currant seed oils are rich in both α-linolenic acid and γ-linolenic acid, which makes them specific among plant oils.[2]

This paper is a continuation of investigations on the chemical composition of edible berries, in pursuit of sources of potentially pharmacologically active compounds.[3–5] Herein, the isolation and structure elucidation of a new dihydrophaseic acid glucoside, along with two known compounds, from the seeds of white currant (*Ribes rubrum*, cv. White Champagne) are described.

---

* Corresponding author. E-mail: dgodjev@chem.bg.ac.rs
doi: 10.2298/JSC110617132G

EXPERIMENTAL

General experimental procedures

The NMR spectra were acquired on a Bruker Avance DRX 500 MHz instrument with a 5 mm inverse detection probe using standard pulse sequences, in acetone-d_6/D_2O (1:1) as a solvent, at 289 K. The spectra were referenced to the residual solvent signal (δ_H 2.05, δ_C 29.92 for acetone-d_6); the chemical shifts are given in δ (ppm), and coupling constants are reported in Hz.

High resolution mass spectral (HR-MS) data (negative ion mode) were generated with an Agilent time-of-flight mass spectrometer equipped with an electrospray ionization source (EPI) (Agilent 6210 system) and Agilent 1200 Series high pressure liquid chromatograph (HPLC). Samples were diluted with water/acetonitrile (1:1) containing 0.1 % formic acid and introduced *via* the HPLC, without a column, using the same solvent system.

Semi-preparative HPLC was performed on an Agilent 1100 system using a Zorbax XDB-C18 column (5 μm, 250 mm×9.4 mm).

Plant material

White currant (*Ribes rubrum*, cv. White Champagne) was grown in the vicinity of Belgrade (experimental orchard of the nursery "Omega", located in Mislođin, Municipality of Obrenovac). Berries at the optimum technological maturity were harvested at the end of June 2009. The seeds from the berries were manually separated from the pulp and dried using filter paper.

Isolation

The samples of whole, dried seeds (20 g) were macerated in 50 mL of 50 % MeOH. The mixtures were sonicated in an ultrasonic bath for 12 h. The extracts were filtered through filter paper, evaporated at reduced pressure at 45 °C, which afforded 500 mg of dry material. The extract was diluted with 1 mL of 0.2 % formic acid/acetonitrile (1:1), and filtered through a 0.45 mm cellulose filter (Millipore).

The separation of the extract was realized using a semi-preparative HPLC method. Mobile phase A was 0.2 % formic acid in water and mobile phase B was acetonitrile. The injection volume was 50 µL, and elution at 4.5 mL min^{-1} with a solvent gradient program (0–20 min, 5–16 % B, 20–28 min, 16–40 % B, 28–30 min, 40–99 % B, 30–35 min, 99 % B, 35–36 min, 99–5 % B). The chromatographic procedure was repeated twenty times, yielding 3 mg of compound **1** (t_R = 11.1 min), 3 mg of compound **2** (t_R = 12.9 min), and 2 mg of compound **3** (t_R = 20.8 min).

Dihydrophaseic acid 3'-O-β-gentiobioside *(**1**)*. Colorless film. ^{1}H-NMR (acetone-d_6/D_2O (1:1), 500 MHz) and ^{13}C-NMR (acetone-d_6/D_2O (1:1), 125 MHz). HR-ESI–MS, *m/z*, 606.2514 (calcd. for $C_{27}H_{42}O_{15}$: 606.2524, error: –1.6 ppm).

Dihydrophaseic acid 3'-O-β-*D-glucopyranoside (**2**)*. Colorless film. ^{1}H-NMR (acetone-d_6/D_2O (1:1), 500 MHz) and ^{13}C-NMR (acetone-d_6/D_2O (1:1), 125 MHz). HR-ESI–MS, *m/z*, 444.1993 (calcd. for $C_{21}H_{32}O_{10}$: 444.1995, error: –0.5 ppm).

3-Carboxymethylindole 1-N-β-*D-glucopyranoside (**3**)*. Colorless film. ^{1}H-NMR (acetone-d_6/D_2O (1:1), 500 MHz) and ^{13}C-NMR (acetone-d_6/D_2O (1:1), 125 MHz). HR-ESI–MS, *m/z*, 337.1161 (calcd. for $C_{16}H_{19}NO_7$: 337.1162, error: –0.3 ppm).

RESULTS AND DISCUSSION

The whole, dried seeds of white currant were extracted with 50 % MeOH. The resulting extract was repeatedly subjected to semi-preparative HPLC to yield three pure compounds. Their structures (Fig. 1) were elucidated by 1D and 2D NMR techniques (^{1}H-, ^{13}C-NMR, COSY, NOESY, HSQC, and HMBC), HR-ESI–MS, and by comparison with literature data. The spectroscopic data for compounds **1** and **2** are given in Table I and for compound **3** in Table II.

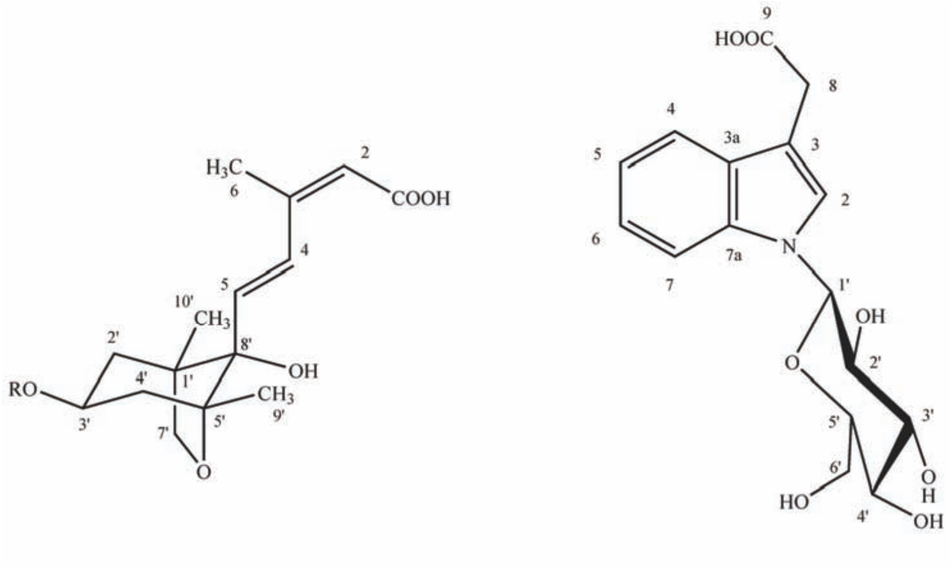

1 R = β-D-Glc(1→6)-β-D-Glc **3**

2 R = β-D-Glc

Fig. 1. Structues of the isolated compounds.

Compound **1** was isolated as a colorless oil and its molecular formula was deduced as $C_{27}H_{42}O_{15}$ based on its negative ESI mass spectrum, which showed $[M–H]^–$ at *m/z* 605.2441. The ^{1}H-NMR spectrum of **1** showed the presence of three methyl singlets at δ 0.84, 1.04, and 1.99 (H-10', 9', and 6, respectively), signals of three methylene groups from the aglycone ring at δ 1.62 (1H, *br d*, H-2'$_{ax}$), 1.89 (1H, *dd*, H-2'$_{eq}$), 1.65 (1H, *br d*, H-4'$_{ax}$), 2.04 (1H, *dd*, H-4'$_{eq}$) and 3.63 ppm (2H, *m*, H-7'), two olefinic methine doublets at δ 6.32 (H-5) and 7.90 ppm (H-4), an olefinic methine singlet at δ 5.69 ppm (H-2), and an oxymethine signal at δ 4.05 ppm (*tdd*, H-3'). The two double bond functionalities of aglycone were also confirmed by the ^{13}C-NMR resonances at δ 119.1, 129.8, 133.7 and 148.0 ppm. A complete assignment of the ^{1}H- and ^{13}C-NMR spectra of the aglycone moiety (Table I) was based on 2D NMR experiments (COSY, NOESY, HSQC and HMBC). A comparison of the NMR data with those from the literature, indicated that compound **1** belongs to dihydrophaseic acid glucoside.[6] The values of vicinal ($^3J_{H,H}$) couplings of H-3' (δ 4.05 ppm, *tdd*, J = 10.5, 6.9 and 6.4 Hz), corresponded to two axial and two equatorial neighbors, revealing the axial position of this proton.[7] Furthermore, the NOESY correlation of protons 3' and 7' was indicative they were on the same side of cyclohexane ring. Similarly, the NOESY correlation of H-2'$_{ax}$ and H-5 suggested that the acyclic moiety of aglycone was attached to the 8' axial position of a bicyclic ring. The configurations of the double bonds (2*Z*, 4*E*) were confirmed by the NOE of H_3-6 with olefinic H-2, and the absence of NOE between olefinic H-4 and H-5. According to the NOESY correlation of H_3-6 with H-5, the 3-*s-trans* conformation is preferred.

TABLE I. ^{1}H-NMR (acetone-d_6/D_2O (1:1), 500 MHz) and ^{13}C-NMR (acetone-d_6/D_2O (1:1), 125 MHz) data of compounds **1** and **2**; assignments were based on COSY, NOESY, HSQC and HMBC experiments. Overlapped proton NMR signals (ovl) are reported without designated multiplicity; n.d. – not determined

Position	Compound					
	1			**2**		
	^{1}H-NMR	*J* / Hz	^{13}C	^{1}H	*J* / Hz	^{13}C-NMR
1	–	–	n.d.	–	–	n.d.
2	5.69 s	–	119.1	5.69 *s*	–	119.1
3	–	–	148.0	–	–	148.3
4	7.90 d	16.0	129.8	7.90 *d*	16.0	129.8
5	6.32	d 16.0	133.7	6.32 *d*	16.0	133.7
6	1.99 *s*	–	20.6	2.00 *s*	–	20.6
1'	–	–	48.0	–	–	47.8
2'$_{ax}$	1.62 *br d*	13.2	41.7	1.62 *br d*	13.5	41.5
2'$_{eq}$	1.89 *dd*	13.2; 6.9	–	1.83 *dd*	13.5; 6.9	–
3'	4.05 *tdd*	10.5; 6.9; 6.4	72.3	4.08 *tdd*	10.5; 6.9; 6.4	71.3
4'$_{ax}$	1.65 *br* d	13.2	41.9	1.65 *br d*	13.5	41.7
4'$_{eq}$	2.04 *dd*	13.2; 6.4	–	2.01 *dd*	13.5; 6.4	–
5'	–	–	85.2	-	–	85.3
7'	3.63 *ovl*	–	74.9	3.60 *ovl*	–	75.1
8'	–	–	81.1	–	–	81.1
9'	1.04 *s*	–	19.5	1.04 *s*	–	19.4
10'	0.84 *s*	–	16.0	0.83 *s*	–	16.0
1''	4.19 *d*	7.8	101.9	4.18 *d*	7.8	101.3
2''	2.90 *ovl*	–	73.1	2.89 *ovl*	–	73.2
3''	3.12 *ovl*	–	76.5	3.12 *ovl*	–	76.5
4''	3.02 *ovl*	–	70.1	3.02 *ovl*	–	70.1
5''	3.33 *ovl*	–	75.6	3.09 *ovl*	–	76.5
6''	3.96 *ovl*	–	68.4	3.42 *ovl*	–	61.0
	3.56 *ovl*	–	–	3.66 *ovl*	–	–
1'''	4.26 *d*	7.8	n.d.	–	–	–
2'''	2.96 *ovl*	–	73.5	–	–	–
3'''	3.13 *ovl*	–	76.6	–	–	–
4'''	3.04 *ovl*	–	70.0	–	–	–
5'''	3.05 *ovl*	–	76.8	–	–	–
6'''	3.67 *ovl*	–	61.0	–	–	–
	3.43 *ovl*	–	–	–	–	–

TABLE II. ^{1}H-NMR (acetone-d_6/D_2O (1:1), 500 MHz) and ^{13}C-NMR (acetone-d_6/D_2O (1:1), 125 MHz) data of compound **3**

Position	^{1}H-NMR	*J* / Hz	^{13}C-NMR
2	7.34 *s*	–	124.1
3	–	–	110.1
3a	–	–	128.0
4	7.50 *d*	8.0	118.8
5	7.02 *t*	8.0	118.9
6	7.12 *t*	8.0	121.1
7	7.50 *d*	8.0	110.3
7a	–	–	136.3
8	3.55 *s*	–	31.9
1'	5.39 *d*	9.1	84.2
2'	3.70 *ovl*	–	71.8
3'	3.45 *ovl*	–	79.1
4'	3.25 *ovl*	–	69.8
5'	3.42 *ovl*	–	77.5
6'	3.44 *ovl*	–	60.8
	3.66 *ovl*	–	–

The ^{1}H-NMR spectrum of **1** also indicated the presence of two anomeric proton doublets at δ 4.19 (H-1'') and 4.26 (H-1'''), suggesting the presence of two sugar moieties. The application of the COSY, NOESY, HSQC, and HMBC spectra enabled the assignment of the remaining ^{1}H- and ^{13}C-NMR sugar resonances, the chemical shifts of which corresponded to glucose. The values of the vicinal couplings of the anomeric protons were consistent with two β-glucopyranosyl units. The occurrence of strong H-1/H-5 and H-1/H-3 NOE cross-peaks indicated a $^4C_1$ conformation for both β-glucopyranosyl units. The interglycosidic linkage was confirmed by NOE cross-peaks of H-1''' with both diastereotopic H-6''. In the preferred conformation of the sugar subunit, the anomeric proton 1'' is close in space to H-4'$_{ax}$ of the aglycone moiety, as shown by the corresponding cross peak in the NOESY spectrum. In this way, it was concluded that the sugar unit was connected to the 3'-position of the aglycone moiety. Based on the above spectral data, the structure of **1** was unambiguously established as dihydrophaseic acid 3'-*O*-β-gentiobioside.

Compound **2** was isolated as a colorless oil, and its molecular formula was deduced as $C_{21}H_{32}O_{10}$ based on its negative ESI mass spectrum, showing $[M–H]^–$ at *m/z* 443.1920. The NMR data of this compound were very similar to those of compound **1**, containing the signals for only one β-glucopyranosyl unit. Thus, compound **2** was identified as dihydrophaseic acid 3'-*O*-β-D-glucopyranoside, which was previously isolated from the aerial parts of *Juniperus phoenicea*.[6]

Compound **3** was isolated as a colorless oil, and its molecular formula was deduced as $C_{16}H_{19}NO_7$ based on its negative ESI mass spectrum, which showed $[M–H]^–$ at *m/z* 336.1088, and $[2M–H]^–$ at *m/z* 637.2256. The ^{1}H- and ^{13}C-NMR chemical shifts corresponded to 3-carboxymethylindole 1-*N*-β-D-glucopyranoside, a nitrogen-containing astringent indole already isolated from red currants.[8]

Acknowledgement. This study was financially supported by the Ministry of Education and Science of the Republic of Serbia, Project No. 172053.

ИЗВОД

ХЕМИЈСКИ САСТАВ ЕКСТРАКТА СЕМЕНКИ БЕЛЕ РИБИЗЛЕ

ДЕЈАН ГОЂЕВАЦ[1], ВЛАТКА ВАЈС[1], СЛОБОДАН МИЛОСАВЉЕВИЋ[2], БОБАН ЂОРЂЕВИЋ[3],
ГОРДАНА ЗДУНИЋ[4] и ВЕЛЕ ТЕШЕВИЋ[2]

[1]*Инсшишуш за хемију, шехнологију и мешалургију, Универзишеш у Београду, Његошева 12, Београд,*
[2]*Хемијски факулшеш, Универзишеш у Београду, Сшуденшски шрг 16, Београд,* [3]*Пољопривредни*
факулшеш, Универзишеш у Београду, Немањина 6, Земун и [4]*Инсшишуш за проучавање*
лековишог биља Др Јосиф Панчић, Тадеуша Кошћушка 1, Београд

Из семена беле рибизле (*Ribes rubrum*, cv. бела шампањска) изолован је нови сесквитерпенски глукозид (**1**), заједно са два позната једињења: 3’-*O*-β-D-глукопиранозидом дихидрофазеинске киселине (**2**) и 3-карбоксиметилиндол-1-*N*-β-D-глукопиранозидом (**3**). На основу детаљних NMR и MS студија, структура новог једињења је одређена као 3’-*O*-β-генциобиозид дихидрофазеинске киселине.

(Примљено 17. јуна 2011)

REFERENCES

1. J. Rajakangas, M. Misikangas, P. Essi, M. Mutanen, *Eur. J. Nutr.* **47** (2008) 115
2. H. M. Leskinen, J.-P. Suomela, H. P. Kallio, *J. Agric. Food Chem.* **57** (2009) 3920
3. M. Stanković, V. Tešević, V. Vajs, N. Todorović, S. Milosavljević, D. Gođevac, *Planta Med.* **74** (2007) 730
4. D. Gođevac, V. Tesević, V. Vajs, S. Milosavljević, M. Stanković, *Food Chem. Toxicol.* **47** (2009) 2853
5. D. Gođevac, V. Tesević, M. Veličković, Lj. Vujisić, V. Vajs, S. Milosavljević, *J. Serb. Chem. Soc.* **72** (2010) 1641
6. Y. Champavier, G. Comte, J. Vercauteren, D. P. Allais, A. J. Chulia, *Phytochemistry* **50** (1999) 1219
7. R. K. Haris, *Nuclear magnetic resonance spectroscopy*, Longman Group, Harlow, UK, 1986, p. 1
8. B. Schwarz, T. Hofmann, *J. Agric. Food. Chem.* **55** (2007) 1405.

Journal of the Serbian Chemical Society
eVersion electronic
JSCS-info@shd.org.rs • www.shd.org.rs/JSCS

J. Serb. Chem. Soc. 76 (11) 1471–1483 (2011)
JSCS–4221

UDC *Conium maculatum:620.266.1:
547.92:543
Original scientific paper

Steroids from poison hemlock (*Conium maculatum* L.): a GC–MS analysis

NIKO S. RADULOVIĆ*# and NEVENKA D. ĐORĐEVIĆ

Department of Chemistry, Faculty of Science and Mathematics, University of Niš, Višegradska 33, 18000 Niš, Serbia

(Received 6 February, revised 16 March 2011)

Abstract: The steroid content of *Conium maculatum* L. (poison hemlock), Apiaceae, a well-known weed plant species, was studied herein for the first time. This was achieved by detailed GC–MS analyses of twenty two samples (dichloromethane extracts of different plant organs of *C. maculatum* at three or four different stages of phenological development, collected from three locations). In total, twenty four different steroids were identified. Six steroids had an ergostane nucleus while the other ones possessed a stigmastane carbon framework. The identity of these compounds was determined by spectral means (MS fragmentation), GC co-injections with authentic standards and chemical transformation (silylation). Steroid compounds were noted to be the main chemical constituents of root extracts (up to 70 %) of this plant species in the last phase of development. The predominant ones were stigmasta-5,22-dien-3β-ol (stigmasterol) and stigmast-5-en-3β-ol (β-sitosterol). In an attempt to classify the samples, principal component analysis (PCA) and agglomerative hierarchical clustering (AHC) were performed using steroid percentages as variables.

Keywords: *Conium maculatum* L.; Apiaceae; GC–MS analyses; steroids; stigmasterol; β-sitosterol.

INTRODUCTION

Poison hemlock, *Conium maculatum* L. (Apiaceae), is an herbaceous weed of European origin found throughout many parts of the world. Every part of this plant, especially the fresh leaves and fruits, contains a volatile, oily alkaloid, which is so poisonous that a few drops prove fatal to small animals.[1] As a medicine, hemlock is a sedative and antispasmodic, and in sufficient doses acts as a paralyser to the centers of motion. Greek and Arabian physicians were in the practice of using it to cure indolent tumors, relieve swellings and pains of the

---

* Corresponding author. E-mail: nikoradulovic@yahoo.com
\# Serbian Chemical Society member.
doi: 10.2298/JSC110206128R

joints, as well as for affections of the skin.[1] Recently, the chemical composition of the leaf and flower essential oils of *C. maculatum* from Serbia as well as the essential oil of Iranian hemlock were published.[2,3] Birkett reported only the major volatile antifeedant constituents from *C. maculatum*.[4] There was a great deal of work performed on the biologically active compounds, such as alkaloids, flavonoids, coumarins, polyacetylenes, vitamins and non-volatile oils, of *C. maculatum*[1,5,6] but there have been no reports on the steroid content of this plant species. During a routine GC–MS screening of Apiaceae taxa from Serbia, steroid compounds were found to be present in high percentages in the dichloromethane extracts of *C. maculatum*. Hence, it was decided to study the steroid profile of hemlock in more detail: 1) to identify the major and minor steroid constituents, 2) to ascertain the sequestration of these compounds (*i.e.*, to determine their plant part distribution pattern) and 3) to track changes in this profile during different phenophases.

EXPERIMENTAL

Plant material

Plant material (roots, preanthesis aerial parts and in full anthesis, and umbels with ripe schizocarps) was collected from three different locations (Crveni krst, Ledena stena and Palilula) in the city Niš (SE Serbia), from March to August 2009 (three or four collections per location). In total 22 samples were subjected to analyses. The plants were identified by Niko Radulović and voucher specimens (numbers from 200905 to 200916) were deposited at the Herbarium of the Faculty of Science and Mathematics, Niš.

Extraction of steroids

The mentioned above fresh plant samples were macerated with an appropriate volume of freshly distilled dichloromethane (50 ml per 10 g of plant material) at room temperature in the dark for one month. The obtained extracts were gravity filtered through small columns packed with 1 g of Celite® (Merck, Germany) in order to remove all insoluble material.

The extracts were dried over anhydrous magnesium sulfate (Aldrich, USA). The solvent was evaporated under a gentle stream of nitrogen at room temperature, in order to exclude any loss of extract volatiles, and analyzed immediately upon isolation. In order to determine the extract yields, the solvent was removed completely by exposing the residues obtained after removal of the bulk of the CH_2Cl_2 under a stream of nitrogen to *vacuum* at room temperature for a short period to eliminate the solvent completely. The pure extracts were then measured on an analytical balance and multiple gravimetric measurements were taken during 24 h to ensure that all of the solvent had evaporated.

Silylation of the extracts

Typical procedure:[7] trimethylchlorosilane (trimethylsilyl chloride, TMSCl, 0.2 mmol) was added with stirring to a mixture of the dry extract (*ca.* 250 mg), dry triethylamine (0.3 mmol) and dimethyl sulfoxide (0.02 mmol) in dry diethyl ether (10 ml). Temperature of the mixture was kept at 10 °C by occasional cooling. After one hour, the reaction mixture was poured into ice-water (10 ml). After washing the ethereal solution with water, the extract was dried over $MgSO_4$ and evaporated *in vacuo*. The obtained residue was completely dissolved in dry diethyl ether (final concentration 10 mg ml^{-1}) and subjected to GC–MS analysis as described below.

Gas chromatography–mass spectrometry (GC–MS) and gas chromatography (GC)

The GC–MS analyses (three repetitions of each sample) were performed using a Hewlett-Packard 6890N gas chromatograph equipped with a fused silica capillary column DB-5MS (5 % phenylmethylsiloxane, 30 m×0.25 mm, film thickness 0.25 μm, Agilent Technologies, USA) and coupled with a 5975B mass selective detector from the same company. The injector and interface were operated at 250 and 320 °C, respectively. The oven temperature was raised from 70 to 315 °C at a heating rate of 5 °C min^{-1} and then held isothermally for 10 min. Helium at a flow rate of 1.0 ml min^{-1} was used as the carrier gas. The samples, 1 μl of the solutions prepared as mentioned above, were injected in a pulsed split mode (the flow was 1.5 ml min^{-1} for the first 0.5 min and then set to 1.0 ml min^{-1} throughout the remainder of the analysis; split ratio 40:1). The MS conditions were as follows: ionization voltage 70 eV, acquisition mass range 35–500 and scan time 0.32 s. The extract constituents were identified by comparison of their linear retention indices (relative to C_7–C_{37} alkanes on the DB-5MS column)[8] with literature values[9-11] and their mass spectra with those of authentic standards (ergost-5-en-3β-ol, stigmasta-5,22-dien-3β-ol, stigmast-5-en-3β-ol, purchased from Sigma-Aldrich, USA), as well as those from the Wiley 6, NIST02, MassFinder 2.3 and a self-made MS library with the spectra corresponding to pure substances and literature data.[12-14] GC (FID) analysis was performed under the same experimental conditions using the same column as described for the GC–MS. The percentage composition of the extracts was computed from the GC peak areas without any corrections.

Data analysis

Principal component analysis (PCA) and agglomerative hierarchical clustering (AHC) were performed using the Excel program plug-in XLSTAT version 2009.4.05. Both methods were applied utilizing the original variables (GC (FID) percentages of the identified extract constituents). The AHC was determined using the Pearson dissimilarity (as aggregation criterion: simple linkage, unweighted pair-group average and complete linkage) and Euclidean distance (aggregation criterion: weighted pair-group average, unweighted pair-group average and the Ward method). The definition of the groups was based on Pearson correlation, using complete linkage and the unweighted pair-group average method.

RESULTS AND DISCUSSION

The chemical composition of CH_2Cl_2 extracts (yields ranged from 0.05 to 2.70 % (w/w) based on fresh plant material weight) of different plant organs of *C. maculatum* was investigated (by GC–MS) at different stages of phenological development, from three locations (22 samples in total). The total ion chromatograms of the CH_2Cl_2 extracts were primarily screened for the presence of steroids (mass spectral comparison with Wiley and NIST data bases). The extracts were additionally submitted to a derivatization procedure (trimethylsilyl chloride) to verify the identification of steroid alcohols through the shift in their RI values. Moreover, the trimethylsilyl ethers yielded informative mass spectra, and, in certain instances, they afforded highly characteristic modes of fragmentation from which structural details were inferred. The identity of the compounds was corroborated whenever possible by GC co-injections of authentic samples. Thus, the identities of the steroids were established by at least three (at best four) independent means.

In three cases, the identification was performed in a less straightforward way and these will be given in more detail. Root samples, after anthesis, contained four different 3,6-diones. Two of them closely eluting were identified as: stigmasta-4,22-diene-3,6-dione (**1**) and stigmast-4-ene-3,6-dione (**2**). Compound **2** possessing an M^+ at *m*/*z* 426 in its MS was identified by mass spectral comparison using in-house MS libraries and with literature data.[12] However compound **1**, having a very similar MS fragmentation pattern and an additional unsaturation, as inferred from its M^+ (*m*/*z* 424), gave no match in the library search. The difference in the amu values of the fragments between compounds **1** and **2** was lost when the *m*/*z* value dropped below the intense *m*/*z* 285 fragment ion that in compound **2** corresponds to a cation formed by the cleavage of the C-17 side-chain (SC). This suggested that the additional double bond (unsaturation) is situated in the side chain of the stigmast-4-ene-3,6-dione framework and that compounds **1** and **2** have identical nuclei (M^+–SC, *m*/*z* 285). The main MS fragmentation pathways for compounds **1** and **2** are shown in Fig. 1. The position between C-22 and 23 of the unsaturation was initially deduced from the ion $(M–112)^+$.[13] Its position was further ascertained according to two additional facts: 1) the retention properties of closely related 5α-stigmasta-3,6-dione and 5α-stigmast-22-ene-3,6-dione (the other two 3,6-diones in the root extracts, identified by MS comparison with literature data)[13] show the same RI increment as the one for **2** and **1**; 2) the difference in the MS caused by the introduction of the double bond within the mentioned analogous pair is the same as the one observed in the case of compounds **1** and **2**.

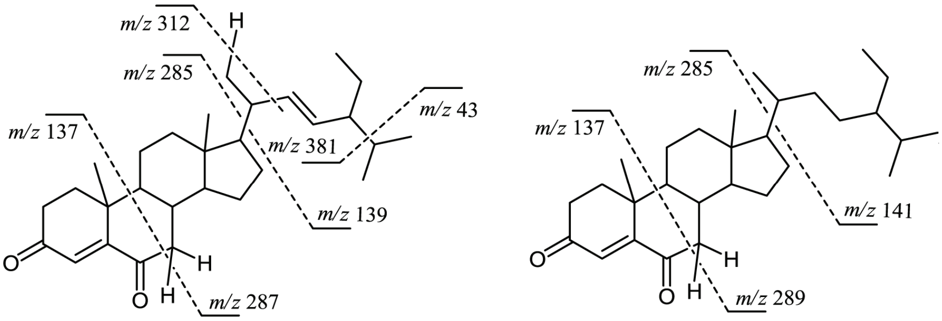

1 **2**

Fig. 1. The main MS fragmentation pathways for stigmasta-4,22-diene-3,6-dione (**1**) and stigmast-4-ene-3,6-dione (**2**).

A similar discussion stands for the identification of 5α-stigmast-22-en-3β-ol (**3**), detected in II (4r) (1.5 %) and III (4s) (0.8 %). 5α-Ergost-22-en-3β-ol possesses an analogous and almost identical MS (NIST07) to that of compound **3** differing in the mass increment of 14 amu and this difference is readily observable in the parent ion at *m*/*z* 414 of the homologous **3**. Stigmasta-4,6-dien-3-one was identified in the same way, by comparing its mass spectrum with that of cholesta-4,6-dien-3-one. The molecular ion of cholesta-4,6-dien-3-one was at *m*/*z* 382 while the molecular ion for the "unknown" compound was at *m*/*z* 410. Subtraction of these molecular ions gives a difference of 28 amu, suggesting that they are members of a homologous series, two methylene units apart.

Silylation provided additional evidence for the proposed structures of other identified compounds (Table I). A non-allylic 3-hydroxy-Δ^5-steroid structure of three detected steroids (ergost-5-en-3β-ol, stigmasta-5,22-dien-3β-ol, stigmast-5-en-3β-ol, Table I) was readily confirmed by their conversion to ethers (sample II (4r) was subjected to TMSCl/Et_3N due to the high content of sterols and the presence of a large number of different components of interest). The trimethylsilyl ether strongly promoted the fragmentations to yield characteristic complementary pair of ions at *m*/*z* 129 and $[M-129]^+$.[15] This allowed the discernment of Δ^5-steroids from other unsaturated 3-ol steroids. Additionally, the silylation permitted the positioning of the double bonds through the retro-Diels–Alder reaction on ring B (together with the corresponding loss of H_2O or TMSOH), which gives *m*/*z* 95 (in both, the free alcohol and TMS ether) for 5α-stigmast-7-en-3β-ol and *m*/*z* 119 for Δ^5-steroids. In general all steroids and their TMS derivatives had the following feature: a prominent ion at *m*/*z* 255 that is ascribed to a fragment derived by loss of molecules of water plus the side-chain in the alcohols or the side-chain plus $HOSiMe_3$ in the ethers.[16]

TABLE I. Identified steroids of dichloromethane extracts of *C. maculatum*; *RI* – retention indices on a DB-5 column relative to C_{31}–C_{37} *n*-alkanes;[8] the experimental values were in good agreement with the literature ones;[9–11] TMS – sterols converted to trimethylsilyl ethers

Steroids	Designation	*RI*	*RI* (Lit.)	*RI* (TMS)	*RI* (Lit.) (TMS)	*m*/*z* (M^+)
Ergosta-5,7,9(11),22-tetraen-3β-ol	E1	3150	–	–	3161[9]	394
Ergosta-5,8,22-trien-3β-ol	E2	3158	3113±5[10]	–	–	396
Ergosta-5,7,22-trien-3β-ol	E3	3187	3152±6[10]	–	3232±2[10]	396
5α-Ergosta-7,22-dien-3β-ol	E4	3202	–	–	–	398
Ergost-5-en-3β-ol[a]	E5	3211	–	3231	3249[11]	400
Stigmasta-5,22-dien-3β-ol[a]	S1	3244	3248[9,10]	3262	3274[9,11]	412
5α-Stigmast-22-en-3β-ol	S2	3253	–	–	–	414
5α-Stigmasta-7,22-dien-3β-ol	S3	3295	3295[9]	–	–	412
Stigmast-5-en-3β-ol[a]	S4	3311	3290±10[10]	3329	3342±4[10]	414
5α-Stigmastan-3β-ol[a]	S5	3325	3317[9]	3343	3349[9]	416
Ergost-4-en-3-one	E6	3354	–	–	–	398
5α-Stigmastan-3-one	S6	3370	–	–	–	414
5α-Stigmast-7-en-3β-ol[a]	S7	3382	–	3401	3404[9]	414
5α-Stigmasta-7,22-dien-3-one	S8	3393	–	–	–	410
Stigmasta-4,22-dien-3-one[a]	S9	3399	–	–	–	410
5α-Stigmasta-7,16-dien-3β-ol[a]	S10	3401	–	–	–	412

TABLE I. Continued

Steroids	Designation	*RI*	*RI* (Lit.)	*RI* (TMS)	*RI* (Lit.) (TMS)	*m*/*z*(M^+)
5*α*-Stigmast-7-en-3-one	S11	3420	–	–	–	412
Stigmast-4-en-3-one	S12	3458	3435±4[10]	–	–	412
Stigmasta-4,6-dien-3-one[a]	S13	3518	–	–	–	410
Stigmasta-4,22-diene-3,6-dione	S14	3538	–	–	–	424
Stigmast-4-ene-3,6-dione[a]	S15	3541	–	–	–	426
5*α*-Stigmasta-22-ene-3,6-dione[a]	S16	3598	–	–	–	426
5*α*-Stigmastane-3,6-dione[a]	S17	3601	–	–	–	428
3*β*-Hydroxystigmast-5-en-7-one[a]	S18	3609	–	–	–	428

[a] EIMS, 70 eV, *m*/*z* (rel. int. %): S10 – 314 (20), 271 (100), 131 (35), 121 (28), 107 (75), 95 (50), 91 (47), 55 (46); S7 – 414 (100), 255 (95), 107 (52), 105 (45), 95 (33), 91 (37), 55 (48), 43 (69); TMS ether of S7 – 486 (32), 471 (18), 381 (10), 255 (60), 229 (18), 213 (14), 147 (10); S13 – 410 (84), 174 (45), 161 (48), 160 (57), 136 (100), 95 (49), 57 (50), 43 (76); S18 – 428 (100), 395 (29), 287 (37), 205 (14), 187 (35), 161 (36), 135 (34), 43 (52); mass spectra of S9, S15, S16 and S17 were identical to those reported previously;[12,13] mass spectra of trimethylsilyl ether derivatives of S5, S4, S1 and E5 were identical to those reported in a previous study[14]

The steroids (Table I) accounted for 5.3–68.3 % of the total extracts (area percentage of the GC chromatograms, Tables II and III). In total, twenty four different steroids were identified in the investigated samples (Tables I–III; out of 22, only one sample did not contain any detectable amount of steroid compounds, II (1a)). The structures of the identified steroids are presented in Fig. 2.

Steroid compounds were noted to be the main chemical constituents of the root extracts (Table II) of this plant species in the late summer when the plant was almost dry (the highest amount of sterols per gram of fresh plant material was 61.0–68.3 %). Only six steroids had an ergostane nucleus (Table I) while the other ones possessed a stigmastane carbon framework. The predominant were stigmasta-5,22-dien-3*β*-ol (stigmasterol, 14.4–15.5%) and stigmast-5-en-3*β*-ol (*β*-sitosterol, 12.5–18.9 %), the former one is the most common phytosterol in terrestrial plants. The two sterols were most abundant in the last phase of development and were present in all investigated samples of *C. maculatum*. Together with *β*-sitosterol and stigmasterol, other minor identified steroids possessed a C-3--oxygenation pattern. The occurrence of C-3-oxygenated steroids was previously reported in higher plants from very diverse plant families. The following *C. maculatum* steroids can serve as examples: 5*α*-stigmast-22-en-3*β*-ol (*Kirganelia reticulate* – Euphorbiaceae, *Allamanda cathartica* – Apocynaceae),[17,18] 5*α*-stigmasta-7,16-dien-3*β*-ol (found only in *Clinopodium vulgare* – Lamiaceae),[19] 5*α*--stigmasta-7,22-dien-3-one (*Gustavia augusta* – Lecythidaceae, *Clinopodium umbrosum* – Lamiaceae),[20,21] 5*α*-stigmasta-7,22-dien-3*β*-ol (*Camellia japonica* – Theaceae, *Bupleurum aureum* – Apiaceae)[22,23] and 5*α*-stigmast-7-en-3*β*-ol (*Cucurbita pepo* – Cucurbitaceae, *Tricholepis glaberrima* – Asteraceae).[24,25] Stigmast-4-ene-3,6-dione was often found to be present with other 4-en-3-ones or 3,6--diones (5*α*-stigmastane-3,6-dione, stigmast-4-en-3-one, stigmasta-4,22-dien-3-one

TABLE II. Percentage of steroids ± standard error from the GC (FID) chromatograms and yields (%, w/w) of dichloromethane extracts of roots of *C. maculatum* at three/four different stages of phenological development, from three locations; I, II, III – three collection locations (Crveni krst, Ledena stena, Palilula, respectively); 1, 2, 3, 4 – different stages of development (preanthesis – 1,2, anthesis – 3, ripe fruits – 4); r – roots; tr – trace amount (<0.05 %)

Steroid[a]	I (1r)	I (2r)	I (3r)	I (4r)	II (1r)	II (2r)	II (3r)	II (4r)	III (2r)	III (3r)	III (4r)
E1[b]	–	–	–	0.3±0.02	–	–	–	0.5±0.04	–	–	0.3±0.01
E2	–	–	–	0.4±0.03	–	–	–	0.5±0.03	–	–	0.3±0.02
E3	–	–	–	6.5±0.35	–	–	–	6.0±0.33	–	–	5.3±0.29
E4	–	–	–	–	–	–	–	0.3±0.01	–	–	0.2±0.01
E5	0.1±0.04	–	0.2±0.01	1.0±0.15	–	0.2±0.01	0.2±0.01	1.4±0.23	–	0.1±0.01	1.0±0.15
S1	3.0±0.21	5.0±0.27	5.0±0.29	15.2±0.93	1.8±0.23	4.6±0.67	4.9±0.23	14.4±0.89	1.1±0.13	3.1±0.26	15.5±0.89
S2	–	–	–	–	–	–	–	1.5±0.19	–	–	–
S3	–	–	–	–	–	–	–	0.1±0.01	–	–	1.0±0.17
S4	2.0±0.19	4.7±0.24	4.1±0.17	12.5±0.85	1.0±0.11	3.5±0.27	4.8±0.20	18.9±0.97	0.7±0.03	2.1±0.16	13.6±0.76
S5	–	–	0.4±0.02	1.9±0.28	–	–	0.5±0.04	2.5±0.14	–	–	–
E6	–	–	–	1.0±0.13	–	–	–	–	–	–	–
S6	–	–	–	1.4±0.19	–	–	–	1.3±0.15	–	–	1.1±0.15
S7	0.2±0.01	0.4±0.06	0.2±0.01	0.9±0.04	–	0.3±0.04	0.2±0.01	1.7±0.18	–	–	1.4±0.23
S8	–	–	–	–	–	–	–	4.9±0.31	–	–	–
S9	–	–	0.2±0.01	9.0±0.54	–	0.1±0.01	0.2±0.01	–	–	–	9.6±0.61
S11	–	–	–	–	–	–	–	0.8±0.03	–	–	1.0±0.12
S12	–	0.3±0.02	0.4±0.02	8.5±0.41	–	0.2±0.02	0.4±0.03	9.7±0.42	–	0.1±0.01	10.1±0.69
S13	–	–	–	0.8±0.23	–	–	–	0.8±0.02	–	–	0.6±0.04
S14	–	–	–	0.6±0.04	–	–	–	0.4±0.02	–	–	tr
S15	–	–	–	1.2±0.15	–	–	–	0.9±0.05	–	–	tr
S16	–	–	–	0.2±0.01	–	–	–	0.6±0.02	–	–	tr
S17	–	–	–	0.3±0.02	–	–	–	1.1±0.23	–	–	tr
S18	–	–	–	0.1±0.01	–	–	–	–	–	–	–
Total	5.1–5.5	10.1–10.5	10.2–10.7	61.5–61.9	2.3–2.7	8.6–8.9	11.0–11.3	68.1–68.4	1.4–1.9	5.3–5.7	59.9–60.2
Yield	0.19	0.17	0.40	0.44	0.21	0.18	0.22	0.40	0.16	0.30	0.35

[a] Compounds listed in order of elution from a DB-5 column; [b] for steroid designation see Table I

TABLE III. Percentage of steroids ± standard error from the GC (FID) chromatograms and yields (%, w/w) of dichloromethane extracts of the aerial parts (a) and fruits (f) of *C. maculatum* at three/four different stages of phenological development, from three locations; I, II, III – three collection locations (Crveni krst, Ledena stena, Palilula, respectively); 1, 2, 3, 4 – different stages of development (preanthesis – 1,2, anthesis – 3, ripe fruits – 4); a - aerial parts; f – fruits; tr – trace amount (<0.05 %)

Steroid[a]	I (1a)	I (2a)	I (3a)	I (4f)	II (2a)	II (3a)	II (4f)	III (2a)	III (3a)	III (4f)
E2[b]	–	–	–	–	–	–	0.2±0.02	–	–	0.4±0.02
E3	–	–	–	1.4±0.16	–	–	2.4±0.27	–	–	2.4±0.29
E5	–	–	0.1±0.01	–	–	–	0.4±0.03	–	0.2±0.01	0.5±0.04
S1	3.3±0.28	4.2±0.36	3.2±0.29	2.3±0.22	5.1±0.37	3.4±0.28	4.5±0.32	1.2±0.11	2.2±0.24	4.0±0.37
S2	–	–	–	–	–	–	–	–	–	0.8±0.07
S3	tr	2.1±0.16	0.9±0.07	–	tr	–	–	–	tr	tr
S4	3.0±0.31	3.0±0.24	1.8±0.19	1.6±0.17	4.1±0.32	2.1±0.25	2.9±0.31	0.8±0.09	2.3±0.20	2.4±0.18
S5	–	–	–	0.3±0.02	–	–	0.8±0.04	–	–	–
S7	1.3±0.11	2.8±0.28	1.2±0.09	0.6±0.04	1.5±0.13	0.8±0.09	1.1±0.12	–	1.5±0.14	1.2±0.11
S9	–	–	–	–	–	–	0.3±0.01	–	–	0.3±0.02
S10	–	0.8±0.05	0.2±0.01	–	–	–	–	–	0.3±0.02	0.2±0.01
S12	–	–	–	–	–	–	–	–	–	0.4±0.02
Total	7.3–7.8	12.7–13.0	7.1–7.6	6.0–6.4	10.5–10.8	6.2–6.5	12.4–12.7	1.9–2.2	6.2–6.6	12.2–12.7
Yield	0.16	0.05	0.31%	2.70%	0.05%	0.16%	1.70%	0.17%	0.60%	1.45%

[a]Compounds listed in order of elution from a DB-5 column; [b]for steroid designation see Table I

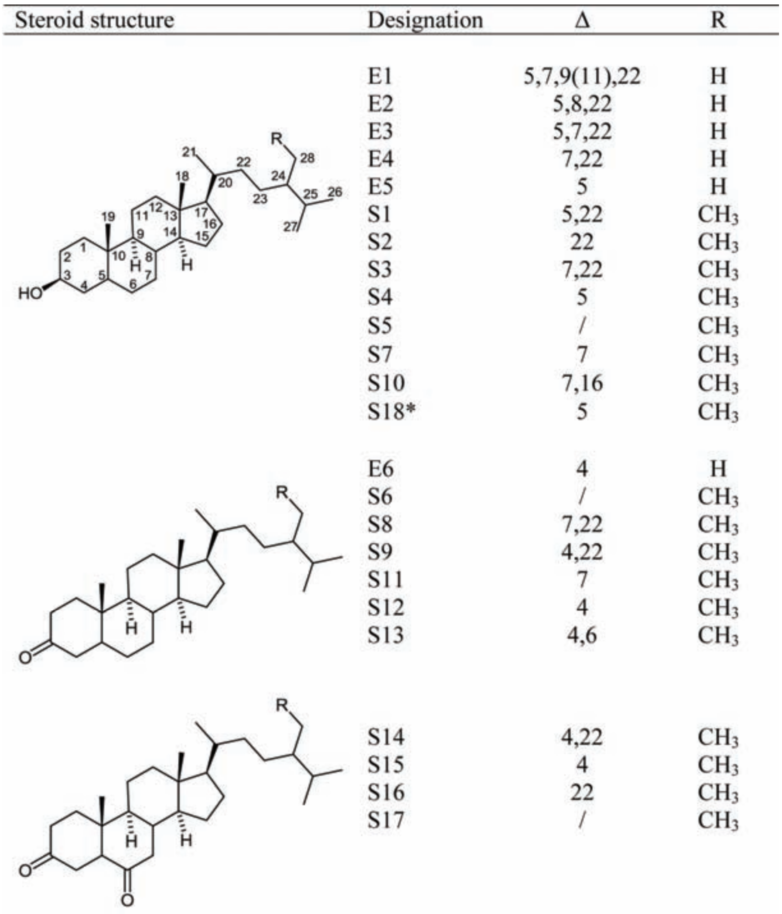

Steroid structure	Designation	Δ	R
	E1	5,7,9(11),22	H
	E2	5,8,22	H
	E3	5,7,22	H
	E4	7,22	H
	E5	5	H
	S1	5,22	CH_3
	S2	22	CH_3
	S3	7,22	CH_3
	S4	5	CH_3
	S5	/	CH_3
	S7	7	CH_3
	S10	7,16	CH_3
	S18*	5	CH_3
	E6	4	H
	S6	/	CH_3
	S8	7,22	CH_3
	S9	4,22	CH_3
	S11	7	CH_3
	S12	4	CH_3
	S13	4,6	CH_3
	S14	4,22	CH_3
	S15	4	CH_3
	S16	22	CH_3
	S17	/	CH_3

Fig. 2. Structures of the identified steroids from *C. maculatum* (*steroid S18 (3β-hydroxy-stigmast-5-en-7-one) has an additional carbonyl group at C-7).

or/and stigmasta-4,22-diene-3,6-dione), for example in *Aristolochia triangularis*, *Aristolochia tubiflora* (Aristolochiaceae), *Polygonum chinensis* (Polygonaceae) and *Ptychopetalum olacoides* (Olacaceae).[26–29] These are interesting due to the noted anti-inflammatory and anti-allergic properties for these sterols (from *P. chinensis*).[28] Stigmasta-4,22-diene-3,6-dione, an allelochemical substance, found also in *Pistia stratiotes* (Araceae) was established to inhibit the growth of some microalgae.[30] Previously, 5α-stigmast-7-en-3-one was reported only from three plant species: *Gypsophila trichotoma* (Caryophyllaceae),[31] *Centratherum anthelminticum* (Asteraceae)[32] and *Coccinia indica* (Cucurbitaceae),[33] while stigmasta-4,6-dien-3-one was only found to occur naturally in *Senecio crassiflorus* (Asteraceae)[34] and *Prosopis alpataco* (Fabaceae).[35] Several of the steroids listed in Table I are quite rare plant constituents. Stigmast-22-ene-3,6-dione, detected only in the last stages of development from all three locations, was previously reported only for the stem extracts of *Phoenix dactylifera* (Arecaceae).[36] 3*β*-Hydroxystigmast-5-en-7-one was detected only in the sample I (4r). Previously, it was reported in *Oryza sativa* (Poaceae).[37]

In order to try to classify the samples, principal component analysis (PCA) and agglomerative hierarchical clustering (AHC) were performed with the GC (FID) percentages of the steroid compounds as variables. The dendrogram obtained as the result of AHC is depicted in Figs. 3 and 4. The AHC analysis performed using the identified extract constituents indicated five groups (classes) of extracts under study.

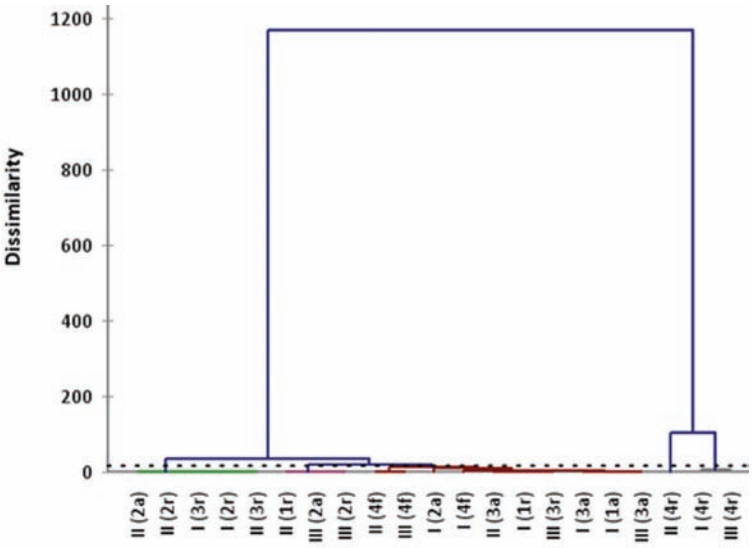

Fig. 3. Dendrogram (AHC analysis) obtained using the percentage of the identified steroid constituents (root and aerial parts extracts) as the original variables obtained by Euclidean distance dissimilarity (dissimilarity within the interval [0,1200]), using the aggregation criterion – the Ward method.

Generally, all samples were statistically very similar (visible from the low dissimilarity values). AHC analysis grouped the root extracts of *C. maculatum* (the last stage of phenological development) from locations I and III together in the dendrogram. They were also closely related to the sample 4r from location II but it formed a separate class. The presence of numerous minor steroids was a mutual feature of samples I, III and II (4r), but they differed in the content of stigmasta-7,22-dien-3-one and stigmasta-4,22-dien-3-one (Table II). The samples II (1r), III (2a) and III (2r) were placed within the same class due to the fact that they contained only two sterols (stigmasterol and *β*-sitosterol) in lower relative amount (0.7–1.8 %) compared to the rest of the samples. Assuming that the intensity of steroid biosynthesis follows the phenological development, the plants from location III seem to have matured slower than those from location II. Since all of the plants eventually reached the same level of steroid production in the last phase, this could be attributed to a whole array of environmental factors (temperature, illumination period variations, *etc*. for the different locations).

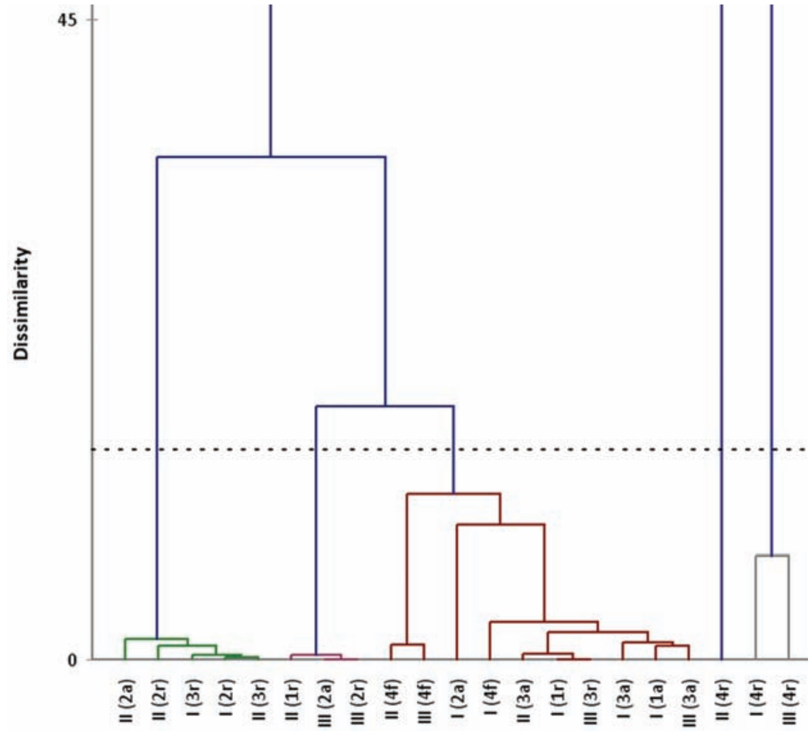

Fig. 4. Enlargement of a part (dissimilarity interval [0,45]) of Fig. 3..

The PCA analysis utilizing the original variables (relative content of the identified compounds) revealed a number of strong dependences between the extract constituents. High coefficients were noted between certain steroids and their dehydro derivatives: ergosta-5,7,9(11),22-tetraen-3β-ol and ergosta-5,7,22-trien-3β-ol (0.901); stigmasta-5,22-dien-3β-ol and stigmast-5-en-3β-ol (0.958); 5α-stigmastan-3-one and stigmast-4-en-3-one (0.983); stigmast-4-en-3-one and stigmasta-4,6-dien-3-one (0.979); 5α-stigmast-22-en-3,6-dione and 5α-stigmastane-3,6-dione (0.998); stigmasta-4,22-diene-3,6-dione and stigmast-4-ene-3,6-dione (0.998), possibly because the biosynthesis of these steroids is mutually interdependent (*i.e.*, substrates of the same dehydrogenase).

CONCLUSIONS

Steroid compounds were noted to be the main chemical constituents of the root extracts (up to 70 %) of *C. maculatum* in the last stage of phenological development. The predominant were stigmasta-5,22-dien-3β-ol (stigmasterol) and stigmast-5-en-3β-ol (β-sitosterol). The identified steroid compounds (and their possible biological/pharmacological properties) contribute to knowledge on *C. maculatum* and add interest to this plant species. These results demonstrate the pronounced variability of the steroid constituents found in *C. maculatum* and stresses the importance of investigations dealing with the chemistry of separate plant organs and different plant harvesting periods and locations.

Acknowledgments. The financial support of this work by the Ministry of Education and Science of the Republic of Serbia is gratefully acknowledged (Project No. 172061).

ИЗВОД

СТЕРОИДИ ИЗ КУКУТЕ (*Conium maculatum* L.): GC–MS АНАЛИЗА

НИКО С. РАДУЛОВИЋ и НЕВЕНКА Д. ЂОРЂЕВИЋ

Дeпартман за хемију, Природно–математички факултет, Универзитет у Нишу,
Вишеградска 33, 18000 Ниш

У овом раду су изнети резултати испитивања стероида биљне врсте *Conium maculatum* L. (кукута), из породице Apiaceae, добро познате отровне коровске биљке. Урађене су детаљне GC–MS анализе двадесет и два узорка (дихлорметански екстракти биљних органа врсте *C. maculatum*; материјал је сакупљан са три локације, у току три или четири фенофазе). Двадесет и четири стероида су идентификована, од којих шест има ергостанско језгро, док остали поседују стигмастански скелет. Идентификација ових једињења је вршена на основу њихове MS фрагментације, као и GC коинјекцијом чистих једињења и хемијском трансформацијом (силиловањем). Уочено је да су стероиди главни састојци екстраката корена (до 70 %) ове биљне врсте у последњој фази фенолошког развића. Најзаступљенији су били стигмаста-5,22-диен-3β-ол (стигмастерол) и стигмаст-5-ен-3β-ол (β-ситостерол). Да бисмо покушали да класификујемо наше узорке, урађена је статистичка обрада добијених резултата коришћењем методе анализе главне компоненте (PCA) и агломеративне хијерархијске кластер анализе (AHC), са релативним садржајем стероида као варијаблама.

(Примљено 6. фебруара, ревидирано 16. марта 2011)

REFERENCES

1. J. Vetter, *Food Chem. Toxicol.* **42** (2004) 1373
2. N. Radulović, D. Zlatković, B. Zlatković, D. Đoković, G. Stojanović, R. Palić, *Chem. Nat. Compd.* **44** (2008) 390
3. S. Masoudi, A. Esmaeili, M. A. Khalilzadeh, A. Rustaiyan, N. Moazami, M. R. Akhgar, M. Varavipoor, *Flavour Frag. J.* **21** (2006) 801
4. M. A. Birkett, C. J. Dodds, I. F. Henderson, L. D. Leake, J. A. Pickett, M. J. Selby, P. Watson, *J. Chem. Ecol.* **30** (2004) 563
5. E. V. Zdanevich, G. A. Belodubrovskaya, *Rastit. Resur.* **33** (1997) 108 (in Russian)

6. M. Khodzhimatov, S. Bobokhodzhaeva, *Izv. Akad. Nauk. Tadzhikskoi SSR*, *Otd. Biol. Nauk.* **2** (1976) 81 (in Russian)
7. R. G. Visser, H. J. T. Bos, L. Brandsma, *Recl. Trav. Chim. Pays-Bas* **99** (1980) 70
8. H. Van Den Dool, P. D. Kratz, *J. Chromatogr.* **11** (1963) 463
9. *Retention data*, NIST Mass Spectrometry Data Center, http://webbook.nist.gov/cgi/ /cbook.cgi?Source=2008TRE%2320876M&Units=SI (accessed 20.12.2010)
10. V. A. Isidorov, L. Szczepaniak, *J. Chromatogr., A* **1216** (2009) 8998
11. P. Jonsson, A. I. Johansson, J. Gullberg, J. Trygg, A. Jiye, B. Grung, S. Marklund, M. Sjöström, H. Antti, T. Moritz, *Anal. Chem.* **77** (2005) 5635
12. K. Ghosh, T. K. Bhattacharya, *Molecules* **10** (2005) 798
13. P. Georges, M. Sylvestre, H. Ruegger, P. Bourgeois, *Steroids* **71** (2006) 647
14. C. J. W. Brooks, E. C. Horning, J. S. Young, *Lipids* **3** (1968) 391
15. C. J. W. Brooks, *Phil. Trans. R. Soc. London* **293** (1979) 53
16. M. Pelillo, G. Iafelice, E. Marconi, M. F. Caboni, *Rapid Commun. Mass Spectrom.* **17** (2003) 2245
17. R. Jain, S. Nagpal, *J. Indian Chem. Soc.* **79** (2002) 776
18. P. K. Agrawal, M. P. Sharma, *Indian J. Pharm. Sci.* **45** (1983) 246
19. P. Hadjieva, E. Popova, A. Tzvetkova, B. Hadjieva, *Bulg. Chem. Ind.* **75** (2004) 96
20. A. D. L. De Souza, A. F. I. Da Rocha, M. L. B. Pinheiro, C. H. de S. Andrade, A. L. de A. Q. Galotta, M. do P. S. S. dos Santos, *Quim. Nova* **24** (2001) 439
21. S. M. Lee, J. S. Lai, Y. H. Kuo, *J. Chin. Chem. Soc.* **40** (1993) 87
22. R. Suau Suarez, *Acta Cient. Compostelana* **8** (1971) 185
23. A. T. Troshchenko, T. I. Limasova, *Khim. Prir. Soedin.* **3** (1967) 145 (in Russian)
24. H. Itokawa, Y. Oshida, A. Ikuta, H. Inatomi, *Yakugaku Zasshi* **102** (1982) 318
25. A. S. Chawla, V. K. Kapoor, P. K. Sangal, A. K. Gupta, F. J. Evans, *Planta Med.* **30** (1976) 151
26. G. Ruecker, B. Langmann, N. S. De Siqueira, *Planta Med.* **41** (1981) 143
27. G. Peng, F. Lou, Y. Chen, S. Zhao, *Zhongcaoyao (Chin. Trad. Herbal Drugs)* **26** (1995) 623
28. P. L. Tsai, J. P. Wang, C. W. Chang, S. C. Kuo, P. D. Chao, *Phytochemistry* **49** (1998) 1663
29. Y. Ito, F. Hirayama, Y. Aikawa, H. Kondo, K. Sagara, J. Shoji, *Nat. Med.* **49** (1995) 487
30. G. Aliotta, P. Monaco, G. Pinto, A. Pollio, L. Previtera, *J. Chem. Ecol.* **17** (1991) 2223
31. I. N. Krasteva, I. S. Popov, V. I. Balabanova, S. D. Nikolov, I. P. Pencheva, *Quim. Nova* **31** (2008) 1125
32. B. K. Mehta, D. Mehta, M. Verma, *Nat. Prod. Res.* **19** (2005) 435
33. W. Sucrow, A. Reimerdes, *Z. Naturforsch., B* **23** (1968) 42
34. M. C. Tettamanzi, E. A. Jares, L. M. Iannone, A. B. Pomilio, *Fitoterapia* **65** (1994) 468
35. M. Mazzuca, V. T. Balzaretti, *J. Sci. Food Agric.* **83** (2003) 1072
36. I. M. Fernandez, J. R. Pedro, E. Seoane, *Phytochemistry* **22** (1983) 2087
37. F. A. Macias, N. Chinchilla, R. M. Varela, J. M. G. Molinillo, *Steroids* **71** (2006) 603.

Journal of the Serbian Chemical Society
JSCS-info@shd.org.rs • www.shd.org.rs/JSCS

J. Serb. Chem. Soc. 76 (11) 1485–1496 (2011)
JSCS–4222

UDC *Phymatopteris hastata:547.56:
547.972:615.27–188
Original scientific paper

Phenolic content and antioxidant activity of *Phymatopteris hastata*

WEI SU[1]*, PEIYUAN LI[2]**, LINI HUO[2], CAIYING WU[1],
NANA GUO[1] and LIANGQUAN LIU[1]

[1]*College of Chemistry and Life Science, Guangxi Teachers Education University, Nanning and* [2]*College of Pharmacy, Guangxi Traditional Chinese Medical University, Nanning, China*

(Received 11 November 2010, revised 11 January 2011)

Abstract: Various solvent extracts of *Phymatopteris hastata*, a traditional Chinese medicinal material, were screened for their antioxidant activities. Four systems of *in vitro* testing were employed to investigate the antiradical and antioxidant effect, *i.e.*, the 2,2-diphenyl-1-picryhydrazyl (DPPH) and 2,2'-azinobis(3-ethylbenzothiazoline-6-sulfonic acid) (ABTS) systems, the hydroxyl radical scavenging assay and the reducing power. In addition, butylated hydroxytoluene (BHT), a widely used synthetic antioxidant, was also studied for comparison. The results revealed that the ethyl acetate extract exhibited outstanding antioxidant activities, which was close or even superior to BHT. Furthermore, the total phenolic (TP) and total flavonoid (TF) contents of different extracts were measured, expressed as gallic acid and rutin equivalent, respectively. The antioxidant activities and the TP/TF content of different extracts followed the same order: ethyl acetate extract > butyl alcohol extract > > petroleum ether extract, showing a good correlation between the antioxidant activities and the TP/TF content. The results showed that these extracts, especially the ethyl acetate extract, were rich in phenolics and flavonoids and could be considered as natural antioxidants.

Keywords: total phenolic content; total flavonoid content; DPPH; ABTS; hydroxyl radical; reducing power; *Phymatopteris hastata*.

INTRODUCTION

Antioxidants are substances that delay the oxidation process, inhibiting free radical initiated chain polymerization and other subsequent oxidizing reactions,[1] and are widely used in the food, cosmetic and pharmaceutical industries.[2] Antioxidants play an important role in biological systems because they defend against oxidative damage and participate in the major signaling pathways of cells.[3] Of particular importance, they can prevent damage in cells caused by the action of reactive oxygen species.[4–6]

Corresponding authors. E-mails: aaasuwei@yahoo.com.cn (*); lipearpear@yahoo.cn (**)
doi: 10.2298/JSC101111130S

Reactive oxygen species (ROS), the major free radicals generated in normal metabolic processes, exist in the form of hydrogen peroxide (H_2O_2), the superoxide anion ($O_2^{\bullet-}$), the hydroxyl radical ($^{\bullet}OH$), *etc*.[7] There is a balance between ROS generation and elimination by endogenous superoxide dismutase, glutathione peroxidase and catalase. However, over-production of ROS, induced by exposure to external oxidant substances or a failure in the defense mechanisms, will cause a variety of biochemical and physiological lesions and often result in metabolic impairment and cell death.[8] Moreover, impairment to cell structures, DNA, lipids and proteins induced by ROS are associated with more than 30 different disease processes,[9] including highly disabling vascular pathologies such as cardiovascular disease (CVD)[10,11] and cardiac failure, alcohol-induced liver disease (ALD) and ulcerative colitis, cancer, and neurodegenerative conditions such as Alzheimer's disease (AD), mild cognitive impairment (MCI) and Parkinson's disease (PD).[12]

Fortunately, the action of active oxygen and free radicals is opposed by a balanced system of antioxidant defenses, hence the presence of antioxidants is essential for human health.[7] The most commonly used synthetic antioxidants, such as butylated hydroxyanisole (BHA), butylated hydroxytoluene (BHT) and propyl gallate (PG) were restricted due to their instability and possible carcinogenicity.[13–15] Hence, there is growing attention for the search for natural antioxidants, which avoid the side effects and can be used to reduce cellular oxidative lesion in foods and even the human body.[16–20] Plants, including herbs and spices, have been considered as potential sources for natural antioxidants,[21,22] because they are rich in phenolic components[23,24] that have antimutagenic, anticarcinogenic, anti-inflammation, and antioxidant activities.[25,26]

Phymatopteris hastata (Thunberg) Pichi Sermolli Webbia, which is widespread in south China, is one of the most important traditional medicines belonging to the Polypodiaceae family. It is used as a remedy for a wide range of diseases, for instance, diarrhea, cough, bronchitis, headache, influenza, fever and urinary tract infection. Moreover, it is especially useful in conditions such as carbuncle, furunculosis and viper bites. However, there is no reported information on the antioxidant activity of *P. hastata*. Thus, in the present study, the antioxidant activities of various solvent extracts from *P. hastata* were investigated by employing four *in vitro* test systems: 2,2-diphenyl-1-picryhydrazyl (DPPH) and 2,2'-azinobis(3-ethylbenzothiazoline-6-sulfonic acid) (ABTS), hydroxyl radical scavenging assay and reducing power. Furthermore, the total phenolic (TP) and total flavonoid (TF) contents of different extracts were measured to expose the relationship between the TP/TF content and antioxidant activity.

EXPERIMENTAL

Sample and reagents

P. hastata whole plant was collected during the summer of 2009 in the Guangxi Province, China. A voucher specimen was identified by Dr. Songji Wei at the Department of Zhuang Pharmacy, Guangxi Traditional Chinese Medical University. 2,2'-Azinobis(3-ethylbenzothiazoline-6-sulfonic acid) (ABTS) and butylated hydroxytoluene (BHT) were purchased from Sigma Aldrich Co., St. Louis, MO, USA; 2,2-diphenyl-1-picryhydrazyl (DPPH) (purity 98 %) was purchased from Wako Chemicals, Japan; rutin and gallic acid standards were purchased from J & K Scientific Ltd., Beijing, China. Other chemicals were purchased from the China National Medicine Group Shanghai Corporation, Shanghai, China. All chemicals and solvents used were of analytical grade.

Preparation of the petroleum ether, ethyl acetate and butyl alcohol extracts

The material was initially air-dried and then reduced to small particles. The particles that passed through a 40-mesh screen were selected for analyses. Fifty grams of air-dried plant material was immersed in 500 mL of ethanol (95 %) and constantly stirred. After 48 h, the filtrate was collected. The extraction was repeated two times more. The combined extracts were then concentrated under reduced pressure at 40 °C using a vacuum rotary evaporator. The above ethanol extract was partitioned with petroleum ether, ethyl acetate and butyl alcohol, and the obtained petroleum ether fractions (PE), ethyl acetate fractions (EE) and butyl alcohol fractions (BE) were collected and concentrated using a vacuum rotary evaporator at 40 °C. The preparation of the petroleum ether, ethyl acetate and butyl alcohol extracts was performed in triplicate.

Determination of the TP and TF contents by spectrophotometric procedures

Determination of the TP content. The total content of soluble phenolics (*TP*) was determined using the Folin-Ciocalteu reagent according to the method of Slinkard and Singleton,[27] with gallic acid as the equivalent. Briefly, the extract solution (0.5 mL, 1 mg mL^{-1}) was diluted with distilled water (46 mL) in a volumetric flask. Folin–Ciocalteu reagent (1 mL) was added and mixed thoroughly. After 3 min, sodium carbonate solution (3 mL, 2 %) was added, and then the mixture was allowed to stand for 2 h with intermittent shaking. The absorbance was measured at 760 nm. The total phenolic content was determined by comparison with a standard calibration curve for gallic acid, and the results are presented as milligrams of gallic acid equivalent per 1 g (dry weight) of extract (mg GAE g^{-1} dw). All tests were conducted in triplicate.

Determination of the TF content. The total flavonoid (*TF*) content was determined following the procedure of Dewanto *et al*.[28] with rutin as the equivalent. The extract solution (3 mL, 0.8 mg mL^{-1}) was placed in a 10-mL volumetric flask and then 5 mL of distilled water was added followed by $NaNO_2$ solution (0.3 mL, 5 %). After 5 min, $AlCl_3$ solution (0.6 mL, 10 %) was added. After another 5 min, NaOH solution (2 mL, 1 M) was added and volume was made up to the mark with 95 % ethanol. The solution was mixed thoroughly and the absorbance measured at 510 nm. The total flavonoid content was expressed as milligrams of rutin equivalent per 1 g (dry weight) of extract (mg RE g^{-1} dw). All tests were performed in triplicate.

Determination of the TP and TF content by HPLC analysis

Preparation of standard and sample solutions. The phenolics and flavonoid compounds in stems extracts of *P. hastata* were determined by HPLC, using a Waters 600 diode array detector (DAD) system equipped with a dualistic pump. The analyses were performed on a Diamonsil C_{18} column (4.6 mm×250 mm, 2.5 μm). Standard stock solutions of gallic acid and rutin were prepared in 95 % EtOH, at concentration of 0.5 mg mL^{-1}. All sample solutions of PE, EAE and BE (1 mg mL^{-1}) were filtered through a 0.45 μm membrane filter (F type, Millipore), and injected directly.

HPLC analysis of the phenolic compounds. The mobile phase consisted of solvent A (0.3 % acetic acid) and solvent B (acetonitrile). The gradient program was as follow: (0–5 min, 20 % B; 5–10 min, 90 % B; 10–15 min, 10 % B; 15–25 min, 20 % B); the flow rate was 1 mL min^{-1}; the volume injected 20 μL; the temperature 25 °C; UV detection wavelength 280 nm. All experimental data are expressed as mean ±*SD* values ($n = 3$).

HPLC analysis of the flavonoid compounds. The mobile phase consisted of the solvents of MeOH–water–acetic acid (40:57.5:2.5) at a flow rate of 1.0 mL min^{-1}. The column temperature was set at 25 °C. The injection volume was 20 μL. The UV detection wavelength was 254 nm. All experimental data are expressed as means ±*SD* values ($n = 3$).

DPPH radical scavenging assay

The scavenging effect of the different fractions on the DPPH radical was measured using a modified version of the method described by Shimada *et al.*[29] In brief, the extract solution (20 μL) in 95 % ethanol at different concentrations (0.2, 0.5, 0.8 and 1.2 mg mL^{-1}) was added to 8 mL of a 0.004 % (w/v) solution of DPPH in 95 % ethanol. The scavenging activities on DPPH radical were determined by measuring the absorbance at 515 nm every 10 min until the reaction reached the steady state. The DPPH radical scavenging activity ($S\%$) was calculated using the following formula: $S\% = ((A_{\text{control}}-A_{\text{sample}})/A_{\text{control}})\times100$, where A_{control} is the absorbance of the blank (containing all reagents except the extract solution) and A_{sample} is the absorbance of the test sample. The DPPH radical scavenging activity of BHT was also assayed for comparison. All tests were performed in triplicate.

ABTS radical scavenging assay

The antioxidant activities of various solvent extracts in the reaction with the stable ABTS^{+} radical cation were determined according to the method of Delgado-Andrade *et al.*[30] Briefly, ABTS^{+} was produced by reacting 7 mM ABTS stock solution with 2.45 mM potassium persulfate and the mixture was left to stand in the dark at room temperature for 12–16 h before use. The ABTS^{+} solution (stable for 2 days) was diluted with 5 mM phosphate-buffered saline (pH 7.4) to an absorbance at 730 nm of 0.70±0.02. After addition of 10 μL of sample to 4 mL of diluted ABTS^{+} solution, the absorbance was read after 30 min. As a positive control, the synthetic antioxidant BHT was used. All the samples were analyzed in triplicate. The ABTS^{+} radical-scavenging activity of the samples was expressed as $S\% = ((A_{\text{control}}-A_{\text{sample}})/A_{\text{control}})\times100$, where A_{control} is the absorbance of the blank control (ABTS^{+} solution without test sample) and A_{sample} is the absorbance of the test sample.

Hydroxyl radical scavenging assay

The hydroxyl radical scavenging activity was performed according to a modified method of Li *et al.*[5] The extract solution (2 mL, 0.2, 0.5, 0.8 and 1.2 mg mL^{-1}), *o*-phenanthroline solution (1.0 mL, 7.5 mmol L^{-1}), phosphate buffer (5 mL, 0.2 M, pH 6.6), ferrous sulfate solution (1.0 mL, 7.5 mmol L^{-1}) and H_2O_2 (1.0 mL, 0.1 %) were mixed and diluted to 25 mL with distilled water. After incubation at room temperature for 30 min, the absorbance was measured at 510 nm. BHT was used as a positive control. The scavenging percentage ($P\%$) was calculated as $P\% = ((A-A_1)/(A_2-A_1))\times100$, where A, A_1 and A_2 are the absorbance value of the system with all solutions including H_2O_2 and extract solution, the system without extract solution, and the system without H_2O_2 and extract solution, respectively. All tests were performed in triplicate.

Measurement of the reducing power

The reducing power of *P. hastata* was determined according to the method of Gulcin.[4] Fractions solutions (100 µL) in 95 % ethanol (0.2, 0.5, 0.8 and 1.2 mg mL^{-1}) were mixed with phosphate buffer (2.5 mL, 0.2 M, pH 7.4) and potassium ferricyanide [$K_3Fe(CN)_6$] (2.5 mL, 1 %). After incubation at 50 °C for 20 min, 2.5 mL of trichloroacetic acid (10 %, w/v) was added and the mixture centrifuged at 3000 rpm for 10 min. 2.5 mL of the upper layer of the above solution was mixed with 2.5 mL of distilled water and 0.5 mL of ferric chloride (0.1 %), and then the absorbance was measured at 700 nm. The higher is the absorbance value, the stronger is the reducing power. The reducing power of BHT was also assayed for comparison. All determinations were performed in triplicate.

Statistical analysis

All tests were conducted in triplicate. The results were expressed as means ±*SD*. Analysis of the variance and significant differences among the means were tested by one-way ANOVA, using SPSS (Version 13.0 for Windows, SPSS Inc., Chicago, IL). P values < 0.05 were regarded as significant.

RESULTS AND DISCUSSION

TP and TF contents determined by spectrophotometric procedures

The total phenolics content (*TP*) and the total flavonoid content (*TF*) of extracts were determined from regression equations for the calibration curves ($y = 0.0796x + 0.0091$, $R^2 = 0.9925$) and ($y = 0.8836x - 0.0255$, $R^2 = 0.9998$), respectively. The TP and TF content of the PE, EE, and BE are listed in Table I. The TP content, as determined by the Folin-Ciocalteu method, is reported as gallic acid equivalents, while the TF content is expressed as rutin equivalents. It is well known that phenolic and flavonoid compounds are potential antioxidants and free-radical scavengers; hence there should be a close correlation between the TP/TF content and the antioxidant activity. The TP/TF content of the three extracts was in the following order: EE > BE > PE.

TABLE I. TP content and TF content of different extracts from *P. hastata* determined by spectrophotometric procedures (results are the mean ± standard deviation of three parallel measurements)

Sample	*TP* / mg GAE g^{-1} dw	*TF* / mg RE g^{-1} dw
EE	70.2±0.28	180.6±0.40
BE	53.6±0.16	98.0±0.22
PE	49.4±0.20	51.2±0.19

TP and TF contents determined by HPLC analysis

Reverse phase-HPLC coupled with UV–Vis DAD was employed to separate, identify and quantify the phenolic compounds in the fractions of *P. hastata*. The concentrations were determined by calculating the HPLC peak areas, which are proportional to the amount of analyte in a peak, and are presented as the mean of three determinations, which were highly repeatable. The standard curves for gallic acid and rutin were $y = 3397.9 + 10474.7x$ ($R^2 = 0.990$) and $y = 4.89 + 16640.2x$ ($R^2 = 0.998$), respectively. The chromatogram of the reference standards gallic acid and rutin is shown in Fig. 1. These compounds were identified in the PE, EE, and BE according to their retention times and the spectral characteristics of their peaks compared to those of the standards. As shown in Table II, the extract with the highest TP amount was EE (83.01±0.56 mg GAE g^{-1} dw), followed by BE (62.92±0.52 mg GAE g^{-1} dw) and PE (36.83±0.78 mg GAE g^{-1} dw). The same trend was observed for the TF content. Of these three extracts, EE contained the higher TP content (83.01±0.56 mg GAE g^{-1} dw) and TF content (73.11±0.61 mg RE g^{-1} dw) than BE and PE, indicating that EE might have the most outstanding antioxidant activity of the various solvent extracts.

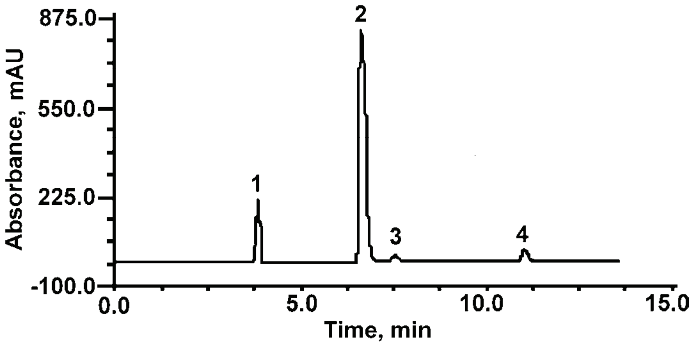

Fig. 1. HPLC chromatogram of the reference standards; 1) gallic acid, 2) rutin and 3) and 4) unknown residues.

TABLE II. TP content and TF content of different extracts from *P. hastata* determined by HPLC (results are the mean ± standard deviation of three parallel measurements; ND – not detected)

Sample	*TP* / mg GAE g^{-1} dw	*TF* / mg RE g^{-1} dw
EE	83.01±0.56	73.11±0.61
BE	62.92±0.52	55.79±0.46
PE	36.83±0.78	ND

DPPH radical scavenging activity

DPPH, a stable radical with a maximum absorption at 517 nm that can readily undergo scavenging by an antioxidant, has been widely employed to investigate the free-radical scavenging ability of various antioxidants because of its advantages of ease, economy and sensitivity to detect active compounds at low concentrations.[21,31]. The DPPH radical scavenging activity of the three extracts is shown in Fig. 2, compared with the synthetic antioxidant BHT. As can be seen, the scavenging effect of EE, BE, PE and BHT increased with increasing concentration. For EE, a sharp increase of its DPPH scavenging activity (43.2–84.2 %) was observed, as its concentration increased from 0.2 to 1.2 mg mL^{-1}. The IC_{50} values on the DPPH radical of BHT and the extracts of *P. hastata* are given in Table III. EE, PE and BE possessed significant scavenging activity on the DPPH radical. Moreover, EE exhibited the highest DPPH scavenging effect (IC_{50} = = 0.25 mg mL^{-1}), which is superior to that of BHT (IC_{50} = 0.45 mg mL^{-1}), indicating that the EE was a prominent scavenger of the DPPH radical.

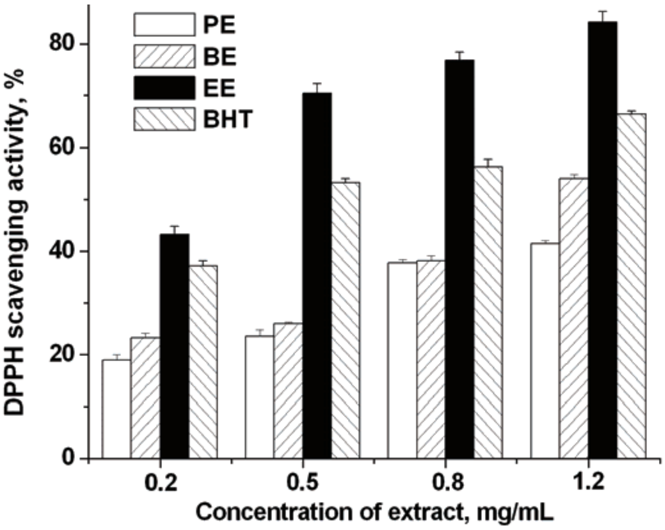

Fig. 2. DPPH radical scavenging activity of the various solvent extracts from *P. hastata*. The results are the mean±*SD* of three parallel measurements. The values are significantly different ($P < 0.05$).

TABLE III. IC_{50} values of different extracts from *P. hastata* and BHT

Extract	IC_{50} / mg mL^{-1}		
	DPPH	ABTS$^+$	•OH
BHT	0.45	0.38	0.59
EE	0.25	0.38	0.62
BE	1.35	0.54	1.64
PE	2.09	33.70	1.66

ABTS$^+$ radical scavenging activity

This method is based on the inhibition by antioxidants of the absorbance of the radical cation of ABTS, which has a characteristic long-wavelength absorption spectrum showing a maximum at 734 nm. The experiments, which can be used in both organic and aqueous solvent systems, are realized using a decolorization assay, which involves the generation of the ABTS$^+$ chromophore by the oxidation of $ABTS^+$ with potassium persulfate.[12] The $ABTS^+$ scavenging capacities of EE, BE, PE and BHT were measured and are compared in Fig. 3, and their IC_{50} values on $ABTS^+$ are presented in Table III.

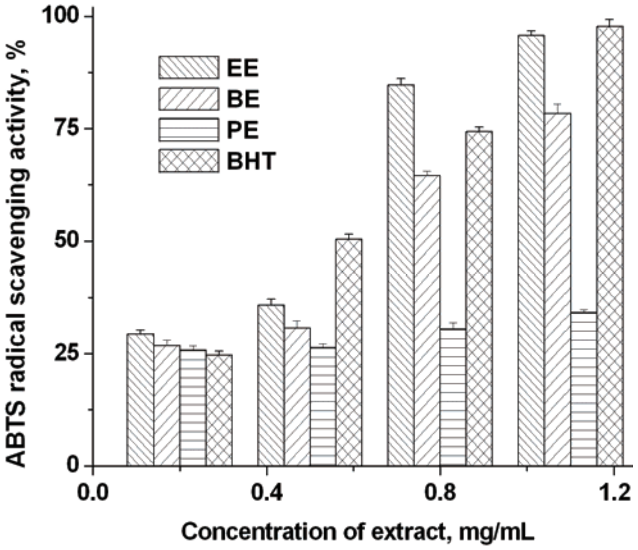

Fig. 3. $ABTS^+$ scavenging activity of the various solvent extracts from *P. hastata.* The results are the mean±*SD* of three parallel measurements. The values are significantly different ($P < 0.05$)

The $ABTS^+$ scavenging activities of all extracts and BHT increased in a concentration dependent manner. The IC_{50} values decreased in the following order: PE (33.70 mg mL^{-1}) < BE (0.54 mg mL^{-1}) < EE/BHT (0.38 mg mL^{-1}). Of the three extracts, EE exhibited the most effective scavenging ability, which was the same as that of BHT, while the lowest one was found to be the PE. The order of scavenging activities on the ABTS radical of the three extracts was similar to those on DPPH. The differences of the $ABTS^+$ scavenging activities of EE, BE and PE indicated that the extraction media significantly influenced the antioxidant abilities of the extracts.

Hydroxyl radical scavenging activity

Hydroxyl radicals, which could be formed from the superoxide anion and hydrogen peroxide, are the most reactive and predominant radicals generated endogenously during aerobic metabolism among the reactive oxygen species (ROS). The Fenton reaction is the most important mechanism for hydroxyl radical formation *in vitro*, in which a transition metal is involved as a pro-oxidant in the catalyzed decomposition of superoxide and hydrogen peroxide.[7]

In present study, the scavenging activity on hydroxyl radicals of EE, BE and PE was investigated (Fig. 4), using ferrous sulfate as the pro-oxidant. BHT was used as a positive control. The IC_{50} values of BHT and extracts of *P. hastata* on hydroxyl radicals are presented in Table III. The three extracts and BHT exhibited strong concentration-dependent scavenging activities on the hydroxyl radical. In the extracts from *P. hastata*, EE was found to be the most powerful scavenger of hydroxyl radicals, with an IC_{50} value of 0.62 mg mL^{-1}, which was similar to that of BHT (IC_{50} = 0.59 mg mL^{-1}). It is worth mentioning that EE showed an inhibition of 10.4 % at a concentration as low as 0.2 mg mL^{-1}. The scavenging activities of the three extracts were in the order: EE > BE > PE.

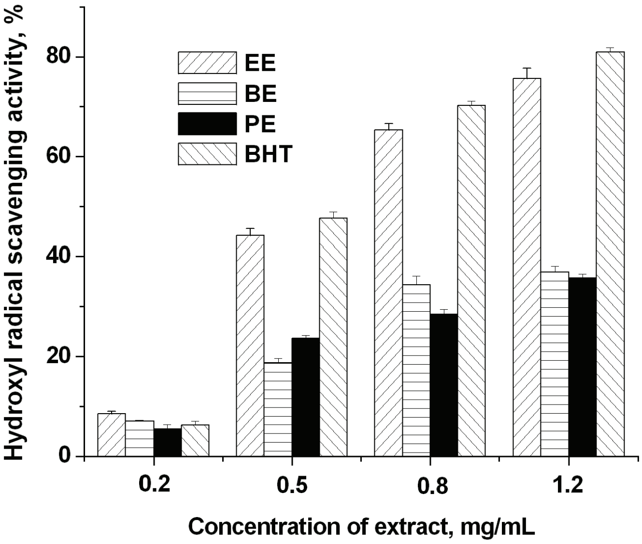

Fig. 4. Hydroxyl radical scavenging activity of the various solvent extracts from *P. hastata*. The results are the mean±*SD* of three parallel measurements. The values are significantly different ($P < 0.05$).

Reducing power

The reducing capacity of a compound, which depends on the presence of reductants that exhibit antioxidant potential by breaking the radical chain and donating a hydrogen atom, may serve as a significant indicator of its potential antioxidant activity.[32] The reducing capability of the extract samples was monitored by measuring the formation of Perls' Prussian blue, absorption at 700 nm, due to the transformation of Fe^{3+}/ferricyanide complex to Fe^{2+}/ferrous form in the presence of reductants in the extracts. Increased absorbance of the reaction mixture indicates increased reducing power.[33]

The reducing power of various solvent extracts from *P. hastata* is shown in Fig. 5. EE, BE and PE exhibited different degrees of electron donating capacities in a concentration-dependent manner, whereby EE was the most outstanding at various concentrations. The reducing capacities at 700 nm for EE, BE, PE and BHT were 0.98, 0.63, 0.52 and 1.02, respectively. Therefore, the reducing power order was: BHT >EE > BE > PE. The absorbance of EE was similar to that of BHT, indicating that EE possessed a comparative reducing power compared to BHT. The trend in the reducing power of the various solvent extracts from *P. hastata* was similar to those of their DPPH, ABTS, hydroxyl radical scavenging activities and the content of TP/TF, indicating that there is a correlation between the TP/TF content and the antioxidant activities of the various solvent extracts from *P. hastata.*

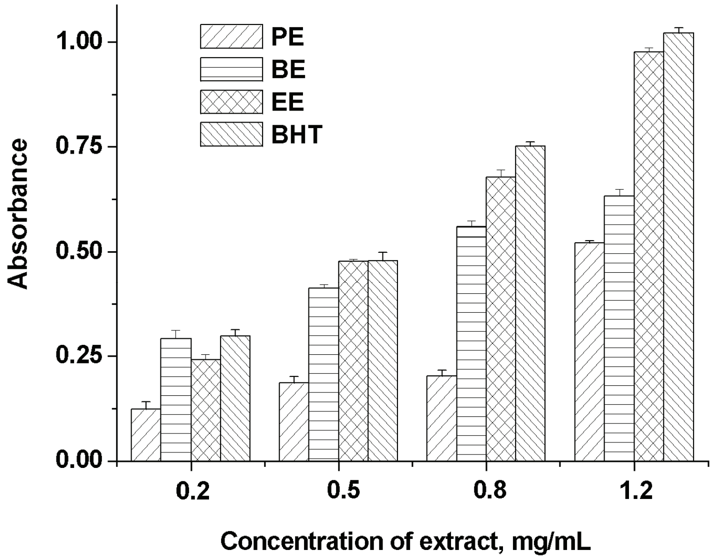

Fig. 5. Reducing power of the various solvent extracts from *P. hastata*. The results are the mean±*SD* of three parallel measurements. The values are significantly different ($P < 0.05$).

CONCLUSIONS

In the present investigation, extracts of *P. hastata* exhibited outstanding scavenging effects on DPPH, ABTS and hydroxyl radical, and possessed a strong reducing power. EE, which had the highest total phenolic (TP) and total flavonoid (TF) contents, was shown to be the most efficient extract and was superior to butylated hydroxytoluene. The TP/TF content of the different extracts and their antioxidant activities in all the tested systems followed the same order: EE > > BE > PE, showing there was a significant correlation between antioxidant activities and TP/TF content. The results indicated that EE, BE and PE possessed sufficient phenolic compounds and exhibited excellent antioxidant activities. Based on the above results, various solvent extracts of *P. hastata*, especially EE extract, were found to be excellent scavengers of free radical and possess remarkable antioxidant ability. The results showed that these extracts could be a promising source of natural antioxidants in the food industry and may be useful for reducing the risks of chronic diseases and preventing diseases progression.

Acknowledgements. The authors thank the National Natural Science Foundation of China (Grant No. 20961001), the Key Project of the Chinese Ministry of Education (Grant No. 2010168), the Guangxi Natural Science Foundation (Grant No. 2010GXNSFB013014), the Scientific Research Fund of the Guangxi Provincial Education Department (Grant No. 200911MS146) and Guangxi Teachers Education University for financial support.

ИЗВОД

ФЕНОЛНИ САДРЖАЈ И АНТИОКСИДАТИВНА АКТИВНОСТ БИЉКЕ *Phymatopteris hastata*

WEI SU[1], PEIYUAN LI[2], LINI HUO[2], CAIYING WU[1], NANA GUO[1] и LIANGQUAN LIU[1]

[1]*College of Chemistry and Life Science, Guangxi Teachers Education University, Nanning* и [2]*College of Pharmacy, Guangxi traditional Chinese Medical University, Nanning, China*

Испитивана је антиоксидативна активност екстраката традиционалне лековите кинеске биљке *Phymatopteris hastata*. Четири методе су коришћене за одређивање антирадикалског и антиоксидативног ефекта: са 2,2-дифенил-1-пикрилхидразидом (DPPH), са 2,2'-азинобис(3--етилбензотиазолин)-6-сулфонском киселином (ABTS), тест за хватање слободних хидроксилних радикала и тест за одређивање редукујуће способности. Резултати су поређени са ефектима бутилованог хидрокситолуена (BHT), синтетичког антиоксиданта. Показано је да етилацетатни екстракт има изузетну антиоксидативну активност, сличну или већу него BHT. Укупни садржај фенола (TP) и флавоноида (TF) је измерен и изражен као еквивалент галне киселине, односно рутина. Антиоксидативна активност и TP/TF садржај различитих екстраката су били у следећем низу: етилацетатни > бутилалкохолни > петролетарски екстракт, указујући на добру корелацију између антиоксидативне активности и садржаја TP/TF. Сви екстракти, а посебно етилацетатни, су богати фенолима и флавоноидима и могу се сматрати природним антиоксидантима.

(Примљено 11. новембра 2010, ревидирано 11. јануара 2011)

REFERENCES

1. C. L. Cespedes, M. El-Hafidi, N. Pavon, J. Alarcon, *Food Chem.* **107** (2008) 820
2. M. Al-Duais, L. Muller, V. Bohm, G. Jetschke, *Eur. Food Res. Technol.* **228** (2009) 813
3. K. S. Kumar, K. Ganesan, P. V. Subba Rao, *Food Chem.* **107** (2008) 289
4. I. Gulcin, R. Elias, A. Gepdiremen, K. Taoubi, E. Koksal, *Wood Sci. Technol.* **43** (2009) 195
5. Y. Li, C. Li, K. Gu, L Ou, J. Yin, *J. Yunnan Univ.* **24** (2002) 302
6. J. Wang, X. Yuan, B. Sun, Y. Tian, Y. Cao, *Food Technol. Biotechnol.* **47** (2009) 39
7. Y. Pan, K. Wang, S. Huang, H. Wang, X. Mu, C. He, X. Ji, J. Zhang, F. Huang, *Food Chem.* **106** (2008), 1264
8. R. P. Pereira, R. Fachinetto, A. S. Prestes, R. L. Puntel, G. N. da Silva, B. M. Heinzmann, T. K. Boschetti, M. L. Athayde, M. E. Burger, A. F. More, V. M. Morsch, J. B. T. Rocha, *Neurochem. Res.* **34** (2009) 973

9. F. Yu, J. Sheng, J. Xu, X. An, Q. Hu, *Eur. Food Res. Technol.* **225** (2007) 843
10. A. T. Hukkanen, S. S. Polonen, S. O. Karenlampi, H. I. Kokko, *J. Agric. Food Chem.* **54** (2006) 112
11. M. Ozgen, R. N. Reese, A. Z. J. Tulio, J. C. Scheerens, A. R. Miller, *J. Agric. Food Chem.* **54** (2006) 1151
12. S. S. Ali, N. Kasoju, A. Luthra, A. Singh, H. Sharanabasava, A. Sahu, U. Bora, *Food Res. Int.* **41** (2008) 1
13. M. Contini, S. Baccelloni, R. Massantini, G. Anelli, *Food Chem.* **110** (2008) 659
14. M. Locatelli, F. Travaglia, J. D. Coïsson, A. Martelli, C. Stévigny, M. Arlorio, *Food Chem.* **119** (2010) 1647
15. T. M. Đordevic, S. S. Šiler-Marinkovic, S. I. Dimitrijevic-Brankovic, *Food Chem.* **119** (2010) 957
16. J. Han, X. Weng, K. Bi, *Food Chem.* **106** (2008) 2
17. J. A. Rufián-Henares, F. J. Morales, *J. Agric. Food Chem.* **55** (2007) 10016
18. J. Zivkovic, Z. Zekovic, I. Mujic, V. Tumbas, D. Cvetkovic, I. Spasojevic, *Food Technol. Biotechnol.* **47** (2009) 421
19. F. Ferreres, C. Sousa, V. Vrchovská, P. Valentão, J. A. Pereira, R. M. Seabra, P. B. Andrade, *Eur. Food Res. Technol.* **222** (2006) 8898
20. N. Gámez-Meza, J. A. Noriega-Rodríguez, L. Leyva-Carrillo, J. Ortega-García, L. Bringas-Alvarado, H. S. García, L. A. Medina-Juárez, *J. Food Process. Pres.* **33** (2009) 110
21. V. Lagouri, A. Bantouna, P. Stathopoulosa, *J. Food Process. Pres.* **34** (2010) 87
22. H. Ayar-Kayali, R. Ozturk Urek, M. Nakiboglu, L. Tarhan, *J. Food Process. Pres.* **33** (2009) 285
23. J. Perez-Jimenez, S. Arranz, M. Tabernero, M. E. Diaz-Rubio, J. Serrano, I. Goni, F. Saura-Calixto, *Food Res. Int.* **41** (2008) 274
24. L. G. L. Ranilla, M. I. S. Genovese, F. M. Lajolo, *J. Agric. Food Chem.* **55** (2007) 90
25. C. Li, H. Du, L. Wang, Q. Shu, Y. Zheng, Y. Xu, J. Zhang, J. Zhang, R. Yang, Y. Ge, *J. Agric. Food Chem.* **57** (2009) 8496
26. N. Erkan, G. Ayranci, E. Ayranci, *Food Chem.* **110** (2008) 76
27. K. Slinkard, V. L. Singleton, *Am. J. Enol. Vitic.* **28** (1977) 49
28. V. Dewanto, X. Wu, K. K. Adom, R H. Liu, *J. Agric. Food Chem.* **50** (2002) 3010
29. K. Shimada, K. Fujikawa, K. Yahara, T. Nakamura. *J. Agric. Food Chem.* **40** (1992) 945
30. C. Delgado-Andrade, J. A. Rufián-Henares, F. J. Morales, *J. Agric. Food Chem.* **53** (2005) 7832
31. M. Suhaj, *J. Food Compos. Anal.* **19** (2006) 531
32. Y. Li, Y. Du, C. Zou, *Eur. Food Res. Technol.* **228** (2009) 1023
33. M. Senevirathne, S. Kim, N. Siriwardhana, J. Ha, K. Lee, Y. Jeon, *Food Sci. Technol. Int.* **12** (2006) 27.

Journal of the Serbian Chemical Society
JSCS-info@shd.org.rs • www.shd.org.rs/JSCS

J. Serb. Chem. Soc. 76 (11) 1497–1504 (2011)
JSCS–4223

UDC 66.017:547.831'269.3:
544.553.537.004.12
Original scientific paper

The synthesis, structure and photoluminescence property of a novel 3D supramolecular compound based on mixed ligands of 8-hydroxyquinoline-5-sulfonate and ethylenediamine

YING WANG[1,2], CHANGFU ZHUANG[1]*, CHUNHUA WU[1], JIAYAN ZHANG[1], LI WANG[2], MINGHONG XIN[2], GUANGSHAN ZHU[2] and JIANING XU[2]

[1]*Southwest Forestry University, Kunming, 650224, and* [2]*State Key Laboratory of Inorganic Synthesis and Preparation, Jilin University, Changchun, 130012, P. R. China*

(Received 29 January, revised 29 September 2011)

Abstract: A new organic–inorganic hybrid coordination compound ZnQS(en)·$2H_2O$ (**1**) in which two different organic ligands, ethylenediamine (en) and 8-hydroxyquinoline-5-sulfonic acid (H_2QS) coordinate with zinc ions, has been synthesized *via* the evaporation method and characterized by single crystal X-ray diffraction analysis, IR spectroscopy and thermogravimetric analysis (TGA). The structure solution showed that compound **1** displays a three-dimensional supramolecular network by synergic linkage of hydrogen and coordinated bonds. Moreover, compound **1** exhibits intense photoluminescence at 513 nm excited at 396 nm in the solid state at room temperature.

Keywords: organic–inorganic hybrid material; 8-hydroxyquinoline-5-sulfonic acid; photoluminescence property.

INTRODUCTION

Due to the potential applications of organic–inorganic hybrid materials in catalysis, gas storage, molecular recognition, optics and magnetic fields,[1–10] the design and synthesis of organic–inorganic hybrid materials have been attracting tremendous attention. To date, much research has focused on constructing organic–inorganic hybrid materials by choosing versatile organic ligands. As functional organic ligands, 8-hydroxyquinoline and its substituted derivatives are attracting more and more attention from synthesis chemists because of their fantastic coordination properties and special photoelectric properties. Many organic–inorganic hybrid materials based on the derivatives of 8-hydroxyquinoline (q) have been synthesized,[11–14] and most of them exhibit amazing optical properties, enabling their application as organic light-emitting devices (OLEDs).[15–17] As organic

---

* Corresponding author. E-mail: cfzhuang_2008@yahoo.com.cn

doi: 10.2298/JSC110129127W

ligand, 8-hydroxyquinoline-5-sulfonate still remains largely unexplored, since sulfonate group is considered as poor ligand and bonds hardly to many metal cations. It is noted that there are only a few articles reporting about organic–inorganic hybrid materials containing the 8-hydroxyquinoline-5-sulfonate group.[18–20] Here, 8-hydroxyquinoline-5-sulfonic acid (H_2QS) and ethylenediamine (en) were employed as reactants to obtain a novel zinc–organic hybrid $ZnQS(en)·2H_2O$ (**1**) by the evaporation method. Interestingly, compound **1** displays a 3D supramolecular structure, which is built from π···π stacking interactions of binuclear complexes and hydrogen bonds interactions of the chelating ethylenediamine, mediated uncoordinated water molecules and QS. Herein, the synthesis, structure and photoluminescence property of compound **1** are reported.

EXPERIMENTAL

All chemicals of reagent quality were obtained from commercial sources and used without further purification. The elemental analysis was performed on a Perkin–Elmer 2400 elemental analyzer. The IR spectra were obtained from KBr pellets in the range of 400–4000 cm^{-1} on a Nicolet Impact 410 FTIR spectrometer. Thermogravimetric analyses (TGA) were performed on a Perkin–Elmer TGA 7 thermogravimetric analyzer at a heating rate of 10 °C min^{-1} in air up to 800 °C. Fluorescence spectra were recorded on a LS 55 fluorescence/phosphorescence spectrophotometer at room temperature.

*Synthesis of $ZnQS(en)·2H_2O$ (**1**)*

A mixture of $Zn(NO_3)_2·6H_2O$ (148 mg, 0.5 mmol) and H_2QS (24 mg, 0.1 mmol) was dissolved in *N*,*N*-dimethylformamide (DMF) (10 mL) at room temperature, and then about 0.1 mL ethylenediamine was added to this mixture under stirring. After the mixture became clear, the beaker was left undisturbed at room temperature for 24 h to give yellow crystals in a yield of 43 % (based on S).

Determination of the single-crystal structure

The intensity data was collected on a Smart CCD diffractometer with graphite-monochromated MoKα (λ = 0.71073 Å) radiation at room temperature in the ω–2θ scan mode. An empirical absorption correction was applied to the data using the SADABS program.[21] The structure was solved by direct methods. All non-hydrogen atoms were refined anisotropically. The hydrogen atoms of the organic ligand were fixed at calculated positions and refined using a riding mode. The hydrogen atoms of the H_2O were located in the difference Fourier map. All calculations were performed using the SHELXTL program.[22]

RESULTS AND DISCUSSION

Description of the structure

The crystallographic data are summarized in Table I, and selected bond lengths and bond angles of compound **1** are listed in Table II.

The zinc atom is five-coordinated in a square-pyramidal coordination environment, coordinating to two oxygen atoms (O1 and O2) and three nitrogen atoms (N1, N2 and N3). O1 and N3 are from the hydroxyl group and the quinoline ring of one ligand, respectively; O2 is from the sulfonate group of the other QS ligand. N1 and N2 are from the same ethylenediamine molecule, *i.e.*, the ethylenediamine molecule as a bidentate chelate ligand is coordinated to the zinc atom. The O2 is in apical position with *d*(Zn–O2) = 2.280(4) Å and the other four coordinated atoms are in bottom positions of the square-pyramid with *d*(Zn––O1) = 2.062(4) Å, *d*(Zn–N1) = 2.102(5) Å, *d*(Zn–N2) = 2.087(5) Å and *d*(Zn––N3) = 2.072(5) Å. The distance of Zn–O2 is significantly longer than that of Zn–O1, but they are in normal range reported for zinc compounds.[23] The Zn–N distances range from 2.072(5) to 2.101(5) Å. These distances are comparable to those reported for other zinc compounds.[24]

TABLE I. Crystal data and structure refinement for compound **1**

Molecular formula	$C_{11}H_{17}N_3O_6SZn$
Formula weight	384.71
T / K	293(2)
λ / Å	0.71073
Crystal system	Monoclinic
Space group	P2(1)/c
a / Å	7.0737(14)
b / Å	19.296(4)
c / Å	10.680(2)
β / °	100.599(4)
V / Å^3	1432.8(5)
Z	4
D_{calc} / kg m^{-3}	1783
μ / mm^{-1}	1.894
F(000)	792
Reflections collected	7434
Independent reflection (R_{int})	2521 (0.2316)
$R_1(I > 2\sigma(I))$	0.0715
wR_2	0.1629

TABLE II. Selected bond lengths and angles for compound **1**

Bond	Distance, Å
Zn(1)–O(1)	2.062(4)
Zn(1)–O(2)	2.280(4)
Zn(1)–N(3)	2.072(5)
Zn(1)–N(1)	2.101(5)
Zn(1)–N(2)	2.087(5)

Bonds	Angle, °	Bonds	Angle, °
O(1)–Zn(1)–N(3)	80.25(16)	N(1)–Zn(1)–O(2)	88.21(17)
O(1)–Zn(1)–N(2)	95.96(17)	N(2)–Zn(1)–O(2)	95.04(18)
O(1)–Zn(1)–N(1)	174.80(18)	N(2)–Zn(1)–N(1)	84.20(18)
O(1)–Zn(1)–O(2)	86.59(15)	N(3)–Zn(1)–N(1)	100.43(18)
N(3)–Zn(1)–N(2)	170.06(19)	N(3)–Zn(1)–O(2)	93.90(16)

Two crystallographically equivalent Zn atoms link to each other through the O2 and its symmetry equivalent at –*x*, 1–*y*, 2–*z* to form a binuclear zinc secondary building unit, as shown in Fig. 1. Weak π···π stacking interactions exist between the two quinoline rings and the contact distance is 3.622 Å. These binuclear zinc secondary building units form a 3D supramolecular network due to the π···π stacking interactions and the complicated hydrogen bonds existing between uncoordinated H_2O molecules and ethylenediamine molecules as well as the QS ligands. There are strong hydrogen bonds between O1w and O1, O2, O4, N2, O2w, respectively. The distances of the hydrogen bonds are O1W–H2W···O1, 2.718 Å, O1W–H1W···O2, 3.240 Å, O1W–H1W···O4, 2.955 Å, N2–H2B···O1W, 3.079 Å and O2W–H3W···O1W, 2.835 Å. Simultaneously, the hydrogen bonds between O2w and O3, N1 are also strong. The distances of the hydrogen bonds are O2W–H4W···O3, 2.844 Å, N1–H1C···O2w, 2.995 Å. Hydrogen bonds also exist between N1 and O3, N2 and O1. Moreover, there are weak hydrogen bonds between S and O1w, O2w, N1. The hydrogen-bond interactions are listed in Table III. The stacking networks based on the hydrogen bonds are shown in Fig. 2.

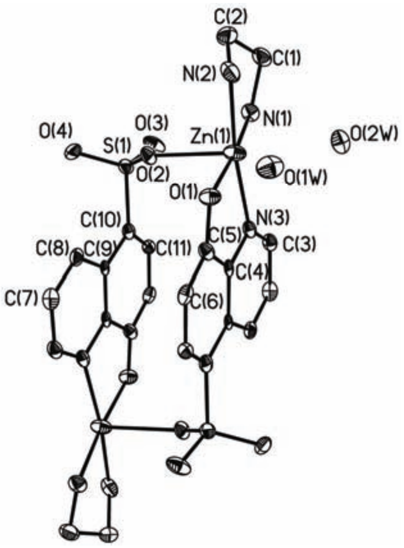

Fig. 1. The binuclear Zn unit of compound **1** showing the atom-labeling scheme (30 % thermal ellipsoids).

Although both compound **1** and the reported compound [Cu(L4)$_2$](H$_2$biim--4)·8H$_2$O[19] are three-dimension supramolecular compounds with two different organic compounds and are both based on the 8-hydroxyquinoline-5-sulfonate organic ligand, there are obvious differences between them. In the latter compound, only the nitrogen atom and hydroxyl oxygen atom of the 8-hydroxyquinoline-5-sulfonate organic ligand coordinate to Cu(II) and none of the oxygen atoms of the sulfonate group, whereas in compound **1**, one oxygen atom of the sulfonate group coordinates to the metal center. Moreover, in compound **1**, besides the 8-hydroxyquinoline-5-sulfonate ligand, ethylenediamine adopts a bidentate chelating mode to coordinate to Zn(II), while in reported $[Cu(L4)_2](H_2biim-4)\cdot 8H_2O$, only 8-hydroxyquinoline-5-sulfonate coordinates to Cu(II). In compound **1**, two crystallographically equivalent Zn(II) link to each other through two bridging oxygen atoms to form a binuclear zinc secondary building unit, and these secondary building units form a 3D supramolecular network due to π···π stacking interactions and hydrogen bonds.

TABLE III. Hydrogen bond lengths and angles in compound **1**

D–H	D···H / Å	H···A / Å	D–H···A / °	D···A / Å	A
N1–H1C	0.900	2.112	166.89	2.995	O2W
N1–H1D	0.900	2.181	154.38	3.018	O3
N1–H1D	0.900	2.963	128.06	3.588	S1
N2–H1	0.899	2.414	148.35	3.214	O1[a]
N2–H2	0.900	2.213	161.32	3.079	O1W[a]
O1W–H1W	0.874	2.352	126.38	2.955	O4[a]
O1W–H1W	0.874	2.395	162.70	3.240	O2[a]
O1W–H1W	0.874	2.799	146.55	3.561	S1[a]
O1W–H2W	0.857	1.863	175.36	2.718	O1
O2W–H3W	0.853	1.990	170.44	2.835	O1W[b]
O2W–H4W	0.856	2.046	154.76	2.844	O3[c]
O2W–H4W	0.856	3.011	130.39	3.626	S1[c]

[a]–*x*, –*y*+1, –*z*+1; [b]–*x*–1, *y*–1/2, –*z*–3/2; [c]*x*–1, *y*, *z*

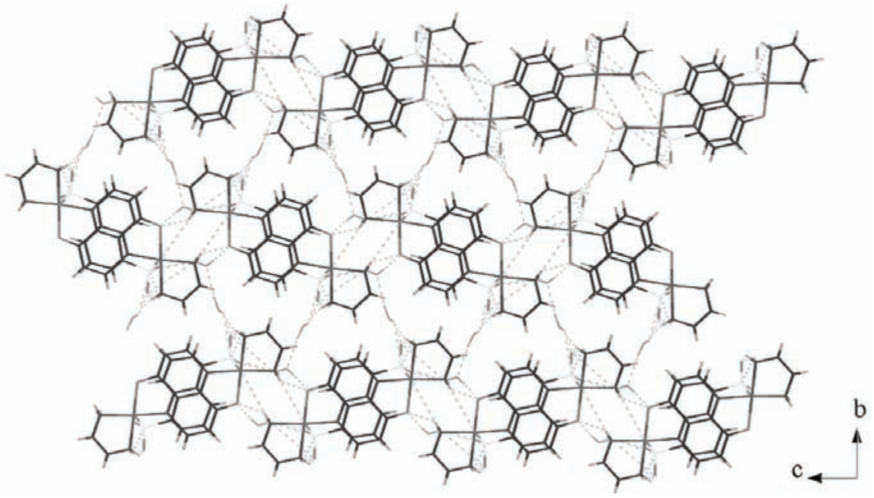

Fig. 2. Stacking hydrogen-bonded network viewed down the *bc* plane.

Characterization

Anal. Calcd. for $ZnO_6SN_3C_{11}H_{17}$: C, 34.31; H, 4.42; N, 10.92%. Found: C, 35.02; H, 4.23; N, 10.85%.

In the IR spectrum, bands in the 1643–1394 cm^{-1} region can be assigned to the vibrations of C=C and C=N of the quinoline ring. The bands in the 1611––1391 cm^{-1} region are characteristic bands of the benzene ring and the bands in the 1354–1199 cm^{-1} region are assigned to the Ar–O. Broad bands due to ν(N–H) are observed in the 3200–3500 cm^{-1} region, while the bending modes for the amine are observed in the range 1300–1650 cm^{-1}. The bands in the 1030–1250 cm^{-1} region are due to the vibration of S–O.[25,26] The absorption bands at around 3303 cm^{-1} are due to the stretching of the hydroxyl groups (from the water molecules), which experience a shift to lower frequency compared with the O–H stretch in free water at 3600 cm^{-1}. This may be due to the formation of hydrogen bonds between the water and the ligands, as well as between the water molecules. In the low-frequency region, the bands are attributed to the lattice vibration of Zn–O and Zn–O–Zn.

To understand the thermal stability of compound **1**, thermogravimetric analysis was performed. There were two separate mass loss steps. The first mass loss of 8.9 % occurred between 50–150 °C, which corresponds to the loss of free H_2O molecules (calcd. 9.4 %) of crystallization. The second mass loss occurred between 300–640 °C, corresponding to the loss of the organic components, and shows that compound **1** may be stable up to 300 °C. The residual mass of about 24.0 % corresponds to ZnO (calcd. 23.3 %).

Photoluminescence

The fluorescence spectrum of compound **1**, measured in the solid state at room temperature, is shown in Fig. 3. The compound was excited at a wavelength of 396 nm. The emission peak at 513 nm is attributed to electron π*–π transitions of the intraligand.[20] The emission peak of compound **1** was blue shifted by ≈ 30 nm compared to that of Znq_2 (542 nm).[26] This blue-shift is connected to the elec-

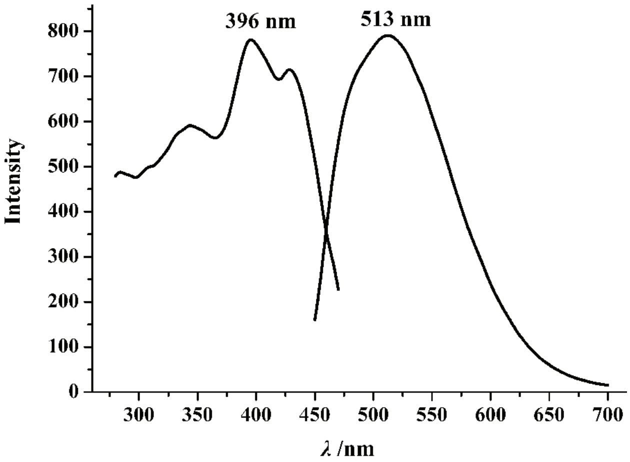

Fig. 3. Fluorescence spectra of compound **1**, excited at 396 nm; emission peak at 513 nm.

tron-withdrawing sulfonate group of the quinoline ring. The sulfonate group in the 5-position of the quinoline ring increases the energy gap between the highest occupied molecular orbital (HOMO) and the lowest unoccupied molecular orbital (LUMO).[27–29] This good fluorescence will have the significant usage property in the OLED devices.

CONCLUSIONS

In summary, a novel organic–inorganic hybrid material ZnQS(en)·$2H_2O$ based on 8-hydroxyquionline-5-sulfonate and ethylenediamine mixed ligands was successfully synthesized and characterized. The compound, synthesized using the solvent evaporation method, displayed a three-dimensional supramolecular network based on multi-type hydrogen bond interactions and $\pi \ldots \pi$ stacking interactions. It is very interesting that this compound exhibited a ≈30 nm blue-shift in its emission band compared to that of Znq_2. This good photoluminescence property has potential significance for its employment in electroluminescent and photoluminescent devices. Further synthesis and characterization studies of other metals with 8-hydroxyquionline-5-sulfonate ligand are in progress.

Supplementary information. Crystallographic data (excluding structure factors) for the structure reported in this paper has been deposited with the Cambridge Crystallographic Data Centre as supplementary publication No. CCDC608873. Copy of the data can be obtained free of charge on application to CCDC, 12 Union Road, Cambridge CB2 1EZ, UK (fax: +44 1223 336 033; e-mail: deposit@ccdc.cam.ac.uk).

Acknowledgements. This work was supported by the Key Foundation of Southwest Forestry University (Grant No.111030), the National Natural Science Foundation of China (Grant No. 31060099) and the Key Program of the Ministry of Education of China (Grant No. 2010Z040).

ИЗВОД

СИНТЕЗА, СТРУКТУРА И ФОТОЛУМИНСЦЕНТНА КАРАКТЕРИСТИКА НОВОГ 3Д СУПРАМОЛЕКУЛАРНОГ ЈЕДИЊЕЊА ДОБИЈЕНОГ ИЗ СМЕШЕ 8-ХИДРОКСИ-ХИНОЛИН-5-СУЛФОНАТА И ЕТИЛЕНДИАМИНА КАО ЛИГАНАДА

YING WANG[1,2], CHANGFU ZHUANG[1], CHUNHUA WU[1], JIAYAN ZHANG[1], LI WANG[2], MINGHONG XIN[2], GUANGSHAN ZHU[2] И JIANING XU[2]

[1]*Southwest Forestry University, Kunming, 650224 и* [2]*State Key Lab of Inorganic Synthesis and Preparation, Jilin University, Changchun, 130012, P. R. China*

Применом технике испаравања синтетизовано је ново органско-неорганско хибридно координационо једињење ZnQS(en)·$2H_2O$ (**1**) у којем су два различита органска лиганда, етилендиамин (en) и 8-хидрокси-хинолин-5-сулфонска киселина (H_2QS), координовани за јон цинка. За карактеризацију овог једињења употребљена је метода дифракције X-зрака са монокристала, као и IR и термогравиметријска анализа (TGA). Испитивање структуре **1** у раствору показује да ово једињење поседује тродимензионалну супрамолекулску синергијску мрежу интеракција водоничних и координационих веза. Истовремено, једињење **1** показује интензивну луминисценцију на 513 nm, ексцитовану на 396 nm у чврстом стању на соб-

ној температури. Кристалографски подаци за једињење **1** су: моноклинична просторна група $P2_1/c$, a = 7,0737(14) Å, b = 19,296(4) Å, c = 10,680(2) Å, β = 100,599(4)°, V = 1432,8(5) Å^3, Z = 4, M_r = 384,71, D_{calc} = 1,783 g·cm^{-3}, MoKα, R_1 = 0,0715, wR_2 = 0,1629, GOF = 1,038.

(Примљено 29. јануара, ревидирано 29. септембра 2011)

REFERENCES

1. K. S. Min, M. P. Suh, *J. Am. Chem. Soc.* **122** (2000) 6834
2. H. Li, M. Eddaoudi, M. O'Keeffe, O. M. Yaghi, *Nature* **402** (1999) 276
3. W. T. Chen, X. N. Fang, Q. Y. Luo, Y. P. Xu, *J. Serb. Chem. Soc.***74** (2009) 755
4. A. P. Mishra, R. K. Mishra, S. P. Shrivastava, *J. Serb. Chem. Soc.***74** (2009) 523
5. B. Moulton, M. J. Zaworotko, *Chem. Rev.* **101** (2001) 1629
6. O. M. Yaghi, H. Li, *J. Am. Chem. Soc.* **118** (1996) 295
7. J. S. Seo, D. M. Whang, H. Y. Lee, S. I. Jun, J. H. Oh, Y. J. Jeon, K. M. Kim, *Nature* **404** (2000) 982
8. T. Sawaki, Y. Aoyama, *J. Am. Chem. Soc.* **121** (1999) 4793
9. S. R. Batten, R. Robson, *Angew. Chem. Int. Ed.* **37** (1998) 1460
10. P. J. Hagrman, D. Hagrman, J. Zubieta, *Angew. Chem. Int. Ed.* **38** (1999) 2638
11. J. Xie, L. Fan, J. Su, H. Tian, *Dyes Pigm.* **59** (2003) 153
12. M. Ghedini, M. L. Deda, I. Aiello, A. Grisolia, *Synth. Met.* **138** (2003) 189
13. M. Ghedini, M. L. Deda, I. Aiello, A. Grisolia, *J. Chem. Soc., Dalton Trans.* (2002) 3406
14. C. Bae, S. Lee, S. Choi, G. Kwag, *Inorg. Chem.* **44** (2005) 7911
15. P. Mark, W. Helfrich, *J. Appl. Phys.* **33** (1962) 205
16. M. Pope, H. P. Kallmann, P. J. Magnante, *J. Chem. Phys.* **38** (1963) 2042
17. W. Helfrich, W. G. Schneidere, *Phys. Rev. Lett.* **14** (1965) 229
18. H. Y. Rao, J. Tao, S. W. Ng, *Acta Cryst.* **E59** (2003) 859
19. W. L. Zhang, Y. Y. Liu, J. F. Ma, H. Jiang, J. Yang, G. J. Ping, *Cryst. Growth Des.* **8** (2008) 1250
20. Y. Wang, M. Xue, J. N. Xu, G. S. Zhu, S. L. Qiu, *Sci. China, Ser. B Chem.* **52** (2009) 1602
21. G. M. Sheldrick, *SADABS*, *Program for Empirical Absorption Correction for Area Detector Data*, University of Göttingen, Göttingen, Germany, 1996
22. G. M. Sheldrick, *SHELXTL*, *v. 5 Reference Manual*, Siemens Analytical X-Ray Systems, Madison, WI, USA, 1997
23. W. T. A. Harrison, Z. Bircsak, L. Hannooman, *J. Solid State Chem.* **134** (1997) 148
24. Y. R. Xie, R. G. Xiong, X. Xue, X. T. Chen, Z. l. Xue, X. Z. You, *Inorg. Chem.* **41** (2002) 3323
25. J. Selbin, L. H. Holmes, S. P. J. McGlynn, *Inorg. Nucl. Chem.* **25** (1963) 1359
26. K. Nakamoto, *Infrared and Raman Spectra of Inorganic and Coordination Compounds*, Wiley, New York, 1978
27. T. A. Hopkins, K. Meerholz, S. Shaheen, M. L. Anderson, A. Schmidt, B. Kippelen, A. B. Padias, H. K. Hall Jr., N. Peyghambarian, N. R. Armstrong, *Chem. Mater.* **8** (1996) 344, and references therein
28. T. A. Albright, J. K. Burdett, M. H. Whangbo, *Orbital Interactions in Chemistry*, Wiley, New York, 1985
29. C. A. Coulson, A. Streitwieser Jr., *Dictionary of pi-Electron Calculations*, Freeman, San Francisco, 1965.

Journal of the Serbian Chemical Society
version electronic
JSCS-info@shd.org.rs • www.shd.org.rs/JSCS
J. Serb. Chem. Soc. *76* (11) 1505–1511 (2011)
JSCS–4224
UDC 547.52/.53+66.095.252.5:54.02
Original scientific paper

A simple mathematical model for the effect of benzo-annelation on cyclic conjugation

IVAN GUTMAN[1*#] and ALEXANDRU T. BALABAN[2]

[1]*Faculty of Science, University of Kragujevac, P. O. Box 60, 34000 Kragujevac, Serbia and*
[2]*Texas A & M University at Galveston, 200 Seawolf Parkway, Galveston, TX 77553, USA*

(Received 28 February 2011)

Abstract: In a series of earlier studies, it was established that benzo-annelation in the angular (resp. linear) position relative to a ring *R* of a polycyclic conjugated π-electron system, increases (resp. decreases) the intensity of the cyclic conjugation in the ring R. Herein, it is shown how this regularity can be explained by means of a simple, Kekulé-structure-based argument, itself based on an idea of Randić from the 1970s.

Keywords: cyclic conjugation; Kekulé structure; benzo-annelation; local aromaticity.

INTRODUCTION

The fact that various parts of a polycyclic conjugated molecules have different π-electron properties (often referred to as differences in their local aromaticity or differences in the magnitude of cyclic conjugation in individual rings) was recognized a long time ago;[1–5] see also recent works along these lines.[6–16] In 2004, within a study[17] of the effect of benzo-annelation on cyclic conjugation in perylene, it was found that in the case of its central six-membered ring:

a) benzo-annelation in an angular position increases the intensity of cyclic conjugation in this ring and that

b) benzo-annelation in a linear position decreases the intensity of cyclic conjugation in this ring.

Several years were needed to recognize that the regularities a and b are not restricted to perylene, but are generally valid, both for benzenoid[18–21] and non-benzenoid[22–26] polycyclic conjugated systems. Initially,[17–26] the rules a and b were verified by calculating the energy effects (*ef*) of the respective rings. This quantity is known[5] to provide a reliable measure of the magnitude of cyclic conjugation in individual rings. Details of the theory on which the *ef*-method is based,

---

* Corresponding author. E-mail: gutman@kg.ac.rs
[#] Serbian Chemical Society member.

doi: 10.2298/JSC110224131G

as well as on its numerous applications, are outlined in two reviews.[27,28] Eventually, in order to eliminate the doubt that the results obtained are artifacts of the *ef*-method, the rules a and b were corroborated by means of several other (more advanced) quantum-theoretical approaches.[29–31] In addition, a general mathematical theory of this phenomenon was elaborated,[32,33] and its applicability demonstrated on the case of benzo-annelated perylenes.[34,35]

In the present paper, it is shown that results equivalent to rules a and b can be deduced by means of a simple approach[3] for quantifying the intensity of cyclic conjugation in a particular ring (or, as it was originally stated,[3] of local aromaticity).

Let G be the molecular graph[36] of a polycyclic conjugated π-electron system, R one of the rings of G, and G–R the subgraph obtained from G by deleting the vertices of R; for an illustrative example see Fig. 1.

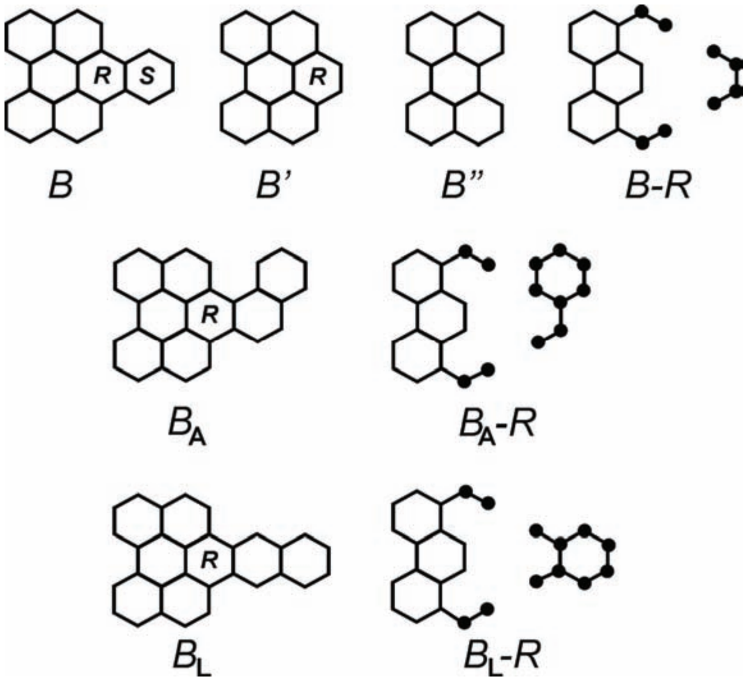

Fig. 1. An example illustrating the notation used in this paper. In naphtho[1,2,3,4-ghi]perylene (B) the ring R has $ef = 0.0261$ and $\Lambda = 0.5263$. In the angularly benzo-annelated derivative (B_A), $ef = 0.0323$, $\Lambda = 0.6897$, and $\Delta = +0.1634$, whereas in the linearly benzo-annelated derivative (B_L), $ef = 0.0223$, $\Lambda = 0.3704$, and $\Delta = -0.1559$.

Let $K(G)$ and $K(G-R)$ be the number of Kekulé structures of G and G–R, respectively. In the following, it is assumed that G is Kekuléan, *i.e.*, that $K(G) > 0$.

According to Randić,[3] the local aromaticity (Λ) pertaining to the ring R in a conjugated system G can be measured by means of the expression:

$$\Lambda = \Lambda(G,R) = \frac{2K(G-R)}{K(G)} \tag{1}$$

A ring is fully aromatic if $\Lambda = 1$, and devoid of any cyclic conjugation if $\Lambda = 0$. The difference between the local aromaticity (of the ring R) after and before benzo-annelation is denoted by $\Delta = \Delta(R)$.

APPLICATION OF EQUATION (1)

The notation used in this section is explained in Fig. 2 (and illustrated by a particular example in Fig. 1).

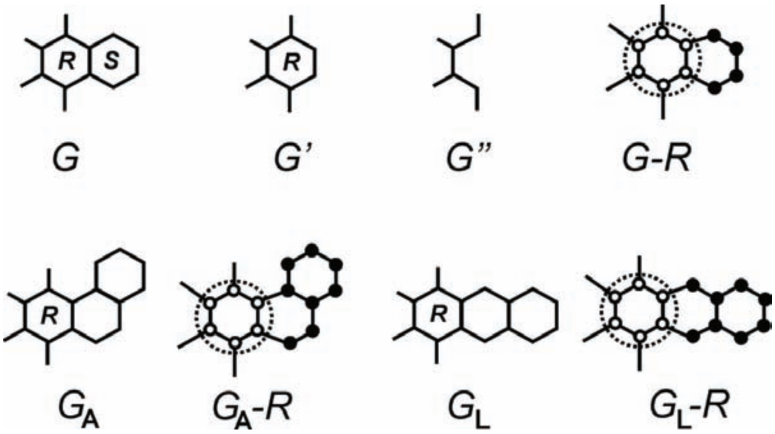

Fig. 2. The notation used. The encircled vertices are those that have been deleted.

Thus, let G be the molecular graph of a polycyclic conjugated system, R the ring whose cyclic conjugation is to be examined, and S the ring adjacent to R. It should be noted that the ring S must be six-membered, but the ring R need not be. In G' the ring S is missing, whereas in G'' both rings R and S are missing. The subgraph $G–R$ is obtained by deleting from G all vertices belonging to the ring R. The angularly and linearly benzo-annelated derivatives of G are denoted by G_A and G_L, respectively, and their subgraphs $G_A–R$ and $G_A–R$ are constructed in full analogy with $G–R$.

In order to apply Eq. (1), the Kekulé structure counts of G, G_A, and G_L must be computed. This can be realized using standard recursive methods,[37,38] namely:

$$K(G) = K(G-e) + K(G-u-v) \tag{2}$$

where e is an edge of G, connecting the vertices u and v, and

$$K(G) = K(G-u-v) \tag{3}$$

if either the vertex *u* or the vertex *v* are pendent (have a single neighbor). The manner in which the formula:

$$K(G) = K(G') + K(G'') \tag{4}$$

is obtained by using Eqs. (2) and (3) is shown in Fig. 3.

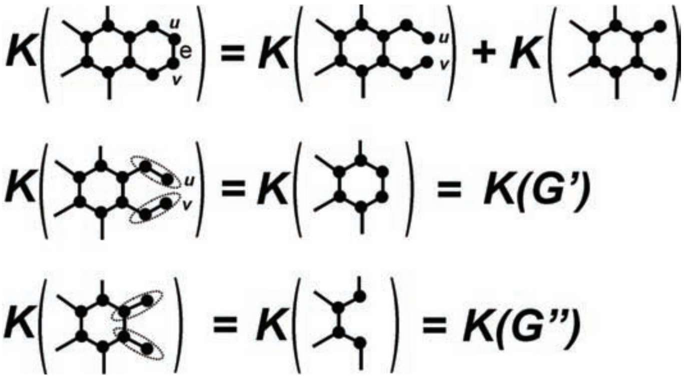

Fig. 3. Deducing Eq. (4).

In an analogous manner, one obtains:

$$K(G_{\mathrm{A}}) = K(G) + K(G') \text{ and } K(G_{\mathrm{L}}) = K(G) + K(G'')$$

which combined with Eq. (4) yield:

$$K(G_{\mathrm{A}}) = 2K(G') + K(G'') \text{ and } K(G_{\mathrm{L}}) = K(G') + 2K(G'')$$

It should be noted that since $K(G) > 0$, then $K(G')$ and $K(G'')$ must also be > 0.

From Figs. 1 and 2, it can be seen that the subgraph G_{A}–R differs from G–R by having a styrene fragment instead of a butadiene fragment. Since styrene has two Kekulé structures, whereas butadiene only one, one has $K(G_{\mathrm{A}}–R) = 2K(G–R)$. On the other hand, the subgraph G_{L}–R possesses an *o*-xylylene fragment, the Kekulé structure count of which is unity. Therefore, $K(G_{\mathrm{L}} - R) = K(G - R)$. Bearing these relations in mind one readily arrives at:

$$\Lambda(G,R) = \frac{2K(G-R)}{K(G)} = \frac{2K(G-R)}{K(G')+K(G'')} \tag{5}$$

$$\Lambda(G_{\mathrm{A}},R) = \frac{2K(G_{\mathrm{A}}-R)}{K(G)} = \frac{4K(G-R)}{2K(G')+K(G'')} \tag{6}$$

and

$$\Lambda(G_{\mathrm{L}},R) = \frac{2K(G_{\mathrm{L}}-R)}{K(G)} = \frac{K(G-R)}{2K(G')+K(G'')} \tag{7}$$

It is now a matter of elementary calculation to verify that if *K*(*G*–*R*) is non-zero, then Eqs. (5)–(7) imply:

$$\Lambda(G_\mathrm{L},R) < \Lambda(G,R) < \Lambda(G_\mathrm{A},R)$$

i.e.,

$\Delta_\mathrm{L}(R) = \Lambda(G_\mathrm{L},R) - \Lambda(G,R) < 0$ and $\Delta_\mathrm{A}(R) = \Lambda(G_\mathrm{A},R) - \Lambda(G,R) > 0$, which is in full agreement with rules a and b. In other words, our finding with regard to the effect of benzo-annelation on cyclic conjugation can be rationalized by means of the simple Kekulé-structure-based formula, Eq. (1). However, this is the case only if the subgraph *G*–*R* is also Kekuléan, *i.e.*, if *K* (*G*–*R*) > 0.

THE CASE *K*(*G*–*R*) = 0

The case *K*(*G*–*R*) = 0 needs to be analyzed separately. This case is important, because it is encountered if the ring R is odd-membered, as in the much studied acenaphthylene and fluoranthene congeners.[22–26] Also, perylene belongs to this case.[17]

If the subgraph *G*–*R* is non-Kekuléan, then from Eqs. (5)–(7), it follows:

$$\Lambda(G,R) = \Lambda(G_\mathrm{A},R) = \Lambda(G_\mathrm{L},R) = 0$$

i.e.,

$$\Delta_\mathrm{L}(R) = \Delta_\mathrm{A}(R) = 0$$

a result that would be expected from a model based solely on Kekulé structures.

The way to circumvent this difficulty is evident: Eq. (1) has to be modified to:

$$\Lambda^* = \Lambda^*(G,R) = \frac{2K^*(G-R)}{K(G)}$$

where K^* is the count of some pertinently chosen resonance structures (with one or more unpaired π-electrons).[39,40] For the present analysis, the actual choice of K^* is immaterial, it is only necessary that $K^*(G–R) > 0$. If so, then from the modifications of Eqs. (5)–(7), namely:

$$\Lambda^*(G,R) = \frac{2K^*(G-R)}{K(G)} = \frac{2K^*(G-R)}{K(G')+K(G'')}$$

$$\Lambda^*(G_\mathrm{A},R) = \frac{2K^*(G_\mathrm{A}-R)}{K(G)} = \frac{4K^*(G-R)}{2K(G')+K(G'')}$$

$$\Lambda^*(G_\mathrm{L},R) = \frac{2K^*(G_\mathrm{L}-R)}{K(G)} = \frac{K^*(G-R)}{2K(G')+K(G'')}$$

one immediately obtains:

$$\Lambda^*(G_\mathrm{L},R) < \Lambda^*(G,R) < \Lambda^*(G_\mathrm{A},R)$$

i.e.,

$$\Delta_{\mathrm{L}}^{*}(R) = \Lambda^{*}(G_{\mathrm{L}}, R) - \Lambda^{*}(G, R) < 0 \text{ and } \Delta_{\mathrm{A}}^{*}(R) = \Lambda^{*}(G_{\mathrm{A}}, R) - \Lambda^{*}(G, R) > 0,$$

that is in harmony with the rules a and b.

Acknowledgement. I. G. thanks for the support of the Ministry of Education and Science of the Republic of Serbia (Grant No. 174033).

ИЗВОД

JEDNOSTAVNI

МАТЕМАТИЧКИ МОДЕЛ ЗА УТИЦАЈ БЕНЗО-АНЕЛАЦИЈЕ НА ЦИКЛИЧНУ КОНЈУГАЦИЈУ

ИВАН ГУТМАН[1] и ALEXANDRU T. BALABAN[2]

[1]Природно–математички факултет Универзитета у Крагујевцу и [2]Texas A & M University at Galveston, Galveston, USA

У низу ранијих истраживања установљено је да бензо-анелација у линеарном (одн. ангуларном) положају у односу на прстен *P* у полицикличном конјугованом π-електронском систему, смањује (одн. увећава) интензитет цикличне конјугације у прстену R. У раду показујемо да се ова правилност може објаснити помоћу једног једноставног, на Кекулеовим структурама заснованог, модела.

(Примљено 28. фебруара 2011)

REFERENCES

1. M. J. S. Dewar, *The Molecular Orbital Theory of Organic Chemistry*, McGraw-Hill, New York, 1969
2. E. Clar, *The Aromatic Sextet*, Wiley, London, 1972
3. M. Randić, *Tetrahedron* **30** (1974) 2067
4. M. Randić, *Tetrahedron* **31** (1975) 1477
5. I. Gutman, S. Bosanac, *Tetrahedron* **33** (1977) 1809
6. M. Randić, *Chem. Rev.* **103** (2003) 3449
7. A. T. Balaban, *Polyc. Arom. Comp.* **24** (2004) 83
8. A. T. Balaban, M. Randić, *J. Math. Chem.* **37** (2005) 443
9. G. Portella, J. Poater, M. Sola, *J. Phys. Org. Chem.* **18** (2005) 785
10. P. Bultinck, S. Fias, R. Ponec, *Chem. Eur. J.* **12** (2006) 8813
11. J. Aihara, T. Ishida, H. Kanno, *Bull. Chem. Soc. Jpn.* **80** (2007) 1518
12. J. Ou, *MATCH Commun. Math. Comput. Chem.* **64** (2010) 157
13. M. Randić, *MATCH Commun. Math. Comput. Chem.* **64** (2010) 303
14. M. V. Putz, *MATCH Commun. Math. Comput. Chem.* **64** (2010) 391
15. A. Ciesielski, T. M. Krygowski, M. K. Cyranski, A. T. Balaban, *Phys. Chem. Chem. Phys.* **13** (2011) 3737
16. A. T. Balaban, M. Randić, in: *Advances in Physics and Chemistry of Carbon Bonding and Structures*, M. V. Putz, Ed., Springer-Verlag, Berlin, 2011, in press
17. I. Gutman, N. Turković, J. Jovičić, *Monatsh. Chem.* **135** (2004) 1389

18. S. Jeremić, S. Radenković, I. Gutman, *Maced. J. Chem. Chem. Eng*. **29** (2010) 63
19. A. T. Balaban, J. Đurđević, I. Gutman, S. Jeremić, S. Radenković, *J. Phys. Chem., A* **114** (2010) 587
20. S. Jeremić, S. Radenković, I. Gutman, *J. Serb. Chem. Soc*. **75** (2010) 943
21. A. T. Balaban, I. Gutman, S. Jeremić, J. Đurđević, *Monatsh. Chem*. **142** (2011) 53
22. I. Gutman, J. Đurđević, A. T. Balaban, *Polyc. Arom. Comp*. **29** (2009) 3
23. J. Đurđević, I. Gutman, J. Terzić, A. T. Balaban, *Polyc. Arom. Comp*. **29** (2009) 90
24. I. Gutman, J. Đurđević, *J. Serb. Chem. Soc*. **74** (2009) 765
25. I. Gutman, S. Jeremić, V. Petrović, *Indian J. Chem., A* **48** (2009) 658
26. B. Furtula, I. Gutman, S. Jeremić, S. Radenković, *J. Serb. Chem. Soc*. **75** (2010) 83
27. I. Gutman, *Monatsh. Chem*. **136** (2005) 1055
28. I. Gutman, in: *Mathematical Methods and Modelling for Students of Chemistry and Biology*, A. Graovac, I. Gutman, D. Vukičević, Eds., Hum, Zagreb, 2009, pp. 13–27
29. J. Đurđević, S. Radenković, I. Gutman, S. Marković, *Monatsh. Chem*. **140** (2009) 1305
30. J. Đurđević, I. Gutman, R. Ponec, *J. Serb. Chem. Soc*. **74** (2009) 549
31. A. T. Balaban, T. K. Dickens, I. Gutman, R. B. Mallion, *Croat. Chem. Acta* **83** (2010) 209
32. S. Radenković, J. Đurđević, I. Gutman, *Chem. Phys. Lett*. **475** (2009) 289
33. I. Gutman, *J. Math. Chem*. **47** (2010) 1309
34. S. Radenković, W. Linert, I. Gutman, S. Jeremić, *Indian J. Chem., A* **48** (2009) 1657
35. I. Gutman, S. Radenković, W. Linert, *Monatsh. Chem*. **141** (2010) 401
36. I. Gutman, O. E. Polansky, *Mathematical Concepts in Organic Chemistry*, Springer-Verlag, Berlin, 1986
37. W. C. Herndon, *J. Chem. Educ.* **51** (1974) 10
38. S. J Cyvin, I. Gutman, *Kekulé Structures in Benzenoid Hydrocarbons*, Springer-Verlag, Berlin, 1988
39. J. R. Dias, *J. Chem. Inf. Comput. Sci*. **41** (2001) 129
40. J. R. Dias, *J. Chem. Inf. Comput. Sci*. **41** (2001) 686.

Journal of the Serbian Chemical Society
JSCS-info@shd.org.rs • www.shd.org.rs/JSCS

J. Serb. Chem. Soc. 76 (11) 1513–1522 (2011)
JSCS–4225

UDC 547.48+66.094.3+547.857.8+
546.215+546–328:544.4
Original scientific paper

A green, reusable and highly efficient solid acid catalyst for the oxidation of aldehydes to the corresponding carboxylic acids using H_2O_2 and $KMnO_4$:$H_5PV_2Mo_{10}O_{40}$ (10-molybdo-2-vanadophosphoric heteropolyacid)

ABDOLLAH FALLAH SHOJAEI[1], MOHAMAD ALI REZVANI[1]* and MAJID HERAVI[2]

[1]*Department of Chemistry, Faculty of Science, University of Guilan, Rasht 419961-3769 and*
[2]*Department of Chemistry, School of Science, Azzahra University, Vanak, Tehran, Iran*

(Received 20 September 2010, revised 23 May 2011)

Abstract: $H_5PV_2Mo_{10}O_{40}$-catalyzed oxidation of aromatic aldehydes to the corresponding carboxylic acids using hydrogen peroxide and $KMnO_4$ as oxidants under mild conditions is reported. This system provides an efficient, convenient and practical method for the oxidation of aromatic aldehydes. In this work, differences between Keggin and Well–Dawson type polyoxometalates are addressed in term of relative stability, hardness and acidity.

Keyword: heteropolyacids; aldehydes; carboxylic acids; microwave irradiation; polyoxometalates.

INTRODUCTION

The catalytic function of heteropolyacids (HPAs) and related polyoxometalate compounds has attracted much attention, particularly over the last two decades.[1–4] In this context, heteropolyacids (HPAs) are promising catalysts. A common and important class of these acids and those used in the majority of catalytic applications are Keggin compounds of the general formula $H_nXM_{12}O_{40}$ (X = P, Si, As, Ge or B; M = Mo and/or W).[5] These solid acids are usually insoluble in non-polar solvents but highly soluble in polar ones. They can be used in bulk or supported forms in both homogeneous and heterogeneous systems. Furthermore, these HPAs have several advantages, including high flexibility in the modification of the acid strength, ease of handling, environmental compatibility, non-toxicity, and experimental simplicity.[6] Keggin type polyoxoanions have been widely studied as homogeneous and heterogeneous catalyst for the oxidation of organic compounds.[7]

---

* Corresponding author. E-mail: marezvani298@yahoo.com
doi: 10.2298/JSC100920135S

Another catalytically important subclass of the Keggin compounds are the mixed vanadium (V) substituted HPAs of the general formula $H_{3+n}PV_nM_{12-n}O_{40}$ (M = Mo and W; n = 1 to 6). These compounds exhibit high activity in acid–base type catalytic reactions; hence, they are used in many catalytic areas as homogeneous and heterogeneous catalysts. The most well known of these HPAs is $H_5PV_2Mo_{10}O_{40}$.

In continuation of ongoing research[8–12] on the syntheses and application of heteropolyacids in organic syntheses and due to the importance of derivatives of aldehydes in chemical processes, the applicability of HPA for efficient oxidation of aldehyde to the corresponding carboxylic acids is reported herein. Ishii and co-workers reported a number of interesting reactions catalyzed by transition metal-substituted heteropolyacids, including oxidation of aldehydes to carboxylic acids.[13] Shimizu and co-workers showed how product selectivity and activity depend on the composition of the heteropolyanion and the type of counter cations as well as the support surface area.[14] In addition, they emphasized that pore size distribution is very important. Mizuno and co-workers examined the oxidation of octanal by O_2 with both nickel- and iron-containing heteropolyacids.[15] Zamaraev and co-workers reported the catalytic properties of several cobalt-containing heteropolyanions, *viz*. tetra-alkylammonium salts of $PW_{11}CoO_{39.5}$ and $CoW_{12}O_{40.6}$, in alkene epoxidation by dioxygen in the presence of *iso*-butyraldehyde, under ambient conditions.[16] The mechanism and the catalytic activity of transition metal-substituted heteropolyacids have been speculated since 1970 and later on, the propensity of them to bind with molecular oxygen and the role of such dioxygen-activated species in the oxidation of organic substrates was explored.[17]

Microwave heating has been used for a wide variety of applications, including the rapid synthesis of organic compounds.[18,19] Now, a very efficient and simple method for the oxidation of aldehydes to the corresponding carboxylic acids using H_2O_2 and $KMnO_4$ as the oxidizing reagent and catalyzed by mixed vanadium (V)-substituted HPAs under mild conditions is reported.

EXPERIMENTAL

All reagents and solvents used in this work are available commercially (Merck) and used as received, unless otherwise indicated. Previously reported methods were used to purify the aldehydes.[20] The preparation of the $H_5PV_2Mo_{10}O_{40}$ catalyst and other mixed heteropolyacids and salts were based on a literature procedure, with modifications as reported below.[21] The acids of $[NaP_5W_{30}O_{110}]^{14-}$, $[P_2W_{18}O_{62}]^{6-}$ and $[P_2Mo_{18}O_{62}]^{6-}$ were prepared according to published methods and were identified by infrared spectroscopy.[22] The ^{1}H-NMR spectra were recorded on a Brucker 100 MHz Aspect 3000 FT-NMR instrument. The IR spectra were recorded on a Buck 500 scientific spectrometer (KBr pellets).

Preparation of $H_5PV_2Mo_{10}O_{40}$[21]

Sodium metavanadate (12.2 g, 100 mmol) was dissolved by boiling in 50 mL of water and then mixed with (3.55 g, 25 mmol) of Na_2HP0_4 in 50 mL of water. After the cooling the solution, concentrated sulphuric acid (5 mL, 17 M, 85 mmol) was added, whereby a red colour developed. $Na_2MoO_4.2H_2O$ (60.5 g, 250 mmol) dissolved in 100 mL of water was added to the red solution under vigorous stirring, followed by the slow addition of concentrated sulphuric acid (42 mL, 17 m, 714 mmol). The hot solution was allowed to cool to room temperature. The 10-molybdo-2-vanadophosphoric acid was then extracted with 500 mL of diethyl ether. Air was passed through the heteropoly etherate (bottom layer) to free it of ether. The solid residue was dissolved in water, concentrated to first crystal formation, as already described, and then allowed to crystallize further. The large red crystals that formed were filtered, washed with water, and air-dried.

Preparation of $H_4PVMo_{11}O_{40}$

Na_2HPO_4 (3.55 g, 25 mmol) was dissolved in 50 mL of water and mixed with (3.05 g, 25 mmol) of sodium metavanadate that had been dissolved by boiling in 50 mL of water. The mixture was cooled and acidified to a red colour with concentrated sulphuric acid (2.5 mL, 17 M, 42.5 mmol). To this mixture was added a solution of $Na_2MoO_4.2H_2O$ (66.5 g, 274.8 mmol) dissolved in 100 mL of water. Finally, 42.5 mL of concentrated sulphuric acid was added slowly to the solution under vigorous stirring. With this addition, the dark red colour changed to a lighter red. After cooling the aqueous solution, heteropoly acid was then extracted into 200 mL of diethyl ether. In this extraction, the heteropoly etherate was present as the middle layer; the bottom layer (water) was yellow and probably contained vanadyl species. After separation, a stream of air was passed through the heteropoly etherate layer to free it of ether. The solid orange residue was dissolved in 50 mL of water, concentrated to the first appearance of crystals in a vacuum desiccator over concentrated sulphuric acid, and then allowed to crystallize further. The orange crystals that formed were filtered, washed with water, and air-dried.

General procedures for the oxidation of benzaldehyde using H_2O_2 as the oxidizing agent

Method A (microwave irradiation conditions). Benzaldehyde, heteropolyacid compound and H_2O_2 are mixed thoroughly in a small beaker. The mixture was placed in microwave oven and irradiated for 3 min. at 10–80 % power (full power 1000 watts). Then to the final mixture was added 10 % aqueous solution of $NaHCO_3$ and the mixture was filtered. The carboxylic acids were precipitated by adding 6 M HCl to the filtrate. The solid product was collected and washed with H_2O. Adding 2,4-dinitrophenylhydrazine (DNP) reagent precipitated the product. The products were characterized by comparison of their spectroscopic data (IR, ^{1}H-NMR and MS), and melting points with those of authentic samples.

Method B (magnetic stirrer (25 °C) conditions). To a stirred mixture of the aldehyde (2 mmol) and H_2O_2 (3 mmol) was added $H_5PV_2Mo_{10}O_{40}$ (0.25 mol %). Then stirring was continued at room temperature under solvent-free conditions. The progress of the reaction was monitored by TLC.

Method C (reflux conditions). The aldehyde (5 mmol) was dissolved in a mixed solvent (10 mL ethanol + 5 mL H_2O). Then heteropolyacid (0.1g, 10^{-2} mmol) was added to the solution. The reaction mixture was refluxed in a 25-mL round-bottom flask equipped with a magnetic stirrer, reflux condenser and thermometer. While the solution was vigorously stirred for 10 min, H_2O_2 (5mL, 165 mmol) was added to the solution. The reaction mixture was stirred and refluxed for 3–10 h at 70 °C.

General procedure for the oxidation of benzyl aldehyde using $KMnO_4$ as the oxidant

Preparation of oxidant ($KMnO_4$). The oxidant is prepared by grinding equal amounts of potassium permanganate and copper sulphate pentahydrate in a mortar until homogeneous or by adding a concentrated aqueous solution of potassium permanganate to alumina, giving a paste that was then ground with an equal amount of copper sulphate pentahydrate. Addition of alumina as a solid support did not improve the yields of these reactions. The best results were obtained when $KMnO_4$ was first mixed with copper sulphate pentahydrate (or a 20/80 mixture of copper sulphate pentahydrate and alumina) to give a reagent that has previously been extensively used as a heterogeneous oxidant.

General procedure for the oxidation using $KMnO_4$ as oxidant

All reaction mixtures were refluxed in a 100-mL, two necked round-bottom flask equipped with a magnetic stirrer, reflux condenser, and thermometer. Benzylaldehyde (5 mmol) and a potion of the oxidant (4 g) was added to the mixed solvent (20 mL ethanol + 10 mL H_2O) and 0.5 g $H_5PV_2Mo_{10}O_{40}$ (0.025 mol). The reaction mixture was stirred vigorously and refluxed for 4–8 h at 80 °C until TLC analysis indicated completion of the reaction. Then the suspension was cooled and the aqueous layer separated by filtration through a short column of sodium chloride. The water layer was acidified to pH 3 by the addition of hydrochloric acid. The precipitate of benzoic acid was separated by filtration and washed with CH_2Cl_2 or cold water (3×10 mL). If greater purity is required, the product could be recrystallized.

Recycling of the catalyst

At the end of the oxidation of aldehydes to carboxylic acids, the catalyst was filtered and washed with dichloromethane. In order to know whether the catalyst would succumb to poisoning and lose its catalytic activity during the reaction, the reusability of the catalyst was investigated. For this purpose, after completion of the reaction, dichloromethane was added to the reaction mixture. All compounds were soluble in dichloromethane except the catalyst. Thus, it could be separated by simple filtration, washed with dichloromethane, dried at 90 °C for 1 h, and reused in another reaction with the same substrate. Even after five runs for the reaction, the catalytic activity of $H_5PV_2Mo_{10}O_{40}$ was almost the same as that of freshly used catalyst. The results are summarized in Table I. The IR spectra of the resulting solids indicate that the catalyst can be recovered without structural degradation.

TABLE I. Reuse of the catalyst in the oxidation of 4-cholorobenzaldehyde (isolated yield is based on the weight of the pure product obtained)

Times used	Isolated yield, %
1	95
2	92
3	94
4	91
5	93

RESULTS AND DISCUSSION

The oxidation of aromatic aldehydes by H_2O_2 or $KMnO_4$ was examined in the presence of a variety of heteropolyacids and transition metal-substituted polyoxometaltes. Although it is difficult to explain the different activities of these HPAs, certainly there is a complex relationship between the activity and structure of the polyanion. By changing the constituent elements of the polyanion (both hetero- and addenda-atoms), the acid strength of the HPAs and their catalytic activity can be varied over a wide range.[24] When the substrate was liquid, the mole ratio of sub:ox:cat was 1:3:10$^{–3}$ but when substrate was solid the mole ratio was 1:15:10$^{–3}$ or 1:30:10$^{–3}$, depending on the reaction conditions. They are summarized in Table II. It is noticeable that the time of reaction under microwave irradiation was very short with respect to the analogous reactions.[25] The Keggin-type polyoxometalates resulted in more effective reactions in comparison to the Well–Dawson-type polyoxometalates (see later Table IV). However, $H_6P_2Mo_{18}O_{62}$ was more effective than $H_3PW_{12}O_{40}$ in the oxidation of aldehydes. This may be due to the difference in the reduction potentials of tungsten and molybdenum.

TABLE II. Oxidation of different aromatic aldehyde using H_2O_2 as oxidant under microwave condition

Entry	Aldehyde aromatic	Power, W	Reaction time, s	Isolated yield, %
1	4-Methylbenzaldehyde	30	100	88
2	4-Cholorobenzaldehyde	300	80	95
3	2,6-Dicholorobenzaldehyde	300	120	92
4	2,4-Dicholorobenzaldehyde	300	130	96
5	3,4-Dicholorobenzaldehyde	350	150	90
6	4-Nitrobenzaldehyde	400	120	97
7	3-Nitrobenzaldehyde	500	130	95
8	3,4-Dinitrobenzaldyde	500	150	94
9	2,3-Dinitrobenzaldyde	500	150	90
10	Benzaldyde	500	150	95

Effect of the aldehyde substituent

The effects of various substituents on the yields of oxidation of a range of aromatic aldehydes were examined using $H_5PV_2Mo_{10}O_{40}$ as the catalyst. The results are given in Tables II and III. Halogens were chosen as electron-withdrawing groups (Table II, entries 2–5), while methyl was chosen as an electron-donating substituent (Table II, entry 1). The yields were generally very good (>80 %) to excellent (>90 %) with no obvious relationship between the aromatic substituent and yield (compare entries 1 with 10 and 2 with 10). A highlight of the method is the ease by which the product may be isolated *via* simple filtration following removal of the solvent.

TABLE III. Oxidation of aromatic aldehydes using H_2O_2 in presence of different solvents under reflux conditions (isolated yield based on the weight of the pure product obtained)

Entry	Aldehyde	Solvent	Time, h	Isolated yield, %
1	4-Nitrobenzaldehyde	20 ml Ethanol + 10 ml H_2O	3	95
		10 ml Ethanol + 20 ml H_2O	3	90
		15 ml ethanol + 15 ml H_2O	4	91
		30 ml Ethanol	5	85
		30 ml H_2O	5	85
		Solvent free	8	65
2	3-Nitrobenzaldehyde	20 ml Ethanol + 10 ml H_2O	5	89

TABLE III. Continued

Entry	Aldehyde	Solvent	Time, h	Isolated yield, %
2	3-Nitrobenzaldehyde	10 ml Ethanol + 20 ml H_2O	7	82
		15 ml Ethanol + 15 ml H_2O	8	80
		30 ml Ethanol	10	75
		30 ml H_2O	10	79
		Solvent free	12	52
3	4-Chlorobenzaldehyde	20 ml Ethanol + 10 ml H_2O	5	94
		10 ml Ethanol + 20 ml H_2O	8	88
		15 ml Ethanol + 15 ml H_2O	10	84
		30 ml Ethanol	10	78
		30 ml H_2O	8	84
		Solvent free	12	63
4	Benzaldehyde	20 ml Ethanol + 10 ml H_2O	6	82
		10 ml Ethanol + 20 ml H_2O	8	79
		15 ml Ethanol + 15 ml H_2O	10	75
		30 ml Ethanol	10	69
		30 ml H_2O	8	75
		Solvent free	12	45

Effect of the catalyst structure

The effect of catalyst structure on the oxidation of aromatic aldehydes is summarized in Table IV. 4-Chlorothiophenol was used as the model compound and the amount of each catalyst was kept constant. In the Keggin-type polyoxometalates series, $H_5PV_2Mo_{10}O_{40}$ showed the highest catalytic activity. In general, the heteropoly salt type catalysts were less efficient than the heteropolyacids. The Keggin-type polyoxometalates led to a more effective reaction in comparison with the Well–Dawson type polyoxometalates. Thus, $H_6P_2Mo_{18}O_{62}$ was again more effective than $H_6P_2W_{18}O_{62}$ in the oxidation of aldehydes, possibly due to the difference in the reduction potentials tungsten and molybdenum. However, the results indicated that the highest yield of products was obtained with $H_5PV_2Mo_{10}O_{40}$ as catalyst (Table III). This behaviour is found to be quite general. The high activity of $H_5PV_2Mo_{10}O_{40}$ in comparison of the other HPAs (Table IV) confirmed that in addition to H^+, the V^{5+} probably played a catalytic role in the reaction.

TABLE IV. Oxidation of aldehydes using $KMnO_4$ as the oxidant in the presence of different heteropolyacids using microwave radiation

Entry	Aldehyde	Catalyst	Reaction time, s	Power, W	Yield, %
1	4-Methylbenzaldehyde	$H_5PV_2Mo_{10}O_{40}$	30	100	88
		$H_6PV_3Mo_9O_{40}$	40	100	86
		$H_4PVMo_{11}O_{40}$	50	100	82
		$H_3PMo_{12}O_{40}$	60	100	78
		$H_6P_2Mo_{18}O_{62}$	80	200	74

TABLE IV. Continued

Entry	Aldehyde	Catalyst	Reaction time, s	Power, W	Yield, %
1	4-Methylbenzaldehyde	$H_3PW_{12}O_{40}$	90	100	70
		$H_6P_2W_{18}O_{62}$	140	200	70
		None	300	500	25
2	4-Chlorobenzaldehyde	$H_5PV_2Mo_{10}O_{40}$	80	300	95
		$H_6PV_3Mo_9O_{40}$	100	280	95
		$H_4PVMo_{11}O_{40}$	110	300	92
		$H_3PMo_{12}O_{40}$	120	500	86
		$H_6P_2Mo_{18}O_{62}$	130	600	82
		$H_3PW_{12}O_{40}$	130	500	88
		$H_6P_2W_{18}O_{62}$	140	1000	81
		None	320	2000	28
3	4-Nitrobenzaldehyde	$H_5PV_2Mo_{10}O_{40}$	120	400	97
		$H_6PV_3Mo_9O_{40}$	100	450	97
		$H_4PVMo_{11}O_{40}$	150	600	96
		$H_3PMo_{12}O_{40}$	180	1000	88
		$H_6P_2Mo_{18}O_{62}$	180	1000	86
		$H_3PW_{12}O_{40}$	170	800	84
		$H_6P_2W_{18}O_{62}$	180	1000	81
		None	480	2000	27
4	3-Nitrobenzaldehyde	$H_5PV_2Mo_{10}O_{40}$	130	500	98
		$H_6PV_3Mo_9O_{40}$	100	500	98
		$H_4PVMo_{11}O_{40}$	160	600	96
		$H_3PMo_{12}O_{40}$	200	1000	87
		$H_6P_2Mo_{18}O_{62}$	280	1000	86
		$H_3PW_{12}O_{40}$	250	1300	84
		$H_6P_2W_{18}O_{62}$	300	1300	82
		None	540	2500	24

Effect of microwave irradiation

In recent years, a practical dimension to microwave heating protocols was added by accomplishing reactions on solid supports under solvent-free conditions.[21] These solvent-free microwave-assisted reactions provide an opportunity to work with open vessels, thus avoiding the risk of high-pressure development and increasing the potential of such reactions to large-scale production. For the first time, results on this environmentally benign microwave approach for the oxidation of aromatic aldehyde in the presence of $H_5PV_2Mo_{10}O_{40}$ are described herein. The results showed that, 4-chlorobenzaldehyde could easily be oxidized but hydroxybenzaldehydes could not. Other mono-substituted benzaldehydes showed different behaviours (Table IV).

A comparison of the methods

The results also showed that under microwave irradiation, the oxidation readily proceeds over mixed addenda heteropolyacid $H_5PV_2Mo_{10}O_{40}$ catalysts loadings under solvent-free conditions in very short times (1–3 min) (Table V). This can be due to the polar nature of the reaction intermediates that couple efficiently with the microwaves and hence, increase the yield and accelerate the rate. Clearly, this method minimizes the longer reaction times required under thermal conditions.

TABLE V. Comparison of the different methods employed

Entry	Aldehyde	Test method	Time	Yield, %
1	4-Methylbenzaldehyde	Reflux (solvent)	4 h	84
		Heated (without solvent)	3.5 h	86
		Magnetic stirrer (25 °C)	10 h	82
		Microwave irradiation	30 s	88
2	4-Chlorobenzaldehyde	Reflux (solvent)	5 h	94
		Heated (without solvent)	5 h	92
		Magnetic stirrer (25 °C)	14 h	90
		Microwave irradiation	80 s	94
3	4-Nitrobenzaldehyde	Reflux (solvent)	3 h	95
		heated (without solvent)	2.5 h	92
		Magnetic stirrer (25 °C)	10 h	96
		Microwave irradiation	120 s	100
4	3-Nitrobenzaldehyde	Reflux (solvent)	5 h	89
		Heated (without solvent)	4.5 h	90
		Magnetic stirrer (25 °C)	12 h	88
		Microwave irradiation	130 s	98
5	Benzaldehyde	Reflux (solvent)	6 h	82
		Heated (without solvent)	7 h	76
		Magnetic stirrer (25 °C)	10 h	74
		Microwave irradiation	150 s	95

Effect of the oxidant

This reaction was carried out using either H_2O_2 or $KMnO_4$ as the oxidizing agent under mild conditions. The effect of the oxidant on the oxidation of aromatic aldehydes in the presence of $H_5PV_2Mo_{10}O_{40}$ is presented in Table VI.

TABLE VI. Oxidation of aldehydes by different oxidants in the presence of $H_5PV_2Mo_{10}O_{40}$

Entry	Aldehyde	Oxidant	Time, h	Yield, %
1	4-Nitrobenzaldehyde	$KMnO_4$	5	97
		H_2O_2	3	95
		None	8	20
2	3-Nitrobenzaldehyde	$KMnO_4$	5	98
		H_2O_2	5	89
		None	8	17
3	4-Chlorobenzaldehyde	$KMnO_4$	7	96
		H_2O_2	5	94
		None	10	18

TABLE VI. Continued

Entry	Aldehyde	Oxidant	Time, h	Yield, %
4	4-Methylbenzaldehyde	$KMnO_4$	4	92
		H_2O_2	4	98
		None	8	27
5	Benzaldehyde	$KMnO_4$	5	96
		H_2O_2	6	69
		None	8	25
6	2,6-Dicholorobenzaldehyde	$KMnO_4$	8	88
		H_2O_2	7	92
		None	10	11
7	2,4-Dicholorobenzaldehyde	$KMnO_4$	8	90
		H_2O_2	7	91
		None	10	10
8	3,4-Dicholorobenzaldehyde	$KMnO_4$	8	87
		H_2O_2	7	91
		None	10	11
9	3,4-Dinitrobenzaldyde	$KMnO_4$	8	89
		H_2O_2	7	92
		None	10	10

CONCLUSIONS

By changing the constituent elements of the polyanion (both hetero and addenda atoms), the acid strength of HPAs as well as their catalytic activity can be varied over a wide range. For the first time, using the inexpensive and easily prepared $H_5PV_2Mo_{10}O_{40}$ solid catalyst, oxidation of aromatic aldehydes with electron-withdrawing and electron-donating groups to the corresponding carboxylic acids was studied. The results showed that the catalyst type is important as well as the solvent and temperature, but that the reaction withstands a range of substituents. The Keggin-type polyoxometalates were superior to the Well–Dawson type polyoxometalates.

ИЗВОД

„ЗЕЛЕНИ“, ПОНОВО УПОТРЕБЉИВ, ВИСОКО ЕФИКАСАН ЧВРСТИ КИСЕЛИ КАТАЛИЗАТОР ЗА ОКСИДАЦИЈУ АЛДЕХИДА ДО ОДГОВАРАЈУЋЕ КИСЕЛИНЕ СА H_2O_2 И $KMNO_4$:$H_5PV_2Mo_{10}O_{40}$ (10-МОЛИБДО-2-ВАНАДО ФОСФОРНЕ ХЕТЕРОПОЛИ КИСЕЛИНЕ)

ABDOLLAH FALLAH SHOJAEI[1], MOHAMAD ALI REZVANI[1] и MAJID HERAVI[2]

[1]*Department of Chemistry, Faculty of Science, University of Guilan, Rasht, 419961-3769* и [2]*Department of Chemistry, School of Science, Azzahra University, Vanak, Tehran, Iran*

Предмет рада је оксидација ароматичних алдехида до одговарајућих карбоксилних киселина, употребом водоник-пероксида као реагенса, уз $H_5PV_2Mo_{10}O_{40}$ као катализатора. Наведени систем представља ефикасан, погодан и практичан метод за оксидацију ароматичних алдехида. Полиоксометалати Keggin и Well–Dawson типа су међусобно упоређени у односу на њихову релативну стабилност, тврдоћу и киселост.

(Примљено 20. септембра 2010, ревидирано 23. маја 2011)

REFERENCES

1. C. A. S. Regino, D. E. Richardson, *Inorg. Chim. Acta* **360** (2007) 3971
2. Y. Izumi, K. Urabe, M. Onaka, *Zeolites Clay and Heteropolyacids in Organic Reactions*, Kodansha, Tokyo, 1992
3. I. V. Kozhevnikov, *Chem. Rev.* **98** (1998) 171
4. I. V. Kozhevnikov, *Catalysis for Fine Chemical Synthesis, Catalysis by Polyoxometalates*, Wiley, New York, 2002
5. X. López, *Ph.D. Thesis*, Rovira i Virgili University, 2003
6. M. Langpape, J. C. M. Millet, *Appl. Catal. A* **89** (2000) 200
7. *Comprehensive Coordination Chemistry*, Vol. 3, M. T. Pope, G. Wilkinson, D. Gillard, J. A. McCleverty, Eds., Pergamon Press, New York, 1987, p. 27
8. V. Kesavan, D. Bonnet-Delpon, J. P. Begue, *Synthesis* (2000) 223
9. M. M. Heravi, Kh. Bakhtiari, F. F. Bamoharram, *Catal. Commun.* **7** (2006) 373
10. F. F. Bamoharram, M. M. Heravi, M. Roshani, M. Akbarpour, *J. Mol. Catal., A* **253** (2006) 16
11. M. M. Heravi, F. K. Behbahani, F. F. Bamoharram, *J. Mol. Catal., A* **253** (2006) 16
12. M. M. Heravi, R. Motamedi, N. Seifi, F. F. Bamoharram, *J. Mol. Catal., A* **249** (2006) 1
13. F. F. Bamoharram, M. M. Heravi, M. Roshani, M. Jahangir, A. Gharib, *J. Appl. Catal., A* **302** (2006) 42
14. Y. Matsumoto, M. Asami, M. Hashimoto, *J. Mol. Catal*. **114** (1996) 161
15. N. Mizuno, T. Hirose, M. Tateishi, *J. Mol. Catal.* **88** (1994) 125
16. M. Hamamoto, Y. Nakayama, Y. Ishii, *J. Org. Chem.* **58** (1993) 6421
17. Proceedings of 3rd World Congress on Oxidation Catalysis, R. K. Grasselli, S. T. Oyama, A. M. Gaffney,J. E. Lyons, Eds., Elsevier, Amsterdam, 1997
18. C. Rong, F. C. Anson, *Inorg. Chem*. **33** (1994) 1064
19. F. Cavani, C. Comuzzi, *J. Catal.* **160** (1996) 317
20. S. Shikata, S. Nakata, T. Okuhara, M. Misono, *J. Catal.* **166** (1997) 263
21. B. L. Hayes, *Microwave Synthesis. Chemistry at the Speed of Light*, CEM Mattehews, NC, USA, 2002.
22. C. O. Kappe, *Angew. Chem., Int. Ed.* **43** (2004) 6250
23. C. Robert, A. Poole, P. Andrew, *Biochem. J.* **259** (1989) 105
24. G. A. Tsigdinos, C. J. Hallada, *Inorg. Chem.* **7** (1968) 437
25. M. H. Alizadeh, S. P. Harmalker, M. T. Pope, *J. Am. Chem. Soc*.**107** (1985) 2662.

Journal of the Serbian Chemical Society
version electronic
JSCS-info@shd.org.rs • www.shd.org.rs/JSCS

J. Serb. Chem. Soc. 76 (11) 1523–1536 (2011)
JSCS–4226
UDC 547.262+66.094.3+546.92+546.811+
546.96+546.97:544.4+539.12
Original scientific paper

Impact of the modification of carbon-supported, Pt-based catalysts by irreversibly adsorbed Sn, Ru and Rh on ethanol oxidation

JELENA D. LOVIĆ*#, AMALIJA V. TRIPKOVIĆ# and KSENIJA DJ. POPOVIĆ#

ICTM – Institute of Electrochemistry, University of Belgrade, Njegoševa 12,
P. O. Box 473, 11000 Belgrade, Serbia

(Received 17 February, revised 7 April 2011)

Abstract: The oxidation of ethanol was studied at Sn_{ad}-, Ru_{ad}- and Rh_{ad}-modified and unmodified PtC, Pt_3Sn/C and Pt_3Ru_2/C catalysts. Potentiodynamic, quasi-steady-state and chronoamperometric measurements were used to investtigate the activity and stability of the catalysts. Irreversible adsorption of a small amount of each of the adatoms (≈10 % surface coverage) enhanced the activity of the Pt/C and Pt_3Sn/C catalysts. The onset potential was shifted by ≈50 mV towards lower values and the current densities over the whole studied potential region were up to two times higher with respect to the unmodified catalysts. On the other hand, the addition of Sn_{ad} or Rh_{ad} slightly increased the activity of Pt_3Ru_2/C, while the presence of Ru_{ad} decreased its activity for ethanol oxidation. The catalytic action of Sn_{ad} and Ru_{ad} was associated mostly with their ability to adsorb oxygen-containing species at lower potentials than Pt, permitting a bifunctional mechanism to proceed. Rh_{ad} also acted on the C–C bond breaking activation as well as source of oxygen containing species, increasing in this way the activity of the modified surfaces for ethanol oxidation.

Keywords: ethanol oxidation; Pt nanocatalyst; Pt–Sn nanocatalyst; Pt–Ru nanocatalyst; Pt–Rh nanocatalyst; adatom modification.

INTRODUCTION

Ethanol is a promising candidate to replace methanol in fuel cells due to its higher energy density that corresponds to 12 electrons per molecule in the total oxidation, low toxicity, mass production from renewable sources and easy storage and transportation. The complete oxidation of ethanol entails dehydrogenation, C–C bond cleavage and the stripping of the resulting adsorbed CO. The fragmentation of ethanol on catalyst surfaces generating stable adsorbates has

---

* Corresponding author. E-mail: jlovic@tmf.bg.ac.rs

Serbian Chemical Society member.

doi: 10.2298/JSC110217136L

been the subject of many previous studies using both *in situ* infrared spectroscopy (FT-IR) and differential electrochemical mass spectrometry (DEMS).[1–5] Although the mechanistic details of ethanol oxidation in acidic solution on a pure Pt electrode still remain unclear, the general view is that acetaldehyde (CH_3CHO) and acetic acid (CH_3COOH) are the main products, with carbon dioxide (CO_2) appearing at very high positive potentials. Thus, the major challenge for the electrocatalysis of ethanol is to achieve its total oxidation to CO_2 at low overpotentials.

Despite of fact that platinum is generally known as one of the best electrocatalyst for alcohol oxidation at low temperatures, it has limited ability for C–C bond scission and is easily poisoned by CO and other carbonaceous intermediates. Different C_1 and C_2 adsorbates formed in the oxidative adsorption of ethanol have been identified.[1,2,6–8] CO_2 is formed from strongly adsorbed intermediates on the electrode, while the products of partial oxidation, acetaldehyde and acetic acid, are formed from weakly adsorbed intermediates.[1,9] The efficiency of C–C bond activation in ethanol oxidation is the key to enable this reaction to be useful in fuel cell applications. Hitherto, this efficiency was quite low and partial oxidation products, acetaldehyde and acetic acid, were observed.[10,11]

The addition of a second metal to Pt by underpotential deposition or by alloying creates bimetallic catalysts and changes the electronic and structural properties of the base material, causing a change of its catalytic activity. It also alters the number of large Pt ensembles on platinum surfaces, which are important for site-demanding processes, such as C–C bond cleavage.

The activity of binary electrocatalysts was attributed to a bifunctional effect (Pt adsorbs alcohol and oxidizes H, while the second metal supplies oxygen-containing species to oxidize the blocking intermediate CO) or to the electronic interaction between Pt and alloyed metals.[12–14] These effects may influence ethanol oxidation on bimetallic catalyst in a way either to accelerate the oxidation of the CO adsorbate, as in the case of PtSn and PtRu bimetallic electrodes,[2,3,15,16] or to improve C–C bond activation, as in the case of PtRh.[17] It was shown that PtSn/C bimetallic carbon-supported materials are more active than PtRu/C electrocatalysts for ethanol oxidation.[15,18] The different promotion effects of PtSn/C and PtRu/C to ethanol oxidation can be explained by the structural effect (difference in alloy phase structure and particle morphology) and by modified bifunctional mechanisms in different potential regions.[18] However, the electro-oxidation of ethanol on PtSn/C or PtRu/C yields almost only partially oxidized products acetaldehyde and acetic acid, *i.e.*, the presence of Sn or Ru did not improve the conversion of ethanol to CO_2. On the other hand, PtRh bimetallic catalysts show significant activity for the production of CO_2 from ethanol, although the reaction currents are almost similar to that of a platinum electrode.[10,19] It was proposed, from the results of DEMS measurements, that the strong CO–Rh bond or slow dehydrogenation on Rh diminish the overall ethanol oxidation reaction (EOR) rate.[17]

In order to improve both the activity and selectivity (the overall reaction rate), ternary catalysts, such as PtSnRh/C, PtRuRh/C or PtRuSn/C, were made using different methods of preparation.[7,19–22] The joint action of the three constituents could explain the large activity of ternary catalysts for ethanol oxidation. In the catalysts containing Rh, the role of Rh was to adsorb and stabilize the key intermediate, which leads to cleavage of C–C bonds, Sn or Ru provides OH species necessary for the oxidation of CO adsorbed on Rh sites, while Pt facilitates ethanol dehydrogenation. It was shown that ternary Pt–Sn–Rh alloy catalysts possess the highest activity for ethanol electro-oxidation at potentials higher than 0.45 V (RHE), as a consequence of geometric and electronic modification due to the formation of a ternary alloy phase.[23] A Pt–Ru–Rh/C catalyst exhibited a compromise between the overall reaction rate and CO_2 yield, *i.e.*, both characteristics were between those of Pt–Ru/C and Pt–Rh/C.[19] In a recent work of Kowal *et al.*,[24] it was stated that a ternary Pt–Rh–SnO_2 electrocatalyst was effective in splitting the C–C bond in ethanol at room temperature and caused its predominant oxidation to CO_2 at very low overpotentials. The catalytic property of this ternary electrocatalyst was attributed to the synergistic effect between all three constituents.

On the other hand, the ternary PtRuSn/C catalyst, benefited from the simultaneous presence of Ru and Sn and the positive effect was ascribed mainly to interactions between Sn and Ru oxides.[17,21,22] The addition of 10 wt. % of Sn to PtRu/C resulted in an excellent performance and a two-fold enhancement compared with PtSn/C.[25]

The irreversible adsorption of Sn, Rh or Ru at Pt/C does not perturb significantly Pt structurally or electronically, as was shown in spectroscopic studies,[26–28] although the presence of the second metal alters the number of large Pt ensembles, which may be important for the site demanding process of C–C bond cleavage. The catalytic action of Sn or Ru atoms was associated mostly with their ability to adsorb oxygenated species at lower potentials than Pt, permitting the bifunctional mechanism to proceed.[15] Both of these two metals are inactive for ethanol adsorption. Moreover, Rh alone is inactive for ethanol oxidation, but it is capable of adsorbing and stabilizing the intermediate formed by ethanol dehydrogenation, which leads to cleavage of C–C bonds at a reasonable rate, as well as to act as a source of oxygenated species.[19]

Recently, the activity of Pt–Sn/C and Pt–Ru/C in ethanol oxidation was correlated with the degree of alloying. Although the results reported so far are generally not in agreement, most of them indicate that highly alloyed catalysts promote ethanol oxidation.[3,23,29,30]

In a previous work,[31] ethanol oxidation was studied at two alloys, Pt_3Sn/C and Pt_3Ru_2/C, as well as on a Pt/C catalyst modified with the corresponding amounts of Sn_{ad} (25 % surface coverage) and Ru_{ad} (40 % surface coverage) in order to simulate the alloy composition of the catalysts. The comparative investigation based on the effects influencing the catalytic properties of these electrodes contributed to a better understanding of the different activities between alloys, as well as between alloys and Pt/C modified by the corresponding amounts of irreversibly adsorbed Sn and Ru.

In the present study, ethanol oxidation was investigated on carbon-supported Pt-based catalysts modified with a small amount (≈10 %) of irreversibly adsorbed Sn, Rh and Ru. The idea of such surface modifications arose from the fact that modification of Pt_3Sn/C with a small amount of Sn_{ad} created a powerful catalyst for overall ethanol oxidation,[31,32] as well as from a previous theoretical study[24] in which it was shown that a low Rh content relative to Pt is likely to facilitate C–C bond breaking in the system.

The main goal of the present work was to examine the influence of electrode composition on the electrocatalytic activity toward the electrochemical oxidation of ethanol in order to explain the difference between modified and unmodified Pt-based catalysts and finally, to determine the optimal concentration of the constituents that gives the most active catalyst for the EOR.

EXPERIMENTAL

Electrode preparation

Commercially available Pt-based catalysts supported on high surface area carbon were used: platinum (Pt/C) with 47.5 wt. % Pt and platinum–ruthenium (Pt_3Ru_2/C) with 33.5 wt. % alloy provided by Tanaka Precious Metals Group (Kikinzoku International K.K) and platinum–tin (Pt_3Sn/C) with 20 wt. % alloy provided by E-Tek, USA. The catalysts were characterized by X-ray diffraction analysis.[31]

The catalysts were applied to a glassy carbon substrate in the form of a thin-film.[15] A suspension of 5 mg of the respective catalyst in a mixture of 1 ml water, 1 ml ethanol and 50 µl of a 5 % aqueous Nafion solution was prepared in an ultrasonic bath and 10 µl of the suspension was placed onto the substrate (5 mm diameter) and dried at room temperature to form a homogenous catalyst layer. The resulting metal loading was 25 µg cm^{-2}.

To avoid the contribution of any other anions, surface modification by the adatoms was achieved by holding a freshly prepared electrode at –0.2 V in 0.1 M $HClO_4$ solution containing Sn, Ru or Rh ions, produced by dissolving the required metal from the alloy matrix of Pt_3Sn/C, Pt_3Ru_2/C and PtRh/C, respectively, during cycling (20 cycles) at different anodic limits. The adatom-modified electrode was then rinsed with water and transferred to the electrochemical cell.

Electrochemical measurements

Electrochemical measurements were performed at room temperature in N_2-purged 0.1 M $HClO_4$ solution in a standard three compartment electrochemical cell with a Pt wire as the counter electrode and a saturated calomel electrode (SCE) as the reference electrode. The reagents used were of p.a. purity (Merck) and solutions were prepared with high purity water

("Millipore", 18 MΩ cm resistivity). Ethanol (0.5 M) was added to the solution while holding the electrode potential at –0.2 V. The catalytic activity was measured using the potentiodynamic (sweep rate 20 mV s^{-1}), quasi-steady-state (sweep rate 1 mV s^{-1}) and chronoamprometric methods. The potentials are given *versus* SCE and the currents were normalized per total mass of metal and are expressed as mA mg^{-1}.

The current–time transient curves were recorded during 30 min upon immersion of the electrode in the solution at –0.2 V for 2 s prior to stepping to 0.2 V.

A VoltaLab PGZ402 (Radiometer Analytical, France) was used in the electrochemical experiments.

RESULTS AND DISCUSSION

Polarization curves for ethanol oxidation on unmodified and Sn_{ad}, Ru_{ad} and Rh_{ad} modified Pt/C, Pt_3Ru_2/C and Pt_3Sn/C catalysts in acid solution are shown in Fig. 1. The positive potential limit was set at 0.3 V to prevent any dissolution of Sn, Rh or Ru.

A comparative investigation of ethanol oxidation on the Pt-based catalysts showed that both alloys are more active than Pt/C, as was found previously.[31] The initial potentials on the Pt_3Sn/C and Pt_3Ru_2/C catalysts were approximately –0.1 V and –0.05 V, respectively, and the reaction rates at the alloyed catalysts were higher than that at Pt/C, particularly at Pt_3Sn/C. On the Pt/C catalyst, the reaction commences at ≈0.1 V, when dissociative adsorption of water occurred providing the OH_{ad} species[33] required for the oxidation of the C_1 and C_2 intermediates generated by dissociative adsorption of ethanol.

The activity of the Pt/C catalyst was improved in the presence of irreversibly adsorbed adatoms and reaction commenced at ≈0.05 V less positive potentials relative to the unmodified Pt/C (Fig. 1). The negative shift of the starting potential was more pronounced at the modified Pt_3Sn/C electrode (≈100 mV), while it was the least expressed on the modified Pt_3Ru_2/C catalyst compared to the unmodified Pt-based alloy catalysts.

The catalytic action of Sn_{ad} or Ru_{ad} on the investigated electrodes was correlated generally to their ability to dissociate water at lower potentials than Pt, enabling the bifunctional mechanism between the adsorbed species on Pt and the OH species adsorbed on the added metals to proceed (Fig. 1a and b).[12] Spectroscopic analysis of Sn_{ad} on Pt/C showed that Sn_{ad} interacted with oxygen species in a similar manner as in the Pt_3Sn/C alloy.[28] The high activity of this alloy originates mainly from the electronic effect resulting in weak bonded adsorbate generated by ethanol adsorption on the Pt sites,[34,35] and an appropriate amount of oxygen-containing species, weakly bound to the Sn sites.[36,37] On the other hand, the underpotential deposition of Sn on Pt/C did not provoke any significant electronic changes in Pt,[27] which means that Sn_{ad} did not interfere remarkably with the ability of Pt to adsorb strongly ethanol or the adsorbate generated by ethanol dissociation. A small amount of Sn (≈10 %) irreversibly adsorbed on Pt_3Sn/C (Fig. 1a) improved the activity of the alloy, creating a powerful catalyst for ethanol oxidation.[31,32] The high activity of this catalyst can be explained by a combination of the electronic effect and the easier mobility of Sn_{ad},[38] with an enhanced amount of oxygen-containing species on the Sn.

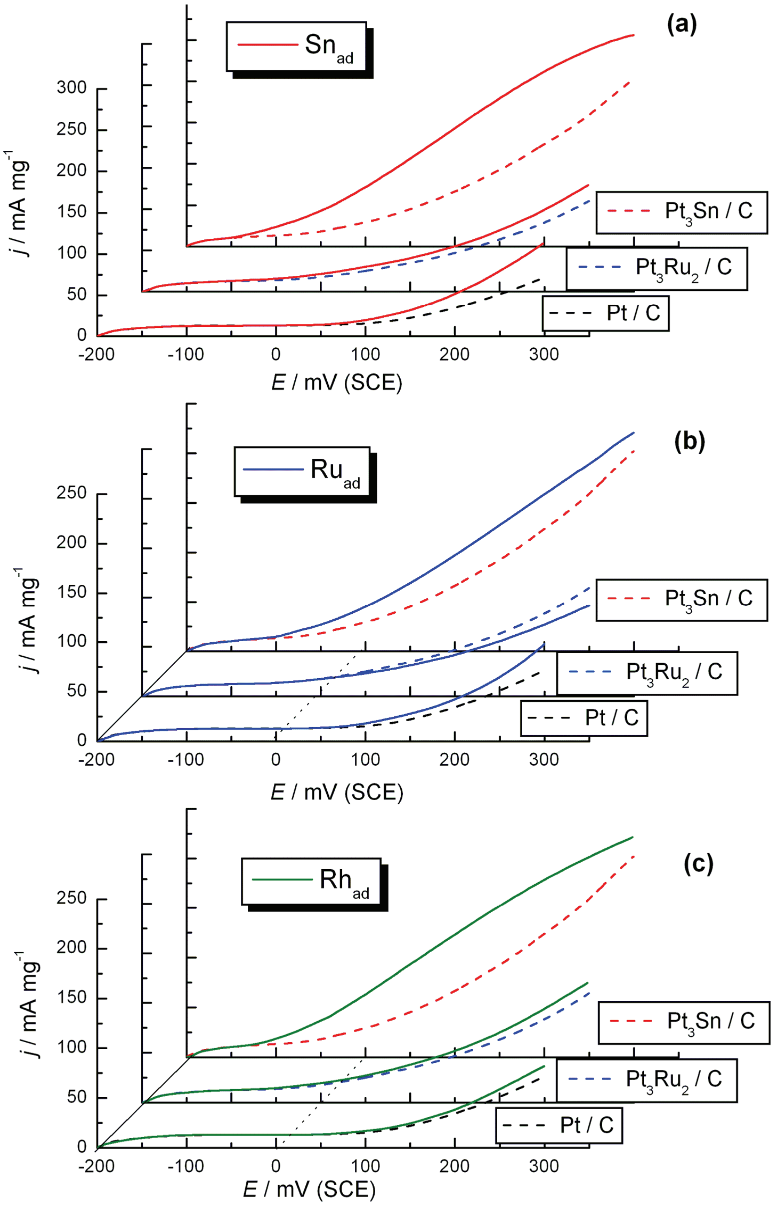

Fig. 1. Potentiodynamic curves for the oxidation of 0.5 M C_2H_5OH in 0.1 M $HClO_4$ at Pt/C, Pt_3Ru_2/C and Pt_3Sn/C: a) unmodified and modified with 10 % Sn_{ad}; b) unmodified and modified with 10 % Ru_{ad}; c) unmodified and modified with 10 % Rh_{ad}. $v = 20$ mV s^{-1}.

Irreversible adsorption of Ru on Pt/C or Pt_3Sn/C did not provoke significant electronic changes in Pt[26,27] and therefore ethanol oxidation on respective catalysts obeyed the conditions relevant for the bifunctional mechanism (Fig. 1b). The addition of 10 % Ru improved slightly the activity of these catalysts due to the increased amount of oxygen-containing species on the Ru sites. On the contrary, the decreased activity of Pt_3Ru_2/C modified by 10 % Ru was the consequence of the disturbance of the conditions relevant for the bifunctional mechanism, *i.e.*, the appropriate ratio between Pt sites, which adsorb ethanol, and Ru sites, which nucleate oxygen containing species necessary to oxidize the adsorbates. The ratio between Pt and Ru that provides the best catalytic performance is 60:40, is fulfilled in the Pt_3Ru_2/C catalyst.[39]

The addition of Rh slightly enhanced the reaction rate on all the investigated catalysts. The effect of Rh_{ad} on Pt/C was less expressed compared to Sn_{ad} or Ru_{ad} (Fig. 1c). The role of Rh is to adsorb C_2 intermediates formed by ethanol dehydrogenation, to stabilize them and permit the cleavage of C–C bonds.[40] Nevertheless, Rh is less efficient for the dehydrogenation reaction compared to Pt; thus a relatively high-energy barrier for the dehydrogenation can hinder C–C bond scission necessary for the formation of CO.[10] Thereby, the CO coverage during the reaction must be lower on surfaces containing Rh. At the same time, the presence of OH_{ad} species on Rh at lower potentials compared to Pt could enhance the oxidation of reaction intermediates. The present results are consistent with a small enhancement of the catalytic effect in ethanol oxidation observed on carbon-supported PtRh (9:1) catalyst relatively to Pt/C and the role of Rh on bimetallic PtRh electrodes was associated with the changes in the electronic properties caused by the addition of Rh to Pt.[10,41]

The catalytic activity of all the investigated catalysts at $E = 0.2$ V are summarized in Table I. The most active was Pt_3Sn/C modified with Sn_{ad}, which was 1.7 times more active than Pt_3Sn/C and even 6 times more active than Pt/C. It is also notable that the Ru modified Pt_3Ru_2/C electrode was less active than Pt_3Ru_2/C by almost 15 %.

TABLE I. Mass-specific current densities (j / mA mg^{-1}) of the respective catalysts at $E = 0.2$ V (SCE)

Catalyst	Unmodified	Sn_{ad}	Rh_{ad}	Ru_{ad}
Pt/C	34.7	52.5	38.4	42.2
Pt_3Sn/C	124.2	212.4	180.0	160.2
Pt_3Ru_2/C	63.6	160.2	70.8	56.0

From a practical point of view, not only is the initial activity of catalysts an important factor, but also the improvement of their poisoning tolerance. This is possible to illustrate by measuring the current densities of ethanol electro-oxidation at a constant potential as a function of time. In this sense, chronoamperometric experiments were performed (Fig. 2). The highest initial current density at 0.2 V on Pt_3Sn/C compared to the other two unmodified catalysts is in accordance with the potentiodynamic measurements (Fig. 1). The currents decayed rapidly at the Pt/C and Pt_3Ru_2/C catalysts, reaching their steady state values within a few minutes. On the contrary, at the Pt_3Sn/C catalyst, the initial current decreased slightly and stabilized in the experimental period of time at a value which was about two times higher than at the Pt_3Ru_2/C catalyst. The Pt_3Sn/C catalyst is evidently less poisoned than Pt_3Ru_2/C or Pt/C, since weaker bound adsorbate on the electronically modified Pt in Pt_3Sn/C could be more easily oxidized than on Pt_3Ru_2/C or Pt/C.

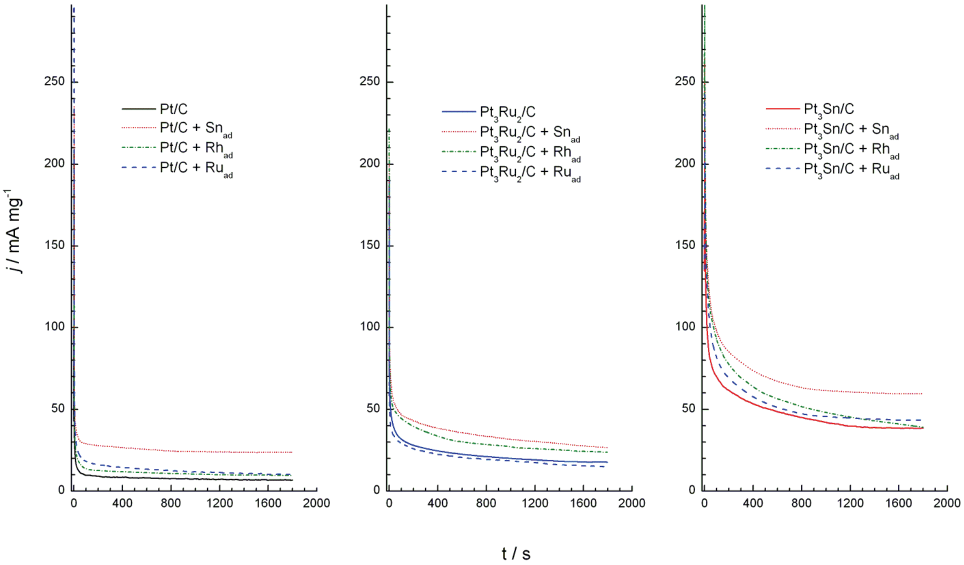

Fig. 2. Chronoamperometric curves for the oxidation of 0.5 M C_2H_5OH in 0.1 M $HClO_4$ at 0.2 V at: a) Pt/C unmodified and modified with 10 % Sn_{ad}, Ru_{ad} and Rh_{ad}; b) Pt_3Ru_2/C unmodified and modified with 10 % Sn_{ad}, Ru_{ad} and Rh_{ad}; c) Pt_3Sn/C unmodified and modified with 10 % Sn_{ad}, Ru_{ad} and Rh_{ad}.

At 0.2 V, the initial current densities at the Sn_{ad}-modified Pt_3Sn/C were significantly increased compared to the unmodified catalyst and they were much higher than at the other catalysts studied with or without Ru_{ad} and Rh_{ad}. The current decayed slower at the Sn_{ad}-modified than on the unmodified Pt_3Sn/C catalyst, indicating less accumulation of CO_{ad} species. Finally, two times higher current densities were achieved at the Sn_{ad}-modified Pt_3Sn/C than on Pt_3Sn/C, which was about 9 times more active than Pt/C. This corresponds with the results obtained in the potentiodynamic measurements (Fig. 1).

The electrocatalytic activity of the catalysts studied for ethanol oxidation after 30 min increased in the sequence: Pt/C < Pt/C+Rh_{ad} < Pt/C+Ru_{ad} < Pt_3Ru_2/C

+ Ru_{ad} < Pt_3Ru_2/C < Pt/C + Sn_{ad} < Pt_3Ru_2/C + Rh_{ad} < Pt_3Ru_2/C + Sn_{ad} < Pt_3Sn/C < Pt_3Sn/C + Ru_{ad} < Pt_3Sn/C + Rh_{ad} < Pt_3Sn/C + Sn_{ad}, suggesting that the activity of the supported Pt-based catalysts can be associated with their CO tolerance, which was the most pronounced at the Sn_{ad}-modified Pt_3Sn/C catalyst.

Moreover, a (di/dt) = f(t) plot at small time values allows an evaluation of the initial poisoning rate, the greater the slope, the greater the initial poisoning of the electrode surface. The initial poisoning rates for the Pt-based catalysts with and without Sn_{ad} are presented in Fig. 3. It appears that Sn_{ad} leads to less poisoning, since the experimental slopes with added Sn were lower by a factor of 1.1, 1.22 and 1.6, compared to those obtained without the addition of Sn_{ad} to Pt/C, Pt_3Ru_2/C and Pt_3Sn/C, respectively.

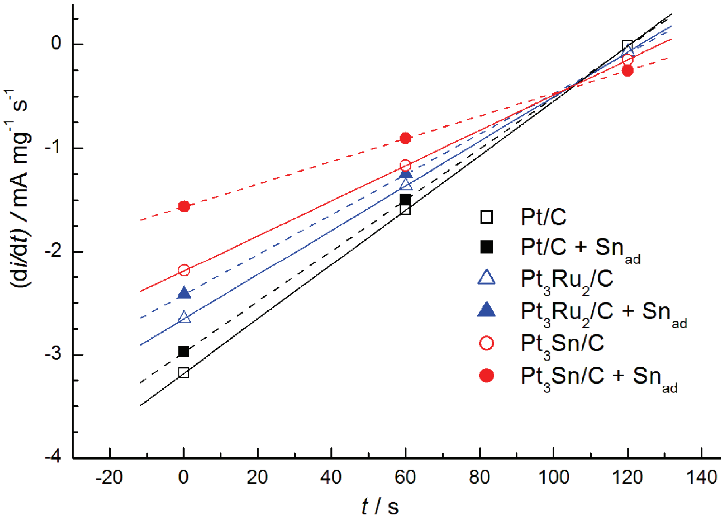

Fig. 3. di/dt = f(t) Curves for Pt/C, Pt_3Ru_2/C and Pt_3Sn/C catalysts with and without 10 % Sn_{ad}.

The quasi-steady-state results of ethanol oxidation on the investigated catalysts are given in Fig. 4. The Tafel slopes of ≈120 mV dec^{-1} obtained at the Sn_{ad}- and Rh_{ad}-modified electrodes and at the unmodified Pt_3Sn/C catalyst indicate that the first electron transfer could be the rate determining step.[29] The higher Tafel slopes of 140–150 mV dec^{-1} at the Ru_{ad}-modified electrodes and the unmodified Pt_3Ru_2/C and Pt/C catalysts could be caused by large poisoning of the Pt.[42]

Hitherto, the mechanism of ethanol oxidation on bimetallic catalysts has been discussed mainly in terms of a bifunctional effect[12,39] and/or electronic effects.[34,35] Since the investigated irreversibly adsorbed adatoms did not change significantly the performance of the supported catalysts regarding ethanol adsorption, their promotional or inhibiting effect (as in the case of Ru_{ad} on Pt_3Ru_2/ /C) on ethanol oxidation requires additional explanation.

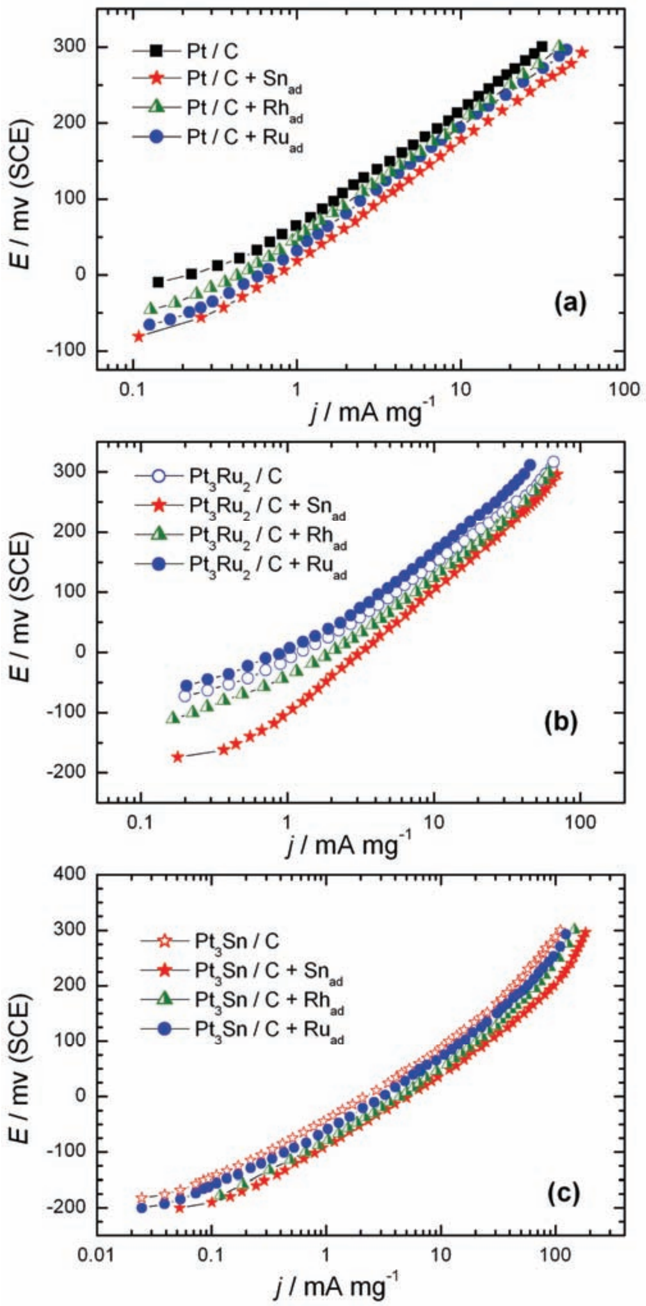

Fig. 4. Tafel plots for oxidation of 0.5 M C_2H_5OH in 0.1 M $HClO_4$ solution at: a) Pt/C unmodified and modified with 10% Sn_{ad}, Ru_{ad} and Rh_{ad}; b) Pt_3Ru_2/C unmodified and modified with 10% Sn_{ad}, Ru_{ad} and Rh_{ad}; c) Pt_3Sn/C unmodified and modified with 10% Sn_{ad}, Ru_{ad} and Rh_{ad}. $\nu = 1$ mV s^{-1}.

With the underpotential deposition of Sn, Ru and Rh, it was intended that different adsorption sites on the Pt particles be occupied. As Sn adatoms are mobile on a Pt surface,[38] it is reasonable to assume that they tend to nucleate on the edges of the Pt particles, preventing strong adsorption of poison and simultaneously providing for the adsorption of OH species on Sn_{ad} at lower potentials than on Pt/C, enabling the oxidation of the intermediates (C_1 and C_2 fragments) on the facet sites. This characteristic of Sn_{ad} should be more pronounced on Pt_3Sn/C than on Pt_3Ru_2/C or on Pt/C due to the change in the electronic structure of Pt on the alloyed surface.

Considering the irreversible adsorption of Ru, it was observed that Ru creates two-dimensional (2D) nanosized and catalytically active islands.[43] There was no preferential deposition of this metal on surface steps under both electrodeposition[44] and spontaneous deposition[45] conditions, indicating that the Ru nucleation does not occur preferentially at crystallographic defects, and that the Ru islands are randomly dispersed over the electrode surface (on facets and step sites), permitting the adsorption of poisoning and reactive species on the Pt active step sites. Although the capability of Ru atoms to dissociate water is larger than that of Sn atoms, Ru-modified surfaces (by irreversible adsorption or alloying) creates catalysts less active than Sn-modified surfaces because of the higher poisoning.[26] This refers to the all the investigated Pt-based catalysts.

Rhodium adlayers also grow in islands, but primarily on the facets, leaving large domains of the surface uncovered, including steps and defect sites.[46,47] As Rh adatoms in the periphery of the islands form steps with the platinum substrate, the islands boundaries (Pt–Rh adsorption sites) could have an enhanced reactivity toward OH and ethanol dissociative adsorption, *i.e.*, the periphery of the islands would contain bifunctional catalytic centers.

In spite of the capability of Ru and Rh atoms to dissociate water at lower potentials with respect to Pt, thereby providing oxygen-containing species to oxidize adsorbed fragments generated from ethanol, the Rh_{ad}-modified Pt/C catalyst was less active than the Ru_{ad}-modified Pt/C catalyst, most likely due to the slightly stronger bond between the adsorbate and Rh.[17]

On both alloys, the effect of Rh_{ad} was more expressed compared to Ru_{ad}. The possible explanation is the presence of larger amount of C_1 and C_2 intermediates in the presence of Rh, which could be oxidized with OH species weakly bound on Sn or Ru sites in the corresponding alloys. This assumption must be supported by quantitative measurements; hence additional study is a necessity.

CONCLUSIONS

In this work, ethanol oxidation was investigated on carbon-supported Pt-based catalysts modified with a small amount (≈10 %) of irreversibly adsorbed Sn, Rh or Ru. The concept of such surface modification was to provide more sites for the adsorption of oxygen-containing species necessary for the oxidation of reaction intermediates and at the same time to maintain large Pt ensembles important for C–C bond scission.

The irreversible adsorption of all types of adatoms enhanced the activity of the Pt/C and Pt_3Sn/C catalysts. The onset potential was shifted by ≈50 mV towards lower values and the current densities over the whole studied potential region were up to two times higher in respect to the unmodified catalysts. On the other hand, the addition of Sn_{ad} or Rh_{ad} slightly increased the activity of Pt_3Ru_2/ /C, while the presence of a Ru_{ad} adlayer decreased its activity for ethanol oxidation. The catalytic actions of Sn_{ad} and Ru_{ad} were associated mostly with their ability to adsorb oxygen-containing species at lower potentials than Pt, permitting the bifunctional mechanism to proceed. Rh adatoms acted on the activation of C–C bond scission and were a source of oxygen-containing species, increasing in this way the activity of the modified surfaces for ethanol oxidation.

Electrochemical measurements revealed that Sn_{ad} had the most pronounced effect on ethanol oxidation on all the investigated Pt-based catalysts. The most active was Pt_3Sn/C modified with Sn_{ad} which was two times more active than Pt_3Sn/C and even 9 times more active than Pt/C according to chronoamerometric measurements. At the same time this catalysts was less prone to poisoning, suggesting a high CO tolerance.

Tafel slopes of ≈120 mV dec^{-1} obtained at the Sn_{ad}- and Rh_{ad}-modified electrodes and at the unmodified Pt_3Sn/C catalyst indicated that the first electron transfer could be the rate determining step. Higher Tafel slopes of 140–150 mV dec^{-1} at the Ru_{ad}-modified electrodes and the unmodified Pt_3Ru_2/C and Pt/C catalysts could be caused by a large poisoning of Pt.

Acknowledgements. This work was financially supported by the Ministry of Education and Science of the Republic of Serbia, Contract No. H-172060.

ИЗВОД

УТИЦАЈ МОДИФИКАЦИЈЕ ПЛАТИНСКИХ НАНОКАТАЛИЗАТОРА ИРЕВЕРЗИБИЛНОМ АДСОРПЦИЈОМ Sn, Ru И Rh НА ОКСИДАЦИЈУ ЕТАНОЛА

ЈЕЛЕНА Д. ЛОВИЋ, АМАЛИЈА В. ТРИПКОВИЋ и КСЕНИЈА Ђ. ПОПОВИЋ

ИХТМ – Центар за електрохемију, Универзитет у Београду, Његошева 12, п. пр. 473, 11000 Београд

Оксидација етанола је испитивана на Pt/C, Pt_3Sn/C и Pt_3Ru_2/C катализаторима модификованим иреверизибилно адсорбованим Sn_{ad}, Ru_{ad} и Rh_{ad} адатомима. Њихова активност и стабилност испитивана је потенциодинамичким, хроноамперометријским и квази-стационарним мерењима. Добијени резултати су показали да мала количина иреверзибилно адсорбованих адатома (10 %) повећава активност Pt/C и Pt_3Sn/C катализатора. Почетак реакције је померен ка негативнијим вредностима за ≈50 mV и добијене су око два пута веће густине струје у поређењу са немодификованим катализаторима. Додатак Sn_{ad} или Rh_{ad} мало повећава активност Pt_3Ru_2/C катализатора, док додатак Ru_{ad} смањује његову активност за оксидацију етанола. Каталитичка активност адатома Sn и Ru се углавном везује са њиховом спо-

собношћу да адсорбују OH честице на нижим потенцијалима од Pt и на тај начин побољшавају бифункционални механизам реакције. Повећана активност катализатора модификованих адатомима Rh може се објаснити лакшим кидањем C–C везе у етанолу, као и повећаном количином OH_{ad} честица на Rh местима.

(Примљено 17. фебруара, ревидирано 7. априла 2011)

REFERENCES

1. G. A. Camara, T. Iwasita, *J. Electroanal. Chem*. **578** (2005) 315
2. H. Wang, Z. Jusys, R. J. Behm, *J. Power Sources* **154** (2006) 351
3. L. Colmenares, H. Wang, Z. Jusys, L. Jiang, S. Yan, G. Q. Sun, R. J. Behm, *Electrochim. Acta* **52** (2006) 221
4. G. A. Camara, R. B. de Lima, T. Iwasita, *J. Electroanal. Chem*. **585** (2005) 128
5. F. Vigier, C. Coutanceau, F. Hahn, E. M. Belgsir, C. Lamy, *J. Electroanal. Chem*. **563** (2004) 81
6. M. H. Shao, R. R. Adžić, *Electrochim. Acta* **50** (2005) 2415
7. C. Coutanceau, S. Brimaud, C. Lamy, J.-M. Leger, L. Dubau, S. Rousseau, F. Vigier, *Electrochim. Acta* **53** (2008) 6865
8. S. C. S. Lai, E. F. Kleyn, V. Rosca, M. T. Koper, *J. Phys. Chem. C* **112** (2008) 19080
9. E. Pastor, T. Iwasita, *Electrochim. Acta* **39** (1994) 547
10. J. P. I. de Souza, S. L. Queiroz, K. Bergamaski, E. R. Gonzalez, F. C. Nart, *J. Phys. Chem. B* **106** (2002) 9825
11. H. Wang, Z. Jusys, R. J. Behm, *J. Phys. Chem. B* **108** (2004) 19413
12. M. Watanabe, S. Motoo, *J. Electroanal. Chem*. **60** (1975) 267
13. C. Lamy, E. M. Belgsir, J.-M. Leger, *J. Appl. Electrochem*. **31** (2001) 799
14. C. Lamy, S. Rousseau, E. M. Belgsir, C. Coutanceau, J.-M. Leger, *Electrochim. Acta* **49** (2004) 3901
15. Q. Wang, G. Q. Sun, L. H. Jiang, Q. Xin, S. G. Sun, Y. X. Jiang, S. P. Chen, Z. Jusys, R. J. Behm, *Phys. Chem. Chem. Phys.* **9** (2007) 2686
16. F. C. Simoes, D. M. dos Anjos, F. Vigier, J.-M. Leger, F. Hahn, C. Coutanceau, E. R. Gonzalez, G. Tremiliosi-Filho, A. R. de Andrade, P. Olivi, K. B. Kokoh, *J .Power Sources* **167** (2007) 1
17. K. Bergamaski, E. R. Gonzalez, F. C. Nart, *Electrochim. Acta* **53** (2008) 4396
18. H. Li, G. Sun. L. Cao, L. Jiang, Q. Xin, *Electrochim. Acta* **52** (2007) 6622
19. F. H. B. Lima, E. R. Gonzalez, *Electrochim. Acta* **53** (2008) 2963
20. A. Kowal, S. Lj. Gojković, K.-S. Lee, P. Olszewski, Y.-E. Sung, *Electrochem. Commun.* **11** (2009) 724
21. G. Wu, R. Swaidan, G. Cui, *J. Power Sources* **172** (2007) 180
22. E. Antolini, F. Colmati, E. R. Gonzalez, *Electrochem. Commun.* **9** (2007) 398
23. F. Colmati, E. Antolini, E. R. Gonzalez, *J. Alloys Comp*. **456** (2008) 264
24. A. Kowal, M. Li, M. Shao, K. Sasaki, M. B. Vukmirović, J. Zhang, N. S. Marinković, P. Liu, A. I. Frenkel, R. R. Adžić, *Nat. Mater*. **8** (2009) 325
25. Y.-W. Chang, C.-W. Liu, Y.-C. Wei, K.-W. Wang, *Electrochem. Commun.* **11** (2009) 2161
26. A. K. Shukla, A. S. Arico, K. M. El-Khatib, H. Kim, P. L. Antonucci, V. Antonucci, *Appl. Surf. Sci*. **137** (1999) 20

27. S. Mukerjee, J. McBreen, in *Proceedings of 2nd International Symp. on New Materials for Fuel Cells and Modern Battery Systems*, O. Savadoga, P. R. Roberge, Eds., Montreal, Canada, 1997, p. 548
28. S. Mukerjee, J. McBreen, *J. Electrochem. Soc*. **146** (1999) 600
29. M. Zhu, G. Sun, Q. Xin, *Electrochim. Acta* **54** (2009) 1511
30. R. F. B. de Souza, L. S. Parreira, D. C. Rascio, J. C. M. Silva, E. Teixeira-Neto, M. L. Calegaro, E. V. Spinace, A. O. Neto, M. C. Santos, *J. Power Sources* **195** (2010) 1589
31. A. V. Tripković, J. D. Lović, K. Dj. Popović, *J. Serb. Chem. Soc*. **75** (2010) 1559
32. A. V. Tripković, K. Dj. Popović, J. D. Lović, V. M. Jovanović, S. I. Stevanović, D. V. Tripković, *Electrochem. Commun.* **11** (2009) 1030.
33. T. Iwasita, *Electrochim. Acta* **47** (2002) 3663
34. I. Pašti, S. Mentus, *Mater. Chem. Phys*. **116** (2009) 94
35. P. Liu, A. Logadottir, J. K. Norskov, *Electrochim. Acta* **48** (2003) 3731
36. A. B. Anderson, E. Grantscharova, P. Schiller, *J. Electrochem. Soc*. **142** (1995) 1880
37. J. H. Kim, S. M. Choi, S. H. Nam, M. H. Seo, S. H. Choi, W. B. Kim, *Appl. Catal. B* **82** (2008) 89
38. Y. Yao, Q. Fu, Z. Zhang, H. Zhang, T. Ma, D. Tan, X. Bao, *Appl. Surf. Sci.* **254** (2008) 3808
39. G. A. Camara, R. B. de Lima, T. Iwasita, *Electrochem. Commun.* **6** (2004) 812
40. M. Li, A. Kowal, K. Sasaki, N. Marinković, D. Su, E. Korach, P. Liu, R. R. Adžić, *Electrochim. Acta* **55** (2010) 4331
41. E. V. Spinacé, R. R. Dias, M. Brandalise, M. Linardi, A. O. Neto, *Ionics* **16** (2010) 91
42. J. D. Lović, A. V. Tripković, S. Lj. Gojković, K. Dj. Popović, D. V. Tripković, P. Olszewski, A. Kowal, *J. Electroanal. Chem*. **581** (2005) 294
43. F. Maillard, G.-Q. Lu, A. Wieckowski, U. Stimming, *J. Phys. Chem. B* **109** (2005) 16230
44. K. A. Friedrich, K. P. Geyzers, A. J. Dickinson, U. Stimming, *J. Electroanal. Chem*. **524–525** (2002) 261
45. G.-Q. Lu, P. Waszczuk, A. Wieckowski, *J. Electroanal. Chem*. **532** (2002) 49
46. F. J. Gutierrez de Dios, R. Gomez, J. M. Feliu, *Electrochem. Commun.* **3** (2001) 659
47. R. Gómez, F. J. Gutiérrez de Dios, J. M. Feliu, *Electrochim. Acta* **49** (2004) 1195.

Journal of the Serbian Chemical Society
JSCS-info@shd.org.rs • www.shd.org.rs/JSCS

J. Serb. Chem. Soc. *76* (11) 1537–1550 (2011)
JSCS–4227

UDC 546.47’73:544.642.076.2:
544.654.2:620.193
Original scientific paper

Microstructure and corrosion behaviour of Zn–Co alloys deposited from three different plating baths

JELENA B. BAJAT[1*#], SANJA I. STEVANOVIĆ[2#] and BOJAN M. JOKIĆ[1#]

[1]*Faculty of Technology and Metallurgy, University of Belgrade, Karnegijeva 4, 11120*
Belgrade and [2]*ICTM – Institute of Electrochemistry, University of Belgrade,*
Njegoševa 12, 11001 Belgrade, Serbia

(Received 31 March, revised 4 July 2011)

Abstract: The effects of plating baths of different composition on the microstructure and corrosion stability of Zn–Co alloy coatings were studied. Zn–Co alloys with the same Co content were deposited from chloride plating baths containing different amounts of Co^{2+}, as well as from a sulphate–chloride plating bath. The surface morphology and crystallite size were investigated by scanning electron microscopy (SEM) and atomic force microscopy (AFM). The corrosion stability of the Zn–Co alloys was determined by following the change of the open circuit potential with time of immersion in a 3 % NaCl solution and by polarization measurements. The results showed a significant influence of the plating bath on the morphology and corrosion stability of the Zn–Co alloys. The surface of the alloy coatings deposited from the chloride baths were uniform and homogenous, whereas the deposit obtained from the sulphate–chloride bath was quite inhomogeneous. The corrosion stability of the homogenous Zn–Co deposits obtained by deposition from both chloride baths was higher than that of the deposit obtained from the sulphate–chloride bath. An increase in the Co content in the chloride-plating bath resulted in a reduction of the alloy crystallite size and it was shown that the alloy with the smaller crystallites of the two alloy deposits, although having the same chemical content, exhibited a lower corrosion rate.

Keywords: electrodeposition; coatings; Zn–Co alloy; corrosion; AFM.

INTRODUCTION

The electrodeposition of zinc alloy coatings has been of interest recently since these alloys provide better corrosion protection than pure zinc coatings.[1–4] The alloying of Zn is easily achieved with more noble metals, mostly with metals of the iron group (Ni, Co and Fe).[5–11] If zinc alloys have effectively a high

---

[*] Corresponding author. E-mail: jela@tmf.bg.ac.rs
[#] Serbian Chemical Society member.
doi: 10.2298/JSC110331137B

amount of zinc, they can still maintain a sufficiently negative potential to steel and yet, offer better corrosion protection than zinc alone.[9] It is stated in the literature that the main corrosion product for all zinc-coatings is zinc hydroxide chloride, $Zn_5(OH)_8Cl_2 \cdot H_2O$ (ZHC).[4,6,11,12] According to the corrosion mechanism suggested by Lambert,[13] zinc dissolves preferentially at the beginning of the corrosion process, providing galvanic protection to the steel. This, however, leads to an enrichment of the alloy with the nobler component (dezincification) and the alloy coating becomes a composite-like structure, consisting of corrosion products and a layer rich in the alloying elements. This newly formed coating acts as a protective barrier layer, which reduces the corrosion rate.[10,13,14] This mechanism was confirmed by Short et al.[14] for Zn–Co alloys containing 1–10 % Co.

It is known that, compared with Zn and other Zn alloys, Zn–Co alloys have other superior properties, namely hardness, ductility, internal stresses, paintability and weldability.[15,16] Different plating baths for Zn–Co co-depositions are reported in the literature, giving deposits with varied properties.[3,17–22] The different properties of alloy coatings depend on their structure and composition, whereby the structure and composition of an alloy coating are determined by the plating parameters. Some of these parameters are: temperature of the plating bath, the type of the bath, the deposition current density or the deposition potential and the deposition mode.[23–25] Each of these parameters has its own influence on the structure and composition of an alloy coating, which, however, could often not be unambiguously defined, but are rather dependent on other plating parameters.

Since there are numerous publications related to Zn–Co alloy coatings having a low Co content (≈ 1 wt. %)[5,7,11,12,15] and not many reported on Zn–Co alloys with higher Co contents, Zn–Co deposits with 6 wt. % Co were investigated in this work. The aim of this work was to study the effects of three different plating baths on the morphology of Zn–Co coatings and their corrosion stability. Namely, it would be of interest to investigate Zn–Co deposits having the same Co content but obtained from different plating baths, and to determine how the type of the plating bath affects the morphology and the corrosion stability of the obtained Zn–Co deposits.

EXPERIMENTAL

Electrodeposition of Zn–Co alloys

Zn–Co alloys were deposited galvanostatically on a steel or platinum panel from three different plating baths (Table I) at room temperature (25±1 °C). The employed plating baths were free of additives since the aim of the study was to investigate only the influence of different deposition baths on the morphology and corrosion stability of Zn–Co deposits.

The electrolytes used were prepared using *p.a.* chemicals and high purity water (Millipore, 18 MΩ cm resistivity).

Deposition times were chosen to obtain Zn–Co deposits of 15-μm thickness.

The working electrodes for polarization measurements and open circuit potential measurements, as well as for scanning electron microscopy (SEM), atomic force microscopy (AFM) and energy dispersive spectroscopy (EDS), were Zn–Co alloys deposited on a steel (ISO T57) panel. The steel substrates were pre-treated by mechanical cleaning (abrading successively with emery papers of the following grades: 280, 360, 800 and 1000) and then degreased in a saturated solution of sodium hydroxide in ethanol, pickled with a 1:1 hydrochloric acid solution for 30 s and finally rinsed with distilled water. For determining the chemical composition, Zn–Co alloys were additionally deposited on platinum panels, then dissolved in a small amount of HCl solution (1:1) (5–10 cm^3) and the chemical composition was determined by atomic absorption spectroscopy. Prior to each electrodeposition, the Pt surface was mechanically polished with a polishing cloth (Buehler Ltd.) impregnated with an aqueous suspension of alumina powder (0.3 µm grade), and then rinsed with pure water in an ultrasonic bath.

TABLE I. Plating baths[26]

Bath	Composition	j_{dep} / A dm^{-2}	pH
Chloride	0.1 mol dm^{-3} $ZnCl_2$ 0.03 or 0.5 mol dm^{-3} $CoCl_2\cdot 6H_2O$ 0.4 mol dm^{-3} H_3BO_3 3 mol dm^{-3} KCl	2	5.5
Sulphate–chloride	0.24 mol dm^{-3} $ZnSO_4\cdot 7H_2O$ 0.1 mol dm^{-3} $CoSO_4\cdot 7H_2O$ 0.32 mol dm^{-3} H_3BO_3 2.0 mol dm^{-3} KCl	8	5.5

The counter electrodes were a zinc panel placed parallel to a steel panel for the electrodeposition of the alloys, or a Pt panel for the polarization and corrosion measurements. The reference electrode used in all experiments was a saturated calomel electrode (SCE).

The plating parameters were chosen (Table I) so that all the alloy deposits had the same Co content (≈ 6 wt. %).[26]

Corrosion measurements

The corrosion rates in aerated 3% NaCl solution (pH 6.7) of the electrodeposited Zn–Co alloys were determined using extrapolation of anodic polarization curves to the open circuit potential (OCP). A potential sweep rate of 0.2 mV s^{-1} was applied starting from the OCP, after a constant OCP had been established. The cathodic and anodic polarization curves were recorded in two separate experiments.

Chemical composition and surface morphology

The surface morphology of different Zn–Co deposits was observed by a JEOL JSM 5800 scanning electron microscope (SEM). The chemical content of deposited alloys was determined using an Oxford System for Energy Dispersive Spectroscopy (EDS) connected to the SEM. In addition, the chemical composition of the Zn–Co alloys was determined by atomic absorption spectroscopy (AAS) using an AAS-PYE Unicam SP9, Philips instrument.

The morphological characterization was performed by atomic force microscopy (AFM) using a NanoScope 3D (Veeco, USA) microscope operated in the tapping mode under ambient conditions. Etched silicon probes with a spring constant of 20–80 N m^{-1} were used.

RESULTS AND DISCUSSION

The effect of the plating bath on alloy deposition

Galvanostatic curves for deposition of Zn–Co alloys from different plating baths are presented in Fig. 1. It could be seen that the deposition potential greatly depends on both the type of the plating bath and the Co^{2+} content in the plating bath. Namely, the Zn–Co alloy deposited mainly at –1.22 V from the chloride bath containing the lower amount of Co^{2+} and the deposition potential advanced to a more noble value, –1.13 V, as the concentration of Co^{2+} in the bath increased. According to the Fig. 1, a higher overpotential was needed to create the initial nucleus during deposition from the bath with the lower Co^{2+} content. Similar results were reported for Zn–Ni deposition.[27] Plating from sulphate–chloride bath was performed at an even lower overpotential, –1.07 V, although the current density of electrodeposition was higher than in the cases of the chloride baths.

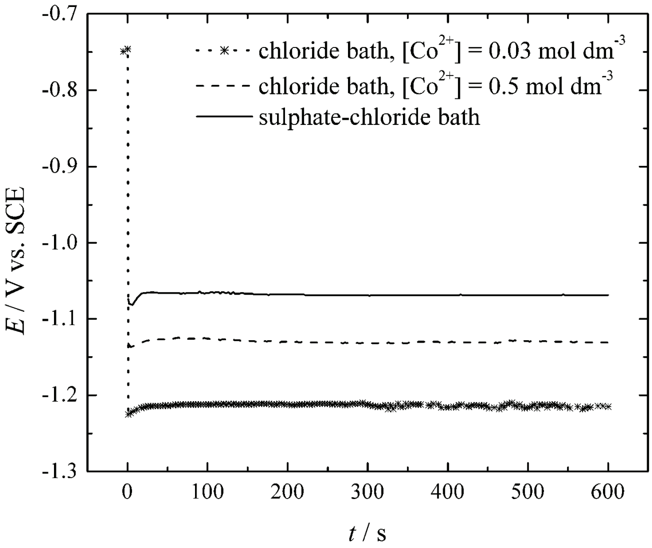

Fig. 1. Galvanostatic curves in different plating baths for the deposition of Zn–Co alloys.

The small potential fluctuation on the galvanostatic curves, especially pronounced for the curve related to Zn–Co deposition from the chloride bath with the lower amount of Co^{2+}, is the result of hydrogen evolution. Namely, the current efficiency for the electrodeposition of this alloy coating was the lowest (23 %)[26] as compared to 75[26] and 40 % for electrodeposition of Zn–Co coatings from the chloride bath with the higher amount of Co^{2+} and from the sulphate–chloride bath, respectively.

The differences in the deposition potentials from the two chloride baths were due not only to the different amounts of Co^{2+}, but also to the different ratios of

Co^{2+} to $Cl^{–}$ in the two plating baths. Namely, different types of complexes could be formed in aqueous halide solutions, depending on the cobalt to chloride ions ratio.[28] In electrolytes with a large excess of $Cl^{–}$ with respect to Co^{2+}, as it was the case in this work for the chloride plating bath with lower Co^{2+} content, at room temperature, it is considered that cobalt reactive species form complexes, $CoCl_4^{2–}$.[28] The $[Cl^{–}]/[Co^{2+}]$ ratio was very high (109) in this plating bath and, thus, electrodeposition was realized from complexes with the highest overpotential (Fig. 1). On the contrary, in plating baths with a low $[Cl^{–}]/[Co^{2+}]$ ratio, the reactive species are metal cations, Co^{2+}. The $[Cl^{–}]/[Co^{2+}]$ ratio was lower (≈8) for the chloride bath with the higher Co^{2+} content, which resulted in deposition with lower overpotential in respect to deposition from the other chloride bath. As a result of all the above-mentioned, the electrodeposition from the two different chloride plating baths resulted in deposits having the same amount of Co (≈6 wt. %) that were obtained at the same deposition current density, but at different overpotentials. The electrodeposition from sulphate–chloride plating bath was also performed at a low $[Cl^{–}]/[Co^{2+}]$ ratio, which was, however, more than two times higher (20) than in the chloride bath with the higher Co^{2+} content; hence, electrodeposition of the Zn–Co deposit with ≈6 wt. % Co from the sulphate–chloride plating bath was realized at a different current density and the lowest overvoltage.

Surface morphology

The surface morphology of electrodeposited Zn–Co alloys was investigated using SEM. SEM and optical microscopy have proved themselves to be convenient methods for the analysis of the surface morphology of electrochemical deposits[29,30] and in determining the crystallite size in alloy deposits. SEM Images of Zn–Co alloys having the same Co content, but deposited from different plating baths, are shown in Fig. 2.

SEM Analyses of the morphology of the samples studied indicate clear difference between the deposits obtained from the different plating baths. The deposit obtained from the chloride bath with the lower Co^{2+} content is illustrated in Fig. 2a. The surface of this alloy coating is uniform, homogenous and consists of irregular crystals particles. The surface morphology of the Zn–Co alloy obtained from the plating bath with the higher Co^{2+} content in the plating bath, at the same current density, is shown in Fig. 2b. This deposit is also homogenous and uniform, with a dense surface morphology covering the entire surface area. EDS Analysis showed the same chemical content over both these alloy deposits. It could be seen that increasing the cobalt content in the plating bath resulted in a reduction of the crystallite size (Figs. 2a and 2b). However, the deposit obtained from the sulphate–chloride bath is quite inhomogeneous (Fig. 2c). The local differences in chemical content for this deposit were determined using EDS. Namely, the Zn–Co alloy deposit obtained from sulphate–chloride bath also contained 6.0 wt. % Co, as determined by AAS. EDS Analysis, however, showed slight differences in the Co content in different areas of deposit, with the Co contents ranging from 5.7–8.3 wt. %. In addition, 3.0 % oxygen was also detected by EDS.

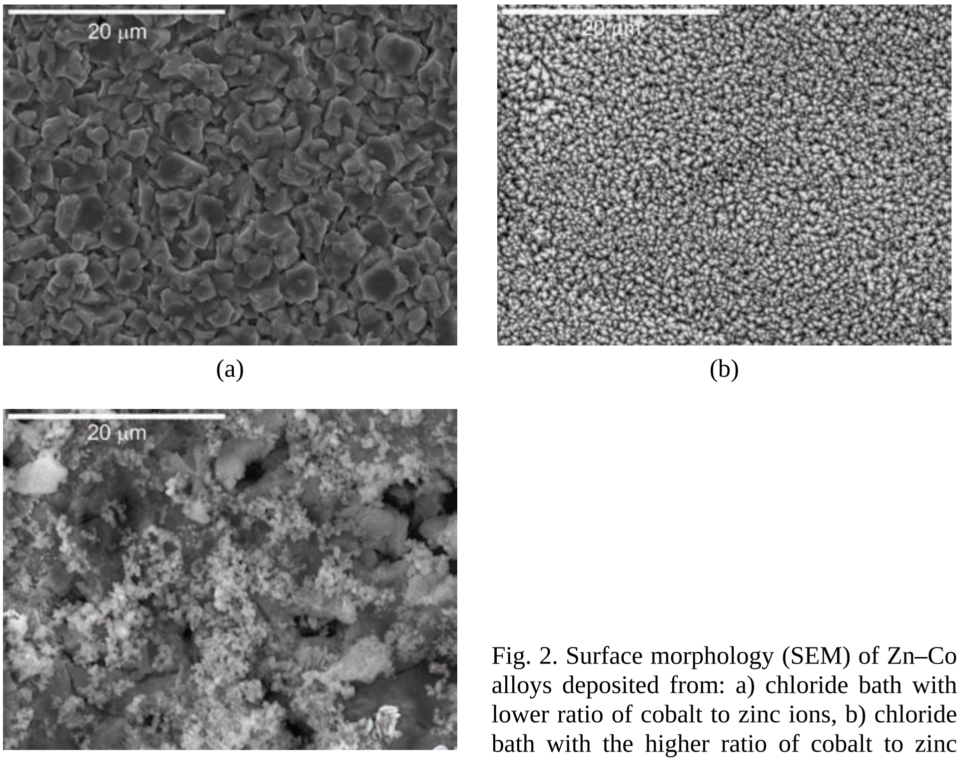

(a) (b)

(c)

Fig. 2. Surface morphology (SEM) of Zn–Co alloys deposited from: a) chloride bath with lower ratio of cobalt to zinc ions, b) chloride bath with the higher ratio of cobalt to zinc ions and c) sulphate–chloride bath.

Corrosion stability

The effect of the plating bath on the corrosion stability of the Zn–Co alloys was determined by following the change of the open circuit potential, E_{ocp}, with time of immersion in a 3 % NaCl solution and by polarization measurements. The open circuit potential of the bare steel surface in 3 % NaCl was –640 mV *vs.* SCE and it is marked with the dotted line in Fig. 3. The potentials of the Zn–Co alloys were more negative than that of the steel base under the same conditions; thus, the Zn–Co alloys provide sacrificial cathodic protection. The OCPs of the alloys deposited from all three baths were initially almost the same, but over time, they increased positively at different rates and reached almost the same values (the steel E_{ocp}) after different time intervals, which represent loss of the coating and the start of the corrosion process.

The results of the visually observed alloy destruction in 3 % NaCl solution, or the appearance of red rust on the steel base, are presented in Table II. The longest time before the appearance of red rust, indicating the best corrosion stability, was observed for Zn–Co alloy deposited from chloride bath with the higher Co^{2+} content, whereas the Zn–Co deposit obtained from the sulphate–chloride bath was destroyed the fastest.

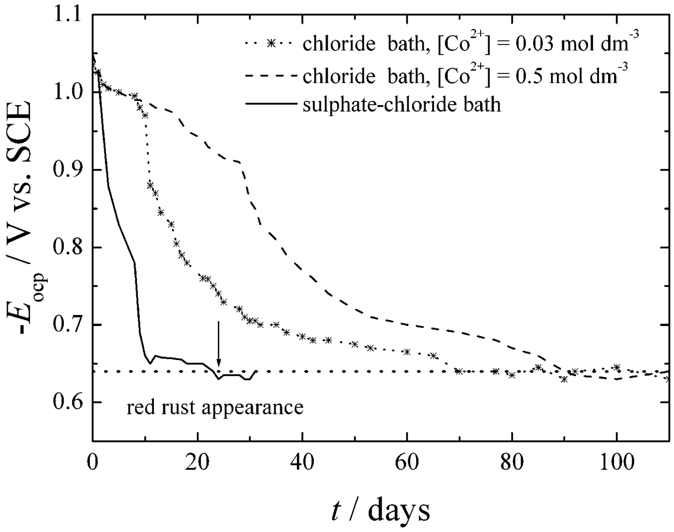

Fig. 3. The dependence of E_{ocp} for the Zn–Co alloys deposited on steel from different plating baths (15-μm thickness).

TABLE II. The time of red rust appearance and corrosion current densities, j_{corr}, for Zn–Co alloys deposited from different plating baths (all the data are mean values of 3–5 measurements)

Bath	Time, days	j_{corr} / μA cm^{-2}
Chloride, $[Co^{2+}]$ = 0.03 mol dm^{-3}	70	12
Chloride, $[Co^{2+}]$ = 0.5 mol dm^{-3}	92	3
Sulphate–chloride	23	40

In addition, polarization curves were obtained in a 3 % NaCl solution and are presented in the form of E–log j plots (Fig. 4). As can be seen, the anodic reaction is activation-controlled alloy dissolution, while the cathodic reaction is oxygen reduction under diffusion control. Thus, the corrosion current densities, j_{corr}, were determined from the intersect of the anodic Tafel plots with the OCP and the values are given in Table II. The data given in Table II are mean values of three to five measurements.

Since the amount of Co in alloy deposits was the same, the corrosion potential differs only slightly for all the alloy deposits. However, a clear difference among the samples could be seen from the potentiodynamic curves (Fig. 4). The corrosion rate of the deposit obtained by plating from the sulphate–chloride bath was higher than the ones deposited from the chloride baths. The highest corrosion stability was observed for the Zn–Co alloy deposited from the chloride bath with the higher Co^{2+} content. These results are in agreement with the results of the appearance of red rust.

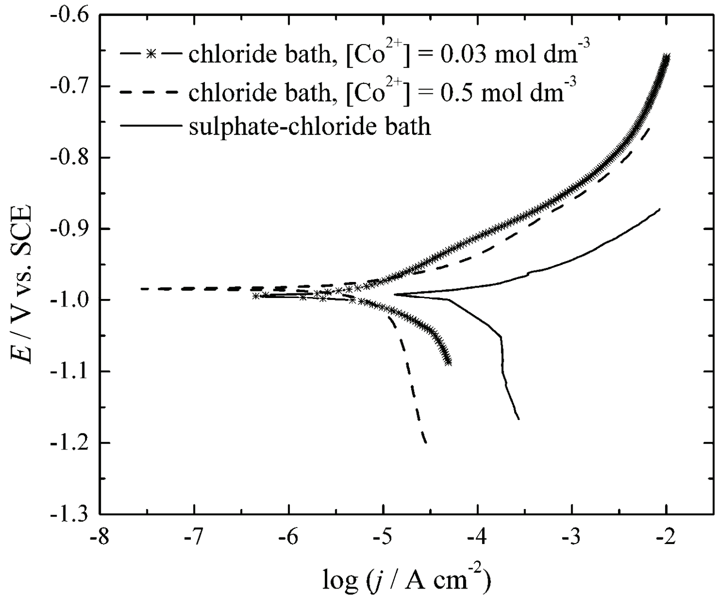

Fig. 4. Anodic polarization curves in 3 % NaCl for the Zn–Co alloys deposited from the different plating baths.

The differences in corrosion properties among the different Zn–Co alloys arise from the different surface morphology obtained by deposition from the different plating baths. Namely, it is well known that Zn coatings deposited from baths of various compositions have differences in porosity, structure and other characteristics, which, in turn, affect the corrosion resistance of the coatings.[9] It was shown in the literature that the phase composition of Zn–Co deposits is determined by their Co content.[22,26,31,32] Zn–Co deposits with between 4 and 10 wt. % Co are composed of quasi-pure Zn and the $Zn_{21}Co_5$ γ-phase.[31] However, since all the investigated Zn–Co alloys contained 6 wt. % Co, it is supposed that all deposits had the same phase structure, and that the differences in corrosion stability arise from the different morphologies of the alloy deposits obtained from the different plating baths.

It was shown in the literature that deposits formed from chloride baths have less inorganic inclusions as compared to deposits from sulphate baths and the presence of inorganic inclusions, in turn, leads to higher corrosion rates.[33] The Zn–Co deposit obtained from the sulphate–chloride bath did contain 3 % of oxygen (from oxide), as shown by EDS analysis. The inhomogeneous morphology of alloy deposit obtained from sulphate–chloride bath is probably another reason for the reduced corrosion stability of this alloy deposit (Figs. 2–4), since different amounts of Co in different areas of Zn–Co alloy deposit obtained from sulphate–chloride bath could lead to the galvanic coupling and, consequently, to a reduction of protective properties. Namely, the local microstructural variations of deposit (as can be seen in Fig. 2c, for Zn–Co deposit obtained from sulphate–chloride bath) adopt different equilibrium potentials in aqueous solutions and are thus, susceptible to local galvanic corrosion.[34]

Therefore, it could be concluded that the type of the plating bath had a significant role in defining the surface properties, such as crystallite size, deposit homogeneity and distribution, as well as corrosion stability, of the alloys. From the SEM micrographs shown in Fig. 2, it could be seen that the Zn–Co alloys deposited from the chloride plating baths with the lower and higher Co^{2+} content have extremely different morphologies as compared to the surface morphology of the Zn–Co alloy deposited from the sulphate–chloride plating bath. It would be of interest to find out the reason for the better corrosion stability of the homogenous deposit obtained from the chloride-plating bath with the higher Co^{2+} content as compared to the also homogenous deposit obtained from the chloride-plating bath with the lower Co^{2+} content. The SEM micrographs showed the differences in morphology of the deposits obtained by deposition from those two chloride baths, and that larger crystallites were obtained for deposition from the bath with the low Co^{2+} content.

In order to gain a deeper insight into the surface morphologies of these alloy deposits, AFM images were taken. Typical three-dimensional (3D) and two-dimensional (2D) AFM images of the Zn–Co deposits obtained in the chloride plating bath with the lower Co^{2+} content are shown in Figs. 5a and 5b. The deposit is made up of crystallite agglomerations which are compact and uniformly cover the entire substrate. The 2D image of this deposit resembles very well the morphology shown in the corresponding SEM micrograph (Fig. 2a). The crystal agglomerations are of diverse dimensions, ranging from 1.5–2.5 μm (Fig. 5b).

The AFM images of the deposit obtained from the chloride plating bath with the higher Co^{2+} content reveal a completely different surface morphology with globular agglomerations (Figs. 6a and 6b). These globules are in the size range 0.7–2.0 μm (Fig. 6b), and are made up of smaller, nanosized crystallites in the 150–300 nm size range (Fig. 6b).

The chemical compositions of deposits shown in Figs. 5 and 6 were the same, but the increase of Co content in the plating bath resulted in a deposit having a smaller crystallite size. This globular surface morphology, in turn, resulted in improved corrosion stability. In addition, the deposit obtained from the chloride bath with the lower Co^{2+} content had a much coarser morphology than the one obtained from the chloride bath with the higher Co^{2+} content. The finer grained structure of the Zn–Co alloy obtained from the chloride bath with the higher Co^{2+} content resulted in better corrosion stability, probably because the small grain size created a high-volume fraction of the boundaries that act as a corrosion barrier.[35] The deposition from the chloride bath with the lower Co^{2+} content resulted in larger crystallite sizes (Figs. 2, 5 and 6) and higher anodic dissolution (Figs. 3 and 4).

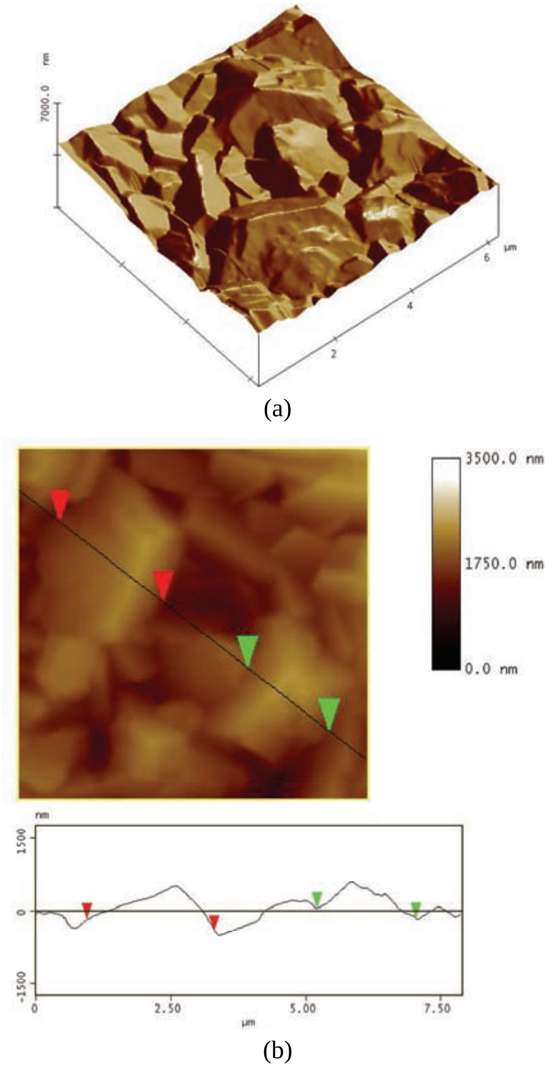

(a)

(b)

Fig. 5. a) 3D AFM Images (5×5×3.5 µm^3) and b) 2D AFM images and height profiles of the Zn–Co alloy deposited from the chloride bath with the lower cobalt content at 2.0 A dm^{-2}.

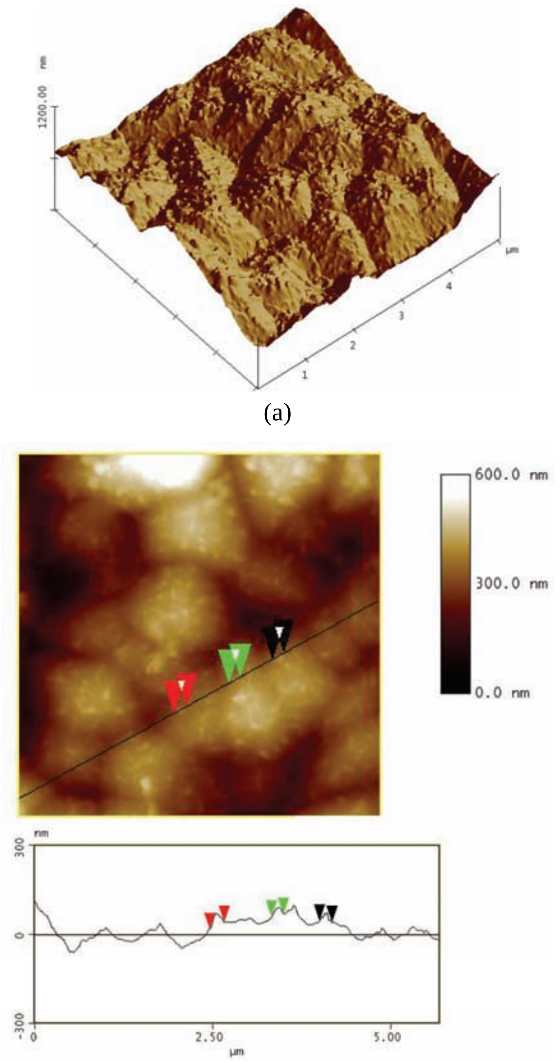

(a)

(b)

Fig. 6. a) 3D AFM Images (5×5×3.5 μm^3) and b) 2D AFM images and height profiles of the Zn–Co alloy deposited from the chloride bath with the higher cobalt content at 2.0 A dm^{-2}.

Another reason for the increased corrosion stability of the Zn–Co alloy coating deposited from the chloride bath with the higher Co^{2+} content could be related to the greater current efficiency obtained during deposition from this bath. Namely, when hydrogen evolution, as a parallel reaction occurring at the cathode, is immense, the hydrogen bubbles formed could be partly incorporated in the alloy deposit. Since the current efficiency was more than three times smaller for the deposition from the chloride bath with the lower Co^{2+} content, these alloy coatings are probably more susceptible to corrosion, as compared to the deposits obtained from the chloride bath with the higher Co^{2+} content.

CONCLUSIONS

Based on the results presented, it could be concluded that the type of the plating bath has a significant influence on the morphology, as well as, on the corrosion stability of electrodeposited Zn–Co alloys.

The surfaces of the alloy coatings deposited from the chloride baths, determined by SEM, were uniform and homogenous, whereas the deposit obtained from the sulphate–chloride bath was quite inhomogeneous. The corrosion stability of the Zn–Co deposits obtained by deposition from both chloride baths was higher than that of the deposit obtained from the sulphate–chloride bath.

The inhomogeneous deposit obtained from the sulphate–chloride bath with oxygen inclusion resulted in reduced corrosion stability, namely the highest corrosion current density, as well as the shortest time before the appearance of red rust. However, the homogenous and dense surface morphology of the Zn–Co deposit obtained from the chloride-plating bath with a higher Co^{2+} content resulted in increased protective properties.

The increase of the cobalt content in the chloride-plating bath resulted in a reduction in the crystallite size of the alloy and an increase in the current efficiency of the alloy deposition. It was shown that the alloy with the smaller crystallite grains of the two alloy deposits obtained from the chloride-plating baths having the same chemical content yielded a lower corrosion rate.

Acknowledgement. This research was financed by the Ministry of Education and Science of the Republic of Serbia, Contract No. III 45019.

ИЗВОД

МИКРОСТРУКТУРА И КОРОЗИОНО ПОНАШАЊЕ Zn–Co ЛЕГУРА ТАЛОЖЕНИХ ИЗ СУЛФАТНОГ И ХЛОРИДНИХ РАСТВОРА

ЈЕЛЕНА Б. БАЈАТ[1], САЊА И. СТЕВАНОВИЋ[2] и БОЈАН М. ЈОКИЋ[1]

[1]*Технолошко–металуршки факултет, Универзитет у Београду, Карнегијева 4, 11120 Београд и*
[2]*ИХТМ – Центар за електрохемију, Универзитет у Београду, Његошева 12, Београд*

У овом раду је проучаван утицај врсте раствора за таложење на микроструктуру и корозиону стабилност превлака Zn–Co легура. Zn–Co легуре са истим садржајем Co су електрохемијски таложене из хлоридних раствора са различитим садржајем јона кобалта, као и из сулфатно–хлоридног раствора. Морфологија површине превлака је испитивана скенирајућом електронском микроскопијом и микроскопијом атомских сила. Корозиона стабилност превлака Zn–Co легура је одређивана праћењем промене потенцијала отвореног кола са временом деловања раствора NaCl концентрације 3%, као и поларизационим мерењима. Добијени резултати су показали значајан утицај врсте раствора за таложење на морфологију и корозиону стабилност превлака Zn–Co легура. Превлаке Zn–Co легура добијене из хлоридних раствора су хомогене, док су превлаке добијене из сулфатно–хлоридног раствора нехомогене. Корозиона стабилност превлака легура добијених из оба хлоридна раствора је већа у односу на стабилност легура добијених из сулфатно–хлоридног раствора. Повећањем садржаја кобалта у хлоридном раствору за таложење добијају се превлаке мањих кристалита и у раду је показано како величина кристалита утиче на корозиону стабилност легура са истим садржајем кобалта.

(Примљено 31. марта, ревидирано 4. јула 2011)

REFERENCES

1. I. H. Karahan, *J. Mater. Sci.* **42** (2007) 10160
2. S. R. Rajagopalan, *Met. Finish.* **70** (1972) 52
3. M. Pushpavanam, S. R. Natarajan, K. Balakrishnan, L. R. Sharma, *J. Appl. Electrochem.* **21** (1991) 642
4. M. H. Gharahcheshmeh, M. H. Sohi, *Mater. Chem. Phys.* **117** (2009) 414
5. R. Ramanauskas, R. Juskenas, A. Kalinicenko, L. F. Garfias-Mesias, *J. Solid State Electrochem.* **8** (2004) 416
6. C. N. Panagopoulos, D. A. Lagaris, P. C. Vatista, *Mater. Chem. Phys.* **126** (2011) 398
7. N. Boshkov, K. Petrov, S. Vitkova, S. Nemska, G. Raichevsky, *Surf. Coat. Technol.* **157** (2002) 171
8. J. B. Bajat, A. B. Petrović, M. D. Maksimović, *J. Serb. Chem. Soc.* **70** (2005) 1427
9. M. A. Pech-Canul, R. Ramanauskas, L. Maldonado, *Electrochim. Acta* **42** (1997) 255
10. W. Kautek, M. Sahre, W. Paatsch, *Electrochim. Acta* **39** (1994) 1151
11. R. Ramanauskas, L. Gudavicinte, L. Diaz-Ballote, P. Bartolo-Perez, P. Quintana, *Surf. Coat. Technol.* 140 (2001) 109
12. R. Fratesi, G. Roventi, C. Branca, S. Simoncini, *Surf. Coat. Technol.* **63** (1994) 97
13. M. R. Lambert, G. R. Hart, H. E. Townsend, *Corrosion mechanism of Zn–Ni alloy electrodeposited coatings, SAE Tech. Pap. Series No. 831817*, Detroit, MI, 1983, p. 81
14. N. R. Short, A. Abibsi, J. K. Dennis, *Trans. Inst. Met. Finish.* **67** (1989) 73
15. P.-Y. Chen, I,-W. Sun, *Electrochim. Acta* **46** (2001) 1169
16. A. Stankeviciute, K. Leinartas, G. Bikulcius. D. Virbalyte, A. Sudavicius, E. Juzeliunas, *J. Appl. Electrochem.* **28** (1998) 89
17. M. S. Chandrasekar, S. Srinivasan, M. Pushpavanam, *J. Solid State Electrochem.* **13** (2009) 781
18. C. N. Panagopoulos, K. G. Georgarakis, S. Petroutzakou, *J. Mater. Process. Tech.* **160** (2005) 234
19. R. D. Srivastava, R. C. Mukerjee, *J Appl. Electrochem.* **6** (1976) 321
20. F. Elkhatabi, M. Benballa, M. Sarret, C. Muller, *Electrochim. Acta* **44** (1999) 1645
21. S. Swathirajan, *J. Electrochem. Soc.* **133** (1986) 671
22. J. B. Bajat, S. Stanković, B. M. Jokić, *J. Solid State Electrochem.* **13** (2009) 755
23. J. Y. Fei, G. D. Wilcox, *Electrochim. Acta* **50** (2005) 2693
24. K. A. Prasad, P. Giridhar, V. Ravindran, *J Solid State Electrochem.* **6** (2001) 63
25. J. B. Bajat, M. D. Maksimović, G. R. Radović, *J. Serb. Chem. Soc.* **67** (2002) 625
26. J. B. Bajat, S. Stanković, B. M. Jokić, S. S. Stevanović, *Surf. Coat. Tech.* **204** (2010) 2745
27. M. M. Abou-Krisha, F. H. Assaf, A. A. Toghan, *J. Solid State Electrochem.* **11** (2007) 244
28. H. Ma, C. Wan, A. H. Zewall, *PNAS* **105** (2008) 12754

29. A. T. Dimitrov, P. Paunović, O. Popovski, D. Slavkov, Ž. Kamberović, S. Hadži Jordanov, *J. Serb. Chem. Soc.* **74** (2009) 279
30. N. D. Nikolić, V. M. Maksimović, M. G. Pavlović, K. I. Popov, *J. Serb. Chem. Soc.* **74** (2009) 689
31. E. Gomez, X. Alcobe, E. Valles, *J. Electroanal. Chem*. **505** (2001) 54
32. Z. F. Lodhi, F. D. Tichelaar, C. Kwakernaak, J. M. C. Mol, H. Terryn, J. H. W. de Wit, *Surf. Coat. Techn.* **202** (2008) 2755
33. L. Felloni, R. Fratesi, E. Quadrini, G. Roventi, *J. Appl. Electrochem.* **133** (1987) 574
34. Z. F. Lodhi, J. M. C. Mol, A. Hovestad, L. ’t Hoen-Velterop, H. Terryn, J. H. W. de Wit, *Surf. Coat. Techn.* **203** (2009) 1415
35. G. B. Hamu, D. Eliezer, L. Wagner, *J. Alloys Comp.* **468** (2009) 222.

Journal of the Serbian Chemical Society
JSCS-info@shd.org.rs • www.shd.org.rs/JSCS

J. Serb. Chem. Soc. *76* (11) 1551–1560 (2011)
JSCS–4228

UDC 577.112.385+547.431:543.4/.5+
546.15+547.564.4'175.5:615
Short communication

SHORT COMMUNICATION

Optimized and validated spectrophotometric methods for the determination of hydroxyzine hydrochloride in pharmaceuticals and urine using iodine and picric acid

NAGARAJU RAJENDRAPRASAD, KANAKAPURA BASAVAIAH* and KANAKAPURA B. VINAY

Department of Studies in Chemistry, Manasagangothri, University of Mysore, Mysore 570 006, India

(Received 7 October 2010, revised 9 February 2011)

Abstract: Two simple, rapid, cost-effective and sensitive spectrophotometric procedures are proposed for the determination of hydroxyzine dihydrochloride (HDH) in pharmaceuticals and in spiked human urine. The methods are based on the charge transfer complexation reaction of the drug with either iodine (I_2) as a σ-acceptor (method A) in dichloromethane or picric acid (PA) as a π-acceptor (method B) in chloroform. The coloured products exhibit absorption maxima at 380 and 400 nm for I_2 and PA, respectively. The Beer Law was obeyed over the concentration ranges of 1.25–15 and 3.75–45 μg mL^{-1} for method A and B, respectively. The molar absorptivity values, Sandell sensitivities, limits of detection (*LOD*) and quantification (*LOQ*) are reported. The accuracy and precision of the methods were evaluated on intra-day and inter-day basis. The proposed methods were successfully applied for the determination of HDH in tablets and spiked human urine.

Keywords: hydroxyzine dihydrochloride; determination; spectrophotometry; charge-transfer complexation; pharmaceuticals; spiked urine.

INTRODUCTION

Hydroxyzine dihydrochloride (HDH), chemically known as 2-[2-[4-[(4-chlorophenyl)phenymethyl]-1-piperazinyl]ethoxy]ethanol, dihydrochloride (Fig. 1), is an H_1 receptor antagonist. It is widely used as an anxiolytic agent to control anxiety[1] and anti-emetic.[2]

The therapeutic importance of HDH initiated several reports on its determination both in pharmaceutical formulations and in biological fluids, *viz*. high-performance liquid chromatography,[3,4] gas chromatography,[5] micellar liquid chromatography,[6] capillary zone electrophoresis,[7] voltammetry,[8] LC–MS,[9] potentio-

---

[*] Corresponding author. E-mail: basavaiahk@yahoo.co.in

doi: 10.2298/JSC101007138R

metry[10] and titrimetry.[11–14] The United States Pharmacopoeia (USP)[15] describes an HPLC method for the determination of HDH in tablets in which HDH is detected at 232 nm with a UV-detector.

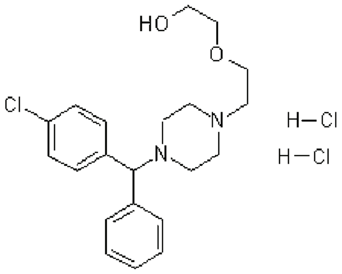

Fig. 1. Structure of hydroxyzine dihydrochloride.

Few visible spectrophotometric methods[12,16–18] have been reported for the determination of HDH in pharmaceuticals. In the method reported by Basavaiah and Charan,[12] different concentrations of the drug are added to a fixed concentration of Hg(II)-diphenylcarbazone complex and the decrease in the absorbance of the Hg(II)-diphenylcarbazone complex, as a consequence of the replacement of diphenylcarbazone in the complex by chloride from the drug, was measured at 540 nm and the method is reported to be applicable in the range 0–60 μg mL^{-1}. Sane *et al.*[16] used three dyes for the determination of the drug content in pharmaceuticals, the method being based on ion-pair formation. Marzanna *et al.*[17] employed Reinecke salt for the assay of the drug. A method based on the charge transfer complex formation reaction with chloranilic acid[18] in acetonitrile was also reported. The method was less sensitive and HDH could be determined only in the concentration range 25–150 μg mL^{-1}.

The aim of the present study was directed at developing and validating two simple, rapid, sensitive and cost-effective spectrophotometric methods based on charge-transfer (C-T) complexation reactions using iodine and picric acid as σ- and π-acceptors, respectively. In the first method (method A), the drug is reacted with iodine in dichloromethane to form a lemon yellow coloured C-T complex with an absorption maximum peaking at 380 nm. The second method (method B) employs picric acid as a π-acceptor to form a yellow C-T complex with the drug in chloroform and the absorbance of the complex is measured at 400 nm. The methods were successfully applied to quantify HDH in pharmaceutical formulations and in spiked human urine. The results obtained were satisfactorily precise and accurate.

EXPERIMENTAL

Apparatus

All absorption measurements were realised using a Systronics Model 106 digital spectrophotometer with 1 cm path length quartz cells.

Materials

Pharmaceutical grade HDH was procured from UCB Pharma Ltd., Mumbai, India, as a gift, and was used as received. Tablets containing HDH, Atarax 25 and Atarax 10 (UCB Pharma Ltd., Mumbai, India) were purchased from the local market and used in the investigation. The urine sample was collected from a healthy volunteer (Male, around 27-year-old) and kept frozen until use after gentle thawing. Chloroform and dichloromethane (spectroscopic grade) were purchased from Merck, Mumbai, India. Distilled water was used wherever required. All other employed chemicals were of analytical reagent grade.

Reagents

A 0.5 % iodine solution was prepared by dissolving 1.25 g of pure resublimed iodine (S.D. Fine Chemicals Ltd., Mumbai, India) in 250 mL of dichloromethane and used after 30 min. Picric acid (0.2 %) was prepared by dissolving 500 mg of pure substance (S.D. Fine Chemicals Ltd., Mumbai, India) in 250 mL of chloroform. To prepare 0.5 mol L^{-1} sodium hydroxide solution, an accurately weighed 2 g of pure NaOH (Merck, India) was dissolved in water, the solution was made up to 100 mL with water.

Standard drug solution

A 250-μg mL^{-1} solution of HDH was prepared by dissolving accurately weighed 25 mg of pure HDH in water and the volume was brought to 100 mL with water and mixed well.

General recommended procedures

Preparation of HDH base (HDN) solution. Method A: HDH solution (10 mL, 250 μg mL^{-1}) was transferred to a 125 mL separating funnel containing 10 mL of a 0.5 mol L^{-1} NaOH solution and the content was mixed well. The hydroxyzine base was extracted with three 15 mL portion of dichloromethane, the extract was passed over anhydrous sodium sulphate and collected in a 100 mL volumetric flask, the volume was made up to the mark with dichloromethane and the resulting solution (25 μg mL^{-1} HDN) was used for the assay in method A.

Method B: HDN solution (75 μg mL^{-1}) was prepared by repeating the above procedure for 30 mL of pure HDH solution (250 μg mL^{-1}) but chloroform was used instead of dichloromethane for extraction. The resulting solution was used for the assay in method B.

Construction of the calibration curves. Method A: Varying aliquots of standard HDN solution equivalent to 1.25–15 μg mL^{-1} (0.25 – 3.0 mL of 25 μg mL^{-1}) were accurately measured and transferred into a series of 5 mL calibrated flasks and 2 mL of 0.5 % iodine solution was added to each flask, the content was mixed well and the flasks were allowed to stand at room temperature (30±2 °C) for 15 min. The volume was brought to the mark with dichloromethane and the absorbance was measured at 380 nm against a reagent blank similarly prepared but without the addition of HDN base solution.

Method B. Into a series of 5 mL calibration flasks, aliquots (0.25–3.0 mL) of standard HDN solution (75 μg mL^{-1}) equivalent to 3.75–45 μg mL^{-1} HDN were accurately transferred, and to each flask 1 mL of 0.2 % picric acid solution was added and the mixture was diluted to 5 mL with chloroform. After 5 minutes, the absorbance of the yellow coloured C-T complex was measured at 400 nm against the reference blank similarly prepared.

Procedure for commercial dosage forms

Twenty tablets were weighed and pulverized. The amount of tablet powder equivalent to 25 mg of HDH was transferred into a 100 mL volumetric flask. The content was shaken well with about 50 mL of water for 20 min, diluted to the mark with water and filtered through Whatmann No. 42 filter paper. The first 10 mL portion of the filtrate was discarded. HDN solutions of concentrations 25 and 75 µg mL^{-1} for method A and B, respectively, were prepared as described under the general procedures for pure drug and a suitable aliquot was used for assay by applying the procedures described earlier.

Procedure for spiked human urine

A spiked urine sample was prepared by adding 20 mg of pure HDH to 10 mL of urine in a separating funnel. Twenty mL of water was added, followed by 10 mL of 0.1 M NaOH solution and the mixture was extracted with three 15 mL portions of dichloromethane. The organic layer was passed over anhydrous sodium sulphate and collected in a 50 mL volumetric flask. The solution was made to the mark with dichloromethane and mixed well. The obtained solution was diluted appropriately to obtain a working concentration of 25 µg mL^{-1} HDN. A 1–2 mL portion of the solution was then subjected to analysis as described for the pure drug in method A. For method B, the required volume of the base solution in dichloromethane was evaporated to dryness. The residue was dissolved in chloroform and diluted with chloroform to a specific volume to obtain a working concentration of 75 µg mL^{-1} HDN. A portion of the solution (*e.g.*, 2 mL) was used for the analysis by following the procedure described earlier.

RESULTS AND DISCUSSION

Molecular interactions between electron donors and electron acceptors are generally associated with the formation of intensely coloured charge-transfer complexes, which absorb radiation in the visible region.[19] Charge transfer complexation reactions have been extensively utilized for the determination of electron-donating basic nitrogenous compounds using either an σ-acceptor (iodine)[20,21] or a π-acceptor (picric acid).[19,22–27] The application of picric acid for the quantitative estimation of orphendrine citrate and phentolamine mesylate injections listed in the USP.[28]

Spectral characteristics

HDN, an *n*-donor (D), forms a lemon yellow-coloured C-T complex with iodine (I_2) (σ-acceptor) in dichloromethane and the resulting coloured species was found to absorb maximally at 380 nm (Fig. 2). The colour of iodine in dichloromethane is violet showing absorption maximum (λ_{max}) at 500 nm. This colour changed into lemon yellow when the iodine was mixed with the drug, and showed an absorption peak at 380 nm (Fig. 2). HDN reacts with picric acid in chloroform medium to yield a yellow-coloured C-T complex peaking at 400 nm (Fig. 3). The interactions between HDN and acceptors to form charge transfer complexes follows according to Schemes 1 and 2.

Optimization of the reaction conditions

Optimum conditions were established by measuring the absorbance of C-T complexes at 380 and 400 nm, for method A and B, respectively, by varying one parameter at a time and keeping the others constant.

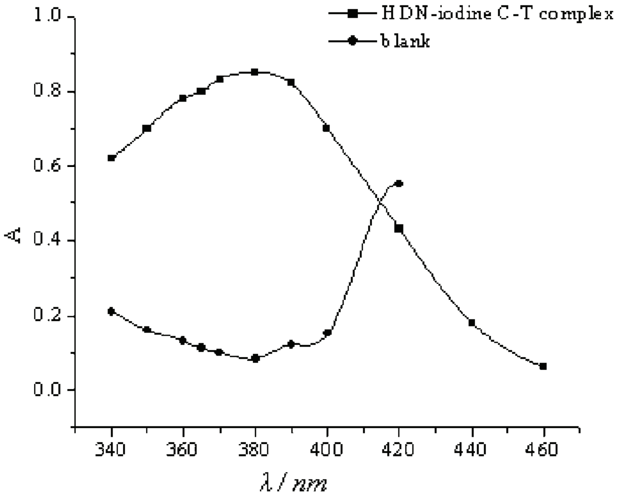

Fig. 2. Absorption spectra of the HDN–I_2 C-T complex (15 µg mL^{-1} HDN) and the reagent blank.

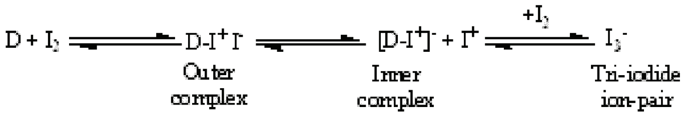

Scheme 1. Reaction pathway for the formation of the C-T complex between HDN and I_2 in dichloromethane

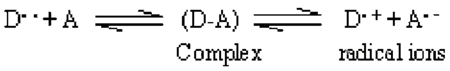

Scheme 2. Reaction pathway for the formation of the electron donor–acceptor complex and radical ions between HDN and picric acid.

Effect of reagent concentration. To establish optimum amounts of the reagents for the sensitive and rapid formation of the HDN charge transfer complexes, the drug (HDN) was allowed to react with different volumes of the reagents (1–4 mL of 0.5 % iodine and 1–3 mL of 0.2 % picric acid in method A and B, respectively). At 2 mL of iodine and 1 mL of picric acid, maximum and minimum absorbance values with respect to the sample and blank were obtained for method A and B, respectively. Therefore, 2 mL of 0.5 % iodine and 1 mL of 0.2 % picric acid in a total volume of 5 mL were used throughout the following investigations.

Choice of solvent. Acetonitrile, chloroform, dichloromethane, ethanol, 2-propanol, methanol, benzene and 1,4-dioxane were the evaluated solvents. Dichloromethane was found to be the ideal solvent for I_2 and showed superior properties compared to the other solvents, since it is favourable for the formation of the triiodide ion-pair (inner complex). With I_2, the other solvents produced lower absorption readings for the sample and higher absorption values for the blanks. In method B, chloroform afforded the maximum sensitivity when compared with all the investigated solvents. Hence, dichloromethane and chloroform were used as solvents for method A and B, respectively.

Reaction time and stability. Complete colour development of the C-T complex was attained after 15 and 5 min in method A and B, respectively, and the coloured species were stable for at least 1 and 16 h, respectively.

Composition of the C-T complexes

The composition of the C-T complex was established by the Job method of continuous variations[29] using equimolar concentrations of the drug (base form) and reagents (4.28×10^{-4} mol L^{-1} in method A and 2.43×10^{-4} mol L^{-1} in method B). The results indicated that a 1:1 (drug:reagent) complex is formed in both cases.

Method validation

A linear correlation was found between the absorbance at λ_{max} and the concentration of HDH in the ranges given in Table I. Regression analysis of the Beer Law data using the least squares method was performed to evaluate the slope (b), intercept (a) and the correlation coefficient (r) for each system and the values are presented in Table I. The optical characteristics such as the limits of the Beer Law, molar absorptivity and the Sandell sensitivity values of both methods are also given in Table I. In addition, the limits of detection (*LOD*) and quantification (*LOQ*), calculated according to ICH guidelines,[30] are also presented in Table I.

TABLE I. Sensitivity and regression parameters

Parameter	Method A	Method B
λ_{max} / nm	380	400
Colour stability, h	1	16
Linear range, μg mL^{-1}	1.25–15	3.75–45
Molar absorptivity (ε), L mol^{-1} cm^{-1}	2.59×10^4	8.06×10^3
Sandell sensitivity, μg cm^{-2}	0.0172	0.0556
LOD / μg mL^{-1}	0.13	0.62
LOQ / μg mL^{-1}	0.39	1.88
Regression equation, Y^a		
Intercept (a)	0.0093	0.0113
Slope (b)	0.0565	0.0174
Standard deviation of a (S_a)	0.0998	0.0998
Standard deviation of b (S_b)	0.0095	0.0030
Regression coefficient (r)	0.9993	0.9995

[a] $Y = a + bX$, where Y is the absorbance, X is concentration in μg mL^{-1}, a is the intercept and b is the slope

Precision and accuracy

For three levels of analyte, the assays were repeated seven times within a day to determine the intra-day precision and five times on different days to determine the inter-day precision of the methods. The percentage relative standard deviation (*RSD*) values were ≤2.29 % (intra-day) and ≤2.98 % (inter-day), indicating the high precision of the methods. The accuracy was evaluated as the percentage relative error (*RE*) between the measured mean concentrations and the taken concentrations for HDN. The RE values of ≤2.40 % demonstrate the high accuracy of the proposed methods.

Robustness and ruggedness

The robustness of the methods was evaluated by making small incremental changes in the volume of reagent (2±0.2 mL of I_2; 1±0.2 mL of PA) and contact time (5±2 min in method B), and the effect of the changes was studied on the absorbance of the complex systems. The changes had negligible influence on the results as revealed by small intermediate precision values expressed as % *RSD* (≤3 %). Method ruggedness was demonstrated by having the analysis performed by four analysts, and by a single analyst performing the analysis on four different instruments in the same laboratory. The intermediate precision values (*RSD*) in both instances were in the range 1.62–3.16 %, indicating acceptable ruggedness.

Applications

Commercial tablets. The proposed methods were applied for the quantification of HDH in commercial tablets. The results were compared with those obtained by the US Pharmacopoeial method.[15] Statistical analysis of the results did not detect any significant difference between the performance of the proposed methods and reference method with respect to accuracy and precision as revealed by the Student's *t*-value and variance ratio *F*-value. The results of the assay are given in Table II.

TABLE II. Results of analysis of tablets by the proposed methods and statistical comparison of the results with the reference method

Tablet brand name	Nominal amount mg/tablet	Found[a] (Percent of label claim ± *SD*)		
		Reference method	Method A	Method B
Atarax 25	25	99.16±0.88	100.6±1.36 *t* = 2.03[b] *F* = 2.39[c]	101.3±1.56 *t* = 2.77 *F* = 3.14
Atarax 10	10	101.6±1.2	100.6±0.96 *t* = 1.46 *F* = 1.56	99.62±1.09 *t* = 2.73 *F* = 1.21

[a] Mean value of 5 determinations; [b] tabulated *t*-value at the 95 % confidence level and for four degrees of freedom is 2.77; [c] tabulated *F*-value at the 95 % confidence level and for four degrees of freedom is 6.39

Recovery from spiked human urine. As another application of the proposed methods, recovery from human urine samples was performed. A prior extraction step, according to Mehran *et al*.[31] was used. The recovery studies were realised with samples containing various amounts of HDN. The results of recovery studies revealed that the other constituents present in the urine did not interfere in the method. The recovery values were in the range 97.2–108.6 %.

Recovery from tablet powder. The recovery test was performed by spiking the pre-analyzed tablet powder with pure HDH at three different levels (50, 100 and 150 % of the content present in the tablet powder (taken) and the total was found by the proposed methods. Each test was repeated three times. In all the cases, the recovery values ranged between 98.40 and 105 %, with a standard deviation in the range 1.04–1.85 %. The closeness of the results to 100 % showed the fairly good accuracy of the methods.

CONCLUSIONS

Two simple, sensitive, extraction-free, rapid and cost-effective spectrophotometric methods based on charge transfer complex formation reactions for the determination of HDH were developed and validated. The suggested methods utilize a single step reaction and single solvent. No substantial differences among the proposed methods arose from analysis of the experimental results. The methods are free from interferences from the common excipients and additives. The statistical parameters and the recovery data reveal good accuracy and precision of the methods. These methods, which can be used as general methods for the determination of HDH in bulk powder, dosage forms and spiked human urine, have many advantages over the separation techniques, *e.g.*, HPLC, such as reduced cost, and speed with high accuracy. Hence, the methods can be used in the routine analysis of drugs in quality control laboratories.

Acknowledgements. The authors thank UCB Pharma Ltd., Mumbai, India, for gifting pure HDH. Two of the authors (NRP and KBV) thank the University of Mysore, Mysore, India, for permission and facilities. NRP also thank the University Grants Commission, New Delhi, India, for the award of a Meritorious Research Fellowship.

ИЗВОД

ОПТИМИЗОВАНА И ВАЛИДИРАНА МЕТОДА ЗА СПЕКТРОФОТОМЕТРИЈСКО ОДРЕЂИВАЊЕ ХИДРОКСИЗИН-ХИДРОХЛОРИДА У ФАРМАЦЕУТСКИМ ПРЕПАРАТИМА И УРИНУ УЗ КОРИШЋЕЊЕ ЈОДА И ПИКРИНСКЕ КИСЕЛИНЕ

NAGARAJU RAJENDRAPRASAD, KANAKAPURA BASAVAIAH и KANAKAPURA B VINAY

Department of Studies in Chemistry, Manasagangothri, University of Mysore, Mysore 570 006, India

Предложене су две економичне и осетљиве спектрофотометриске процедуре за одређивање хидроксизин-дихидрохлорида (HDH) у фармацеутским препаратима и оптерећеном урину. Метода се заснива на трансферу наелектрисдања комплексометријске реакције у леку са јодом као σ-акцептором (метода А) у дихлор-метану и са пикринском киселином као π-акцептором (метода Б) у хлороформу. Обојени производи имају апсорпционе максимуме на 380 and 400 nm за I_2 и пикринску киселину. Сагласност са Beer-овим законом је постигнута у опсегу концентрација 1,25–15 и 3,75–45 μg mL^{-1}, за обе методе. Дате су вредности моларне апсорптивности, Санделовог индекса, граница детекције и квантификације и евалуирана тачност и прецизност методе. Предложене методе су успешно примењене за одређивање HDH у таблетама и оптерећеном хуманом урину.

(Примљено 7. октобра 2010, ревидирано 9. фебруара 2011)

REFERENCES

1. M. Ferreri, E. G. Hantouche, *Acta Psychia. Scand. Suppl.* **393** (1998) 102
2. J. E. F. Reynolds, *Martindale: The Extra Pharmacopoeia*, 30th ed., The Pharmaceutical Press, London, 1993
3. D. Boberić-Borojević, D. Radulović, D. Ivanović, P. Ristić, *J. Pharm. Biomed. Anal.* **21** (1999) 15
4. F. Pehoursq, *J. Pharmacol. Toxicol. Methods* **50** (2004) 41
5. P. Kintz, B. Godelar, P. Mangin, *Forensic Sci. Int.* **48** (1990) 139
6. C. Martinez-Algaba, J. M. Bermudez-Saldana, R. M. Villanueva-Camanas, S. Sagrado, M. J. Medina-Hernandez, *J. Pharm. Biomed. Anal.* **40** (2006) 312
7. M. E. Capella-Peiro, A. Bossi, Esteve-Romero, *Anal. Biochem. J.* **352** (2006), 41
8. A. M. Beltagi, O. M. Abdallah, M. M. Ghoneim, *Talanta* **74** (2008) 851
9. N. Zhou, L. Yi-Zeng, C. Ben-Mei, P. Wang, X. Chen, L. Feng-Ping, *Chromatographia* **66** (2007) 481
10. A. Bouklouze, M. Elbouzekraoui, Y. Cherrah, M. Hassar, J. M. Kauffmann, *Electroanalysis* **14** (2002) 1369
11. K. Basavaiah, V. S. Charan, *Acta Cienc. Indica, Chem.* **27** (2001) 91
12. K. Basaviah, V. S. Charan, *Farmaco* **57** (2002) 9
13. K. Basaviah, V. S. Charan, V. Chandrashekar, *Indian J. Pharm. Sci.* **64** (2002) 251
14. B. Dembinski, *Chem. Anal. (Warsaw).* **38** (1993) 183
15. *The US Pharmacopeia (USP 28), The National Formulary (NF 23)*, US Pharmacopeial Convention Inc., Rockville, MD, USA, 2005, p. 982
16. R. T. Sane, U. M. Vaidya, V. G. Nayak, A. Y. Dhamankar, S. K. Joshi, V. J. Doshi, S. V. Sawant, V. B. Malkar, V. R. Pandit, A. Y. Sathe, S. Jukar, A. D. Nadakarni, *Indian Drugs* **19** (1982) 398
17. K. Marzanna, D. Brunon, S.-C. Aleksandra, S. Pat, *Acta. Pol. Pharma.* **56** (1999) 415
18. K. Basaviah, V. S. Charan, *Indian J. Pharm. Sci.* **65** (2003) 660
19. R. Foster, *Organic Charge-transfer Complexes*, Academic Press, New York, 1969, p. 51
20. A. S. Gamal, *Talanta* **46** (1998) 111
21. A. M. Azza, I. B. Lories, H. R. Heba, *J. Pharm. Biomed. Anal.* **27** (2002) 889
22. M. A.-A. Mohammad, *Bull. Fac. Pharm. Cairo Univ.* **42** (2004) 27
23. E. H. El-Mossalamy, *Spectrochim. Acta, A* **60** (2004) 1161
24. C. S. Xuan, Z. Y. Wang, J. L. Song, *Anal. Lett.* **31** (1998) 1185
25. Y. M. Issa, A. S. Amin, *Anal. Lett.* **26** (1993) 2397
26. M. E. Mahrous, *Anal. Lett.* **25** (1992) 269
27. S. Sadeghi, M. Shamsipur, *Anal. Lett.* **31** (1998) 2691
28. *The United State Pharmacopeia (USP 25), National Formulary (NF 19)*, The United States Pharmacopeial Convention, Inc., Rockville, MD, USA, 2002, p. 1270

29. A. S. Douglas, M. W. Donald, *Principles of Instrumental Analysis*, Holt, Renehart, Winston, New York, 1971, p. 104
30. *International Conference on Harmonisation of Technical Requirements for Registration of Pharmaceuticals for Human Use*, *ICH Harmonised Tripartite Guideline*, *Validation of Analytical Procedures: Text and Methodology Q2(R 1), Complementary Guideline on Methodology*, dated 06 November 1996, incorporated in November 2005, London
31. J. Mehran, E. F. Solmaz, M. Ali, A. Mazid, R. G. Mohammad, N. Parviz, S. Leila, *Anal. Chim. Acta* **612** (2008) 65.

Journal of the Serbian Chemical Society
JSCS-info@shd.org.rs • www.shd.org.rs/JSCS

J. Serb. Chem. Soc. *76* (11) 1561–1566 (2011)
JSCS–4229

UDC 546.46+549.623:548.2:535.004.12
Original scientific paper

The growth of Mg_2TiO_4 single crystals using a four-mirror furnace

ALEKSANDAR GOLUBOVIĆ*# and MARKO RADOVIĆ

University of Belgrade, Institute of Physics, Pregrevica 118, P. O. Box 68,
11080 Belgrade-Zemun, Serbia

(Received 18 August 2010, revised 9 February 2011)

Abstract: A single crystal of Mg_2TiO_4 was grown by the travelling solvent float zone (TSFZ) method. The lattice parameter a = 0.8444(8) nm was determined by X-ray powder diffraction analysis. The optical properties of the Mg_2TiO_4 single crystals were studied using spectroscopic ellipsometry. The obtained results are discussed and compared with published data.

Keywords: Mg_2TiO_4; crystal growth; single crystal; four-mirror furnace; spectroscopic ellipsometry.

INTRODUCTION

Magnesium orthotitanate, Mg_2TiO_4, has been used as a heat resistor, a dielectric for microwave technology, a capacitor for temperature compensation and as a refractory material.[1] Mg_2TiO_4 is a cubic crystal with a crystal structure of the inverse spinel type.

Mg_2TiO_4 is a metastable system. It can be obtained below 800 °C, but it decomposes to $MgTiO_3$ and MgO on further heating.[2] Mg_2TiO_4 crystallizes in the cubic system, with a $Mg(MgTi)O_4$ inverse spinel structure, in which magnesium occupies both tetrahedral and octahedral sites but titanium occupies only octahedral sites. The sites formula can be written as $(A_{1-x}B_x)^{tet.}(A_xB_{2-x})^{oct.}O_4$, where x is called to inversion parameter. In the present case, the spinel is named to (inverse) since x is equal to 1.[3] Mg_2TiO_4 single crystals could be grown by the Verneuil Method, but there are considerable difficulties due to fact that the chemical composition of Mg_2TiO_4 is covered by the primary crystallization field of MgO before Mg_2TiO_4 during cooling.[4] This problem can be solved using the travelling solvent float zone (TSFZ) method.[4] The TSFZ method is essentially identical to the floating zone method, with the exception that the chemical com-

---

* Corresponding author. E-mail: golubovic@ipb.ac.rs
# Serbian Chemical Society member.
doi: 10.2298/JSC100818134G

position of the grown crystal is appreciably different from that of the melt zone. The aim of the present research was to obtain Mg_2TiO_4 single crystals using a four-mirror furnace and determine their optical properties using ellipsometry.

EXPERIMENTAL

The apparatus used for crystal growth was a four-mirror furnace FZ-T-10000-H-HR-I-VPO-PC (Crystal System Corp., Japan). The apparatus has a mirror the shape of an ellipsoid and the focus positions are occupied by halogen lamps. The upper charge feeding and the lower seed holding shafts are located so that the other focus position is always occupied by the melt zone, into which the charge is dissolved and from which crystallization takes place on the seed. The crystal growth was performed in the chamber isolated by a silica glass tube for atmosphere control. An external camera was fixed at a position enabling the solid–liquid boundary to be observed during the crystal growth run and this is presented in Fig. 1.

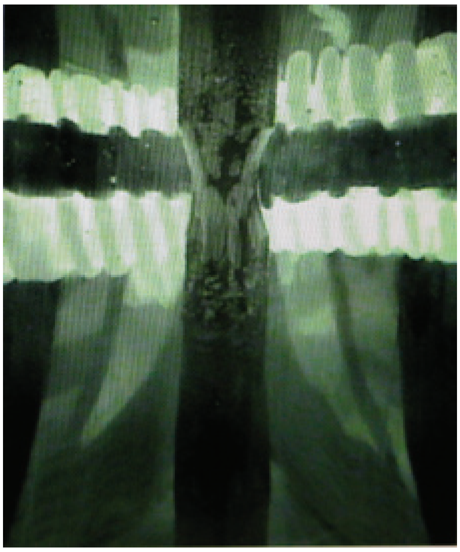

Fig. 1. A view of the floating zone in the display of the four-mirror furnace during a crystal growth run.

Powders of MgO (p.a., Centrohem) and TiO_2 (99.9 % pure, Degussa) were mechanically mixed in the molar ratios of 2:1 and 3:2 for preparation of the materials of the Mg_2TiO_4 charge and the solvent zone, respectively. Each of the mixed batches was placed into a sealed rubber tube and hydrostatically pressed (Crystal System HPTS-M-2000-W hydrostatic press) under a pressure of 80 MPa to give a rod of the desired diameter and length (approximately 10 and 100 mm, respectively). The rods were then sintered at a temperature of 1300 °C (the seed, exactly the solvent zone) and 1500 °C (the charge). In this way, the obtained rods had a density of approximately 85 % of the theoretical value.

Powder X-ray diffraction (XRD) was used for identification of crystalline phases, quantitative phase analysis and estimation of crystallite size and strain. The XRD patterns were collected using a Philips PW 1729 X-ray generator on a Philips diffractometer (PW1710) employing CuKα radiation. Step scanning was performed within the 2θ range from 5 to 70° with a step size of 0.06° and a fixed counting time of 0.41 per step. For product identification, the Fullprof computer program and JCPDS (ASTM) card files were used.

Ellipsometric measurements were performed using a high-resolution variable angle spectroscopic ellipsometer (SOPRA GES5E - IRSE) of the rotating polarizer type. The light source was a short arc Xe lamp while the detector was a photomultiplier tube.

RESULTS AND DISCUSSION

The formation of a steady TSFZ system for successful single crystal growth depends on the following three essential conditions: the degree of sintering of the charge rod, the growth rate, and the chemical composition of the charge rod. In a successful TSFZ crystal growth run, a steady solid–liquid interface is essential for avoiding the precipitation of foreign phases on the growing crystal. The phase diagram of the system MgO–TiO_2 was well described by Woerman *et al.*[5] This system is of interest because of the occurrence of four different eutectics. Such eutectics in this and other systems have been used to prepare some interesting two-phase materials. For example, when a liquid with a composition in the MgO-rich region is cooled from the eutectic temperature at 1707 °C, a material that consists of alternating lamellae of nearly pure MgO and Mg_2TiO_4 will be produced.[6] Other systems show different structures, which are determined in part by the interfacial energies. Of course, interfacial energies are usually not considered in the analysis of phase diagrams.

When the charge rod is in contact with the molten solvent zone under dynamic equilibrium, the liquid phase penetrates into the charge rod to the point where the temperature corresponds to the invariant situation. Consequently, that part of the charge rod is adjacent to the melt zone, thus causing an uneven solid–liquid interface. During floating-zone run, a too wide molten zone may result in the zone becoming unstable and precipitating, while a too narrow zone can lead to the formation of a bridge of solid (or partially solid) material between the growing crystal and the feed rod.[7] While this may not necessarily prevent crystal growth in all materials,[8] it can lead to strain being imparted into the growing crystal, especially if rotation is employed.

The growth rate is the second variable in the system and it was concluded after many experiments that the maximum growth rate of Mg_2TiO_4 single crystals was 2 mm h^{-1}. A higher growth rate resulted in opaque crystals due to foreign phase precipitation and incorporation, while a lower rate lead to many problems during the crystal growth run due to inappropriate surface tensions. The value of crystal growth rate of 2 mm h^{-1} is in accordance with literature data,[4] but the employed rotation rate of 5 rpm was not (the literature value is 30 rpm, [4] but using this value of the rotation, unstable experimental conditions were obtained in this study).

The third important condition for a successful Mg_2TiO_4 crystal growth run is the composition of the rods. The charge rod had the composition MgO:TiO_2 = 2:1, while the seed rod had the composition MgO:TiO_2 = 3:2. The composition of seed was chosen according to the composition obtained from the liquidus curve.[4]

Some authors[4] use solvent zone material in the shape of disk, which is put on the end of a pressed charge rod and then again hydrostatically pressed to give a charge rod with solvent material affixed. As the composition of solvent zone was unknown, it was decided that a seed should be made from the same material (the composition $MgO:TiO_2 = 3:2$).

Blue–grey crystals were obtained after the crystal growth run but after annealing for 12 h at 1000 °C in an oxygen atmosphere, the grown crystals became colourless and transparent. The structural properties were obtained using X-ray diffraction analysis of powdered samples. The unit cell of Mg_2TiO_4 was calculated by the least square method. The parameter of the cubic unit cell is given to be $a = 0.8444$ (8) nm, while the literature value is $a = 0.84443$ (4) nm, according to corresponding JCPDS card 87-1174. The XRD pattern of a powdered Mg_2TiO_4 single crystal is presented in Fig. 2.

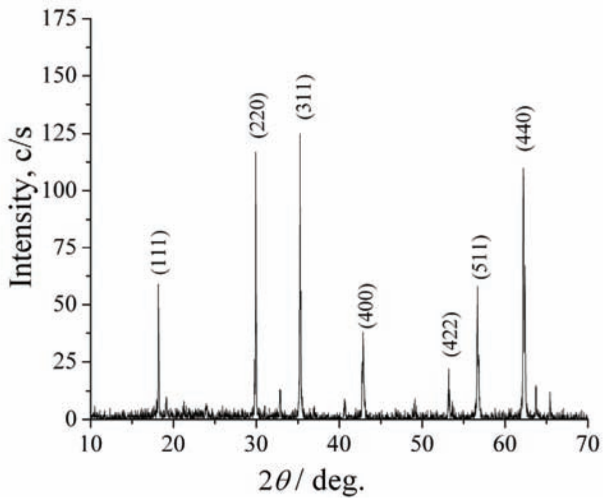

Fig. 2. XRD Pattern of the obtained Mg_2TiO_4 single crystal.

The optical properties of an Mg_2TiO_4 single crystal were studied using spectroscopic ellipsometry in the 1.5–6 eV photon energy range at a 70° angle of incidence. The extraction of refractive index (*n*) and extinction coefficient (*k*) from the ellipsometric data was performed using a two-phase model. The spectral dispersions obtained for *n* and *k* are shown in Fig. 3.

Since inverse spinels have a direct band gap (E_g),[9] the value of E_g for the Mg_2TiO_4 single crystal was evaluated from the general relation:

$$\alpha E = b\sqrt{E - E_g} \tag{1}$$

where *E* is the photon energy, *b* is a constant related to the density of states in conduction band and α is the absorption coefficient derived from extinction coefficient *k* through the relation:

$$\alpha = \frac{4\pi k}{\lambda} \qquad (2)$$

where λ is the wavelength of light.

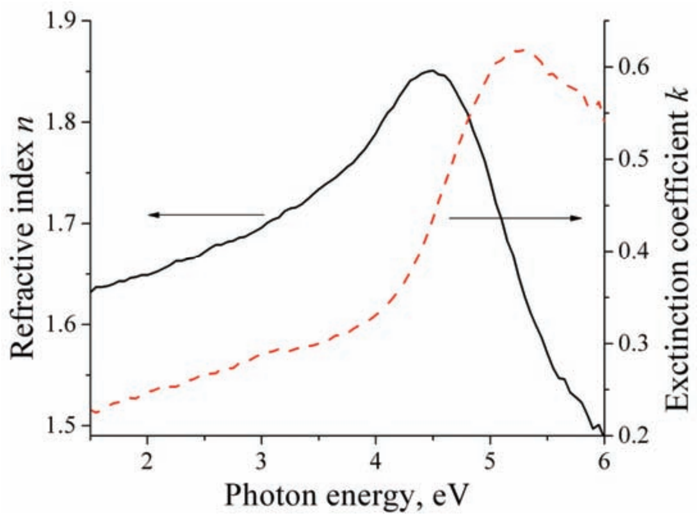

Fig. 3. The photon energy dependence of the refractive index and extinction coefficient for the Mg_2TiO_4 single crystal.

A plot of $(\alpha E)^2$ *vs*. photon energy is shown in Fig. 4. The linear extrapolation towards zero energy gives the value of E_g = 4.25 eV for the direct band gap transition, which is comparable with previously reported results,[10,11] (E_g = 4 eV) and (E_g = 4.4 eV), respectively. The position and slope of the optical absorption edge makes this material a suitable UV-B light absorber.

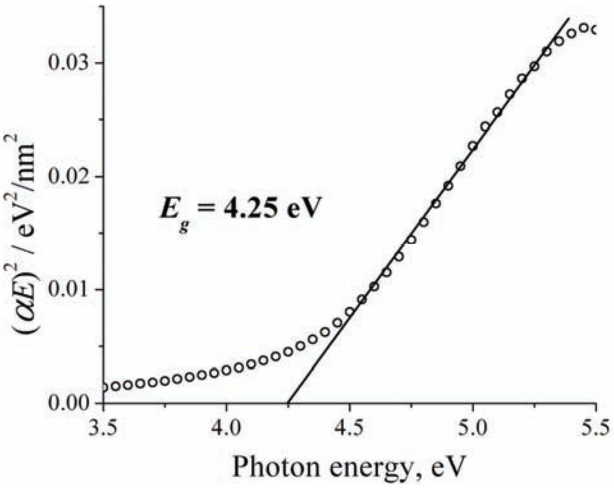

Fig. 4. A plot of $(\alpha E)^2$ *vs*. photon energy, showing the linear extrapolation towards zero energy.

CONCLUSIONS

Good quality Mg_2TiO_4 single crystals were obtained using a four-mirror furnace. The optimum experimental conditions, crystal growth rate of 2 mm h^{-1} and rotation rate of 5 rpm, were experimentally obtained. The unit cell of parameter a = 0.8444 (8) nm and the value of the band gap energy of 4.25 eV for the obtained Mg_2TiO_4 single crystal were in good accordance to data reported in the literature.

Acknowledgement. This work was financially supported by the Ministry of Education and Science of the Republic of Serbia under projects No. ON171032 and III45018

ИЗВОД

РАСТ МОНОКРИСТАЛА Mg_2TiO_4 ПОМОЋУ ПЕЋИ СА ЧЕТИРИ ОГЛЕДАЛА

АЛЕКСАНДАР ГОЛУБОВИЋ и МАРКО РАДОВИЋ

Универзитет у Београду, Институт за физику, Прегревица 118, п. пр. 68, 11080 Земун

Монокристал Mg_2TiO_4 је добијен методом лебдеће зоне са путујућим растварачем (TSFZ). Параметар јединичне ћелије, a = 0,8444 (8) nm, је одређен помоћу дифракције x-зрака на праху. Оптичка својства монокристала Mg_2TiO_4 су проучавана елипсометријом. Добијени резултати су дискутовани и упоређивани са подацима из литературе.

(Примљено 18. августа 2010, ревидирано 9. фебруара 2011)

REFERENCES

1. M. J. Martinez-Lope, M. P. Baura-Pena, M. E. Garcia-Clavel, *Thermochim. Acta* **194** (1992) 59
2. M. R. S. Silva, S. C. Souza, I. M. G. Santos, M. R. Cassia-Santos, L. E. B. Soledade, A. G. Souza, S. J. G. Lima, E. Longo, *J. Therm. Anal. Calorim.* **79** (2005) 421
3. G. Pfaff, *Ceram. Int.* **20** (1994) 111
4. I. Shindo, S. Kimura, K. Kitamura, *J. Mater. Sci.* **14** (1979) 1901
5. E. Woermann, B. Brezny, A. Muan, *Amer. J. Sci.* **267A** (1969) 467
6. Y. M. Chiang, D. Birnie III, W. D. Kingery, *Physical Ceramics*, Wiley, New York, USA, 1997, p. 127
7. S. M. Koohpayeh, D. Fort, J. S. Abell, *J. Cryst. Growth* **282** (2005) 190
8. D. Fort, *J. Cryst. Growth* **94** (1989) 85
9. S.-H. Wei, S. B. Zhang, *Phys. Rev. B* **63** (2001) 045112
10. J. Stade, D. Hahn, R. Dittmann, *J. Lumin.* **8** (1974) 308
11. H. Kominami, M. Tanaka, K. Hara, Y. Nakanishi, Y. Hatanaka, *Phys. Status Solidi, C* **3** (2006) 2758.

Journal of the Serbian Chemical Society
eVersion electronic
JSCS-info@shd.org.rs • www.shd.org.rs/JSCS

J. Serb. Chem. Soc. 76 (11) 1567–1581 (2011)
JSCS–4230
UDC 665:536.421.3:536.5:536.655
Original scientific paper

An analytical study of the effects of vaporization of two-dimensional laminar droplets on a triple flame

MEHDI BIDABADI, GHAZAL BARARI* and MILAD AZIMI

Combustion Research Laboratory, Department of Mechanical Engineering;
Iran University of Science and Technology, Tehran, Iran

(Received 13 August 2010, revised 10 January 2011)

Abstract: The structure of triple flame propagation in combustion systems, containing uniformly distributed volatile fuel droplet was analyzed. The analysis was established for a one-step irreversible reaction with an asymptotic limit, where the value of the Zeldovich number is large. Here, using unit Lewis number, the analytical results for the triple flame temperature were obtained considering two sections. In the first section, a non-vaporizing fuel stream was studied and in the second section, a volatile droplet fuel stream was taken into account. It is presumed that the fuel droplets vaporize to yield a gaseous fuel of known chemical structure, which is subsequently oxidized in the gaseous phase. Here two different cases are studied. In the first case, only the velocity parallel to the reactant flow was considered; while for the latter one, the vertical velocity was considered in addition. The energy equations were solved and the temperature field equations are presented. The results are first presented for a non-vaporizing fuel and compared to the experiment results. In addition, some other results of the temperature field for a vaporizing fuel stream are demonstrated within the comparison between the above-mentioned cases which revealed the effect of the considering the vertical velocity component on the flame temperature field.

Keywords: triple-flame; volatile droplet; flame temperature.

INTRODUCTION

The importance of triple flames is now well established in applications involving combustion phenomena, such as flame spread over solid or liquid fuel surfaces, flame propagation in mixing layers, dynamic extinction of diffusion flames and flame stabilization in reactive streams.

A flame propagating through a fuel/air mixing layer, mainly when the fuel concentration is ranged from lean to rich, may display a triple flame structure, which is composed of a lean and a rich premixed flame wing with a trailing dif-

---

* Corresponding author. E-mail: ghazal_barary@mecheng.iust.ac.ir
doi: 10.2298/JSC100813133B

fusion flame, all extending from a single point. Mixing layers are frequently encountered in combustion problems, including two-dimensional (2-D) mixing layers, heterogeneous propellant combustion, opposed flame spread, jets and boundary layers. The schematic of a triple flame is shown in Fig. 1.

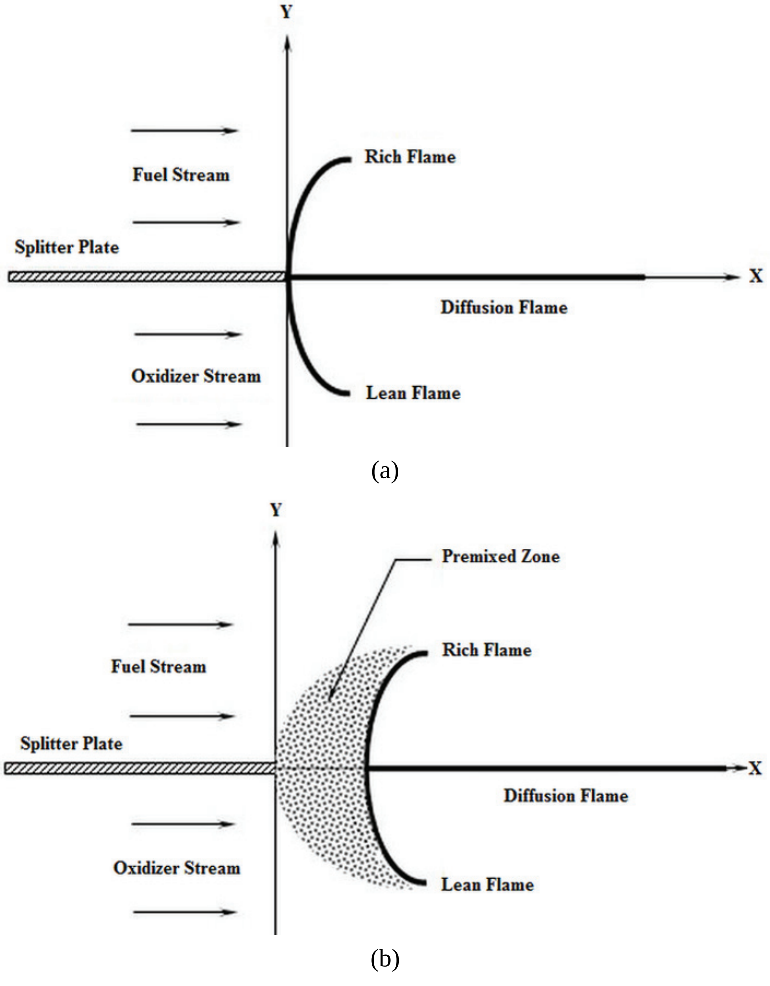

Fig. 1. Triple flame schematic; a) the assumed configuration for the present work; b) the configuration which existed in reality.

The stabilization, propagation and instability of triple flames were studied by Chung.[1] The prospect of establishing a planar turbulent triple flame was considered in the work of Bray and Champion.[2] The local flame speed of a two-dimensional methane–air triple flame in a rectangular burner was investigated by Hirota *et al.*[3] The effect of reversibility of the chemical reaction on triple flame propagation was studied by Ali and Daou.[4] The effects of hydrogen enrichment on the propagation of laminar methane–air triple flames in axisymmetric co-flowing jets were numerically investigated by Briones *et al*.[5] A numerical study of a laminar methane–air triple flame in two-dimensional mixing layers was performed by Guo *et.al*.[6] The effect of flow strain on triple flame propagation was investigated by Hong and Chen.[7] Flame spread in laminar mixing layers was investigated both experimentally and numerically by Kioni *et al*.[8] The dynamics of a laminar triple flame was numerically investigated for different degrees of mixture by Dobrego *et al*.[9] The interaction of non-unity Lewis numbers (due to preferential diffusion and/or unequal rates of heat and mass transfer, was investigated by Shamim.[10]

The aim of this work is to extend current knowledge of triple flames by taking into consideration the influence of a vaporization term for the fuel droplets. This aspect of the problem seems to have received no attention. The purpose of this paper was to investigate how triple flames, and their propagation regimes, are affected by the vaporization term of perfectly volatile fuel droplets in this configuration. In addition, the influence of flow velocity components on the triple flame temperature field was studied.

The paper is structured as follows: the problem is first formulated for a non-vaporizing fuel stream, as a one-step combustion process considering constant density and constant conductivity properties as well as an equal ratio of mass diffusivity to temperature diffusivity (unit Lewis number). The basic equations are solved in terms of dimensionless variables with specified dimensionless boundary conditions. The results are then compared to the experimental work.[11] Then, using the same approach mentioned above, a vaporizing fuel stream will be studied for two different cases related to the flow velocity components. The results obtained in both cases are described and compared.

FORMULATIONS FOR A NON-VAPORIZING FUEL STREAM

The problem addressed herein is the steady propagation of a non-premixed flame consisting of fuel and oxidizer streams. All external forces, including gravitational effects, are assumed to be negligible.

Other approximations introduced are that diffusion caused by a pressure gradient and heat transport by radiation are negligible. The combustion process is modeled by a single, irreversible, one-step reaction of the form $v_F F + v_X X \rightarrow v_P P$, where v_F molecules of a fuel (molecular mass m_F) react with v_X molecules of an oxidizer (molecular mass m_X) to form v_p product molecules (molecular mass m_p). At the first step in the analysis, the problem will be solved within the approximations above. The reactants and products are assumed to be in the gaseous phase. For simplicity and in order to be able to compare the results with the experiments, in this paper, only the case of unity Lewis number, *i.e*., the rate of temperature diffusivity and mass diffusivity of the two species are the same, will be considered.

Basic equations

The time evolution of the mass fractions of the two reactants, Y_F (the fuel mass fraction) and Y_X (the oxidizer mass fraction) is described by:[12]

$$\rho \frac{DY_i}{Dt} = D_i \nabla^2 Y_i - \nu_i m_i \omega \tag{1}$$

where $I = F$ or X, $D/Dt = \partial/\partial t + u\nabla$ is the material derivative, ρ and u are the fluid density and velocity, respectively, ω is the rate of reaction in unit volume per unit time , and D_i is the mass diffusivity of the species i. The time evolution of the temperature, T, is described by:

$$\rho c_\mathrm{p} \frac{DT}{Dt} = D_\mathrm{T} \nabla^2 T + Q\omega \tag{2}$$

where c_p is the specific heat at constant pressure referred to unit mass of gas, Q is the amount of heat released per reaction and D_T is the thermal conductivity. The Lewis numbers will be assumed unity, thus:

$$\frac{D_\mathrm{F}}{\rho_\infty} = \frac{D_\mathrm{X}}{\rho_\infty} = \frac{D_\mathrm{T}}{\rho_\infty c_\mathrm{p}} \equiv k \tag{3}$$

where ρ_∞ is the density of un-burnt gas far upstream, which is assumed to be constant. Therefore Eqs. (1) and (2) become:

$$\rho \frac{DY_i}{Dt} = k\rho_\infty \nabla^2 Y_i - \nu_i m_i \omega \tag{4}$$

and

$$\rho c_\mathrm{P} \frac{DT}{Dt} = k\rho_\infty c_\mathrm{p} \nabla^2 T + Q\omega \tag{5}$$

For the reaction rate, the well known Arrhenius law will be applied by [12]

$$\omega = A\rho^{\nu_\mathrm{F}+\nu_\mathrm{X}} Y_\mathrm{F}^{\nu_\mathrm{F}} Y_\mathrm{X}^{\nu_\mathrm{X}} \exp(-T_\mathrm{a}/T) \tag{6}$$

where T_a is the activation temperature, which is constant for a given reaction, and the exponential factor A is assumed to be approximately constant and has no temperature dependence.

The problem is considered as a uniform flow along the x-axis between $x=(-l,l)$, by $U_\infty x$, where U_∞ is the propagation speed of the triple flame far upstream. It is assumed that the fuel mass fraction varies from $Y_\mathrm{F} = 1$ in the fuel stream ($y \rightarrow +L$) to $Y_\mathrm{F} = 0$ in the oxidizer stream ($y \rightarrow -L$). Similarly, the oxidizer mass fraction varies from $Y_\mathrm{X} = 1$ in oxidizer stream ($y \rightarrow -L$) to $Y_\mathrm{X} = 0$ in fuel stream ($y \rightarrow +L$), *i.e.*:

$$\begin{array}{lll} y \to +L & Y_\mathrm{F} = 1 & Y_\mathrm{X} = 0 \\ y \to -L & Y_\mathrm{F} = 0 & Y_\mathrm{X} = 1 \end{array} \tag{7}$$

such that for upstream:

$$Y_\mathrm{F}(-l, y) + Y_\mathrm{X}(-l, y) = 1 \tag{8}$$

The fuel and oxidizer are assumed to be at the same constant temperature far upstream, $T = T_\infty$. Therefore, the boundary conditions in a limited domain are:

$$\begin{gathered} T(-l,y)=T_\infty \\ T(0,y)=T_s \\ T_y(x,0)=0 \\ T(x,-L)=T_\infty \end{gathered} \tag{9}$$

The fuel mixture fraction, Z, is then defined as:[13]

$$Z=\frac{rY_F-Y_X+1}{1+r} \tag{10}$$

where $r = \nu_X m_X/\nu_F m_F$. Clearly, $Z = 1$ in the fuel stream, $Z = 0$ in the oxidizer stream and $Z = Z_s = 1/(1+r)$ under stoichiometric condition.

It follows from Eqs. (5) and (10) that Z evolves as a passive scalar:

$$\rho\frac{DZ}{Dt}=k\rho_\infty\nabla^2 Z \tag{11}$$

By eliminating the source terms as well as the vaporization terms from Eqs. (4) and (6), it can be shown that the specific enthalpy, which is defined below by Eq. (12), also evolves as a passive scalar (Eq. (13)):

$$H_i=T+\frac{QY_i}{\nu_i m_i c_p} \tag{12}$$

$$\rho\frac{DH_i}{Dt}=k\rho_\infty\nabla^2 H_i \tag{13}$$

From Eq. (10) and (11) and the condition that $T = T_\infty$ far upstream, H_i can be expressed as a linear function of Z as $H_i = A_i + B_iZ$, where A_i and B_i are constants determined from the conditions $Y_F = 1$ in the fuel stream and $Y_F = 0$ in the oxidizer stream. Thus, using the definition of H_i, the reactants mass fractions, Y_F and Y_X, may be expressed in terms of Z and T as follows:

$$Y_F=(T_\infty-T)\frac{m_F\nu_F c_p}{Q}+Z \tag{14}$$

$$Y_X=(T_\infty-T)\frac{m_X\nu_X c_p}{Q}-Z+1 \tag{15}$$

Dimensionless system of the governing equations

In order to express the basic equations in terms of dimensionless variables, suitable dimensionless parameters have to be identified so that the magnitude of the parameters will be of the order unity. Thus, the dimensionless density $\bar{\varpi}=\rho/\rho_\infty$ and the dimensionless velocity components $(U,V)=(u/U_\infty,v/U_\infty)$, as well as dimensionless coordinates $(X,Y)=(x\,U_\infty/k,y\,U_\infty/k)$. The maximum temperature is reached just behind the flame front along the stoichiometric line, where the combustion is complete and neither fuel nor oxidizer are left in the product stream. This "adiabatic flame temperature", T_s, is obtained by substituting $Z = Z_s = 1/(1+r)$ and $Y_F = 0$ in Eq.(14):

$$T_s=T_\infty+\frac{Q}{m_F\nu_F c_p}\frac{1}{1+r}=T_\infty+\frac{Q}{(m_F\nu_F+m_X\nu_X)c_p} \tag{16}$$

The dimensionless parameter α characterizes the temperature rise, or the amount of heat released in the flame:

$$\alpha \equiv \frac{T_\mathrm{s} - T_\infty}{T_\mathrm{s}} = \left[1 + \frac{(m_\mathrm{F}\nu_\mathrm{F} + m_\mathrm{X}\nu_\mathrm{X})c_\mathrm{p}T_\infty}{Q}\right]^{-1} \tag{17}$$

Further, the dimensionless temperature, Θ, and the Zeldovich Number, β, are introduced, which are defined as:

$$\Theta = \frac{T - T_\infty}{T_\mathrm{s} - T_\infty} \tag{18}$$

$$\beta \equiv \alpha \frac{T_\mathrm{a}}{T_\mathrm{s}} \tag{19}$$

In terms of dimensionless variables, Eq. (5) may be written as:

$$\bar{\varpi}(U\frac{\partial \Theta}{\partial X} + V\frac{\partial \Theta}{\partial Y}) = \frac{\partial^2 \Theta}{\partial X^2} + \frac{\partial^2 \Theta}{\partial Y^2} + \lambda \bar{\varpi}^{\nu_\mathrm{F}+\nu_\mathrm{X}} \Sigma(Z/Z_\mathrm{s}, \Theta)\exp\left[-\frac{\beta(1-\Theta)}{1-\alpha(1-\Theta)}\right] \tag{20}$$

where Σ is defined by the following expression:[13]

$$\Sigma(x, y) \equiv (x - y)^{\nu_\mathrm{F}}\left[(1-x) + r(1-y)\right]^{\nu_\mathrm{X}} \tag{21}$$

and λ is defined by:

$$\lambda = \frac{kQA}{c_\mathrm{p}T_\mathrm{s}\alpha}\frac{\rho_\infty^{\nu_\mathrm{F}+\nu_\mathrm{X}-1}}{(1+r)^{\nu_\mathrm{F}+\nu_\mathrm{X}}}\exp(-\beta/\alpha)\frac{1}{U_\infty^2} \tag{22}$$

The dimensionless boundary conditions therefore become:

$$\begin{aligned} \Theta(-l, y) &= 0 \\ \Theta(0, y) &= 1 \\ \Theta_\mathrm{y}(x, 0) &= 0 \\ \Theta(x, -L) &= 0 \end{aligned} \tag{23}$$

Activation energy asymptotic

In order to obtain an analytical solution, some approximations are introduced, whereby $\bar{\varpi}$ may be taken unity. In addition, it is assumed $U = 1$ and $V = 0$.

Equation (20) thus becomes:

$$\frac{\partial \Theta}{\partial X} = \frac{\partial^2 \Theta}{\partial X^2} + \frac{\partial^2 \Theta}{\partial Y^2} + \lambda \Sigma(Z/Z_\mathrm{s}, \Theta)\exp\left[-\beta(1-\Theta)\right] \tag{24}$$

The Zeldovich Number, β, defined by Eq. (19) is considered large for many practical processes. Thus, the basic dimensionless equations describing flames are studied in the asymptotic limit of $\beta \rightarrow \infty$. This limit is known as the activation energy asymptotic (AEA). It is clear from Eq. (24) that the source term vanishes and becomes:

$$\frac{\partial \Theta}{\partial X} = \frac{\partial^2 \Theta}{\partial X^2} + \frac{\partial^2 \Theta}{\partial Y^2} \tag{25}$$

Equation (25) is a linear homogeneous partial differential equation which is converted to Helmholtz differential equation by changing the variable Θ to ψ by the following substitution:[14]

$$\Theta(X,Y)=\exp(\frac{1}{2}X)\psi(X,Y) \tag{26}$$

Hence, Eq. (25) becomes:

$$\frac{\partial^2\psi}{\partial X^2}+\frac{\partial^2\psi}{\partial Y^2}-\frac{1}{4}\psi=0 \tag{27}$$

Equation (27) is a two-dimensional homogeneous Helmholtz equation in the rectangular Cartesian system of coordinates, which may be solved by the separation of variables method. The boundary conditions also become:

$$\begin{aligned} \psi(-l,y) &=0\\ \psi(0,y) &=1\\ \psi_y(x,0) &=0\\ \psi(x,-L) &=0 \end{aligned} \tag{28}$$

Therefore,

$$\psi=\sum_{\kappa_n=1}^{\infty}\frac{2}{L\kappa_n}\sin(\kappa_n L)\frac{e^{-\sqrt{\kappa_n{}^2+1/4}X}-e^{\sqrt{\kappa_n{}^2+1/4}(2l+X)}}{1-e^{2l\sqrt{\kappa_n{}^2+1/4}}}\cos\kappa_n Y \tag{29}$$

From Eq. (26) the triple flame temperature is obtained as:

$$\Theta=\sum_{\kappa_n=1}^{\infty}e^{\frac{1}{2}(X)}\frac{2}{L\kappa_n}\sin(\kappa_n L)\left(\frac{e^{-\sqrt{\kappa_n{}^2+1/4}X}-e^{\sqrt{\kappa_n{}^2+1/4}(2l+X)}}{1-e^{2l\sqrt{\kappa_n{}^2+1/4}}}\right)\cos\kappa_n Y \tag{30}$$

where $\kappa_n=\frac{(2n-1)\pi}{2L}$.

FORMULATIONS WITH VAPORIZATION

The problem presented here will undergo the same method as presented in the previous section; however, here the fuel stream consists of uniformly distributed volatile fuel droplets. It is presumed that the fuel droplets vaporize to form a known gaseous compound which is then oxidized and the products are assumed to be in the gaseous phase.

Basic equations with vaporization

The kinetic of vaporization are presumed to be represented by the expression:[15]

$$W_v=Bn_s(4\pi r^2)T^n \tag{31}$$

where W_v is the mass of gaseous fuel vaporized per unit volume per second. The quantities B and n are constants, which are presumed to be known, and T denotes the gas temperature. For simplicity, it is assumed that the droplet temperature is approximately equal to the gas temperature.

The time evolution of the temperature, T, is given by:

$$\rho c_P\frac{DT}{Dt}=D_T\nabla^2T+Q\omega-W_vQ_v \tag{32}$$

where W_v is vaporization term described by Eq. (31) and Q_v is the heat associated with a vaporizing unit mass of the fuel. With the Lewis number unity, Eq. (32) becomes:

$$\rho c_P\frac{DT}{Dt}=k\rho_\infty c_p\nabla^2T+Q\omega-W_vQ_v \tag{33}$$

Dimensionless system of governing equations

Following the same approach as in the preceding section, Eq. (32) may be written in terms of dimensionless variables as:

$$\bar{\omega}\left(U\frac{\partial \Theta}{\partial X}+V\frac{\partial \Theta}{\partial Y}\right)=\frac{\partial^2 \Theta}{\partial X^2}+\frac{\partial^2 \Theta}{\partial Y^2}+\lambda\bar{\omega}^{\nu_{\mathrm{F}}+\nu_{\mathrm{X}}}\Sigma(Z/Z_{\mathrm{s}},\Theta)\exp\left[-\frac{\beta(1-\Theta)}{1-\alpha(1-\Theta)}\right]-\gamma\Theta^n Q_{\mathrm{v}} \quad (34)$$

where γ is defined by:

$$\gamma=\frac{Bn_{\mathrm{s}}(4\pi r^2)}{c_{\mathrm{p}}}\left(\frac{QZ_{\mathrm{s}}}{m_{\mathrm{F}}\nu_{\mathrm{F}}c_{\mathrm{p}}}\right)^{n-1} \quad (35)$$

Activation energy asymptotic

Here, as in the previous section, $\bar{\omega}$ is introduced and taken to be unity. Two cases are studied, the first $U = 1$ and $V = 0$ and the second $V = 1$, $U = 1$, in order to study the effects the flow velocity components on the flame temperature field.

Case 1, $U = 1$ and $V = 0$: Eq. (34) becomes:

$$\frac{\partial \Theta}{\partial X}=\frac{\partial^2 \Theta}{\partial X^2}+\frac{\partial^2 \Theta}{\partial Y^2}+\lambda\Sigma(Z/Z_{\mathrm{s}},\Theta)\exp\left[-\beta(1-\Theta)\right]-\gamma\Theta^n Q_{\mathrm{v}} \quad (36)$$

and with the AEA assumption, one obtains:

$$\frac{\partial \Theta}{\partial X}=\frac{\partial^2 \Theta}{\partial X^2}+\frac{\partial^2 \Theta}{\partial Y^2}-\gamma^*\Theta \quad (37)$$

where $\gamma^*=\gamma Q_{\mathrm{v}}$. Equation (37) is a linear homogeneous partial differential equation which is converted to a Helmholtz differential equation by changing the variable Θ to ψ by the same substitution, $\Theta(X,Y)=\exp(1/2X)\psi(X,Y)$.

Hence, Eq. (37) becomes:

$$\frac{\partial^2 \psi}{\partial X^2}+\frac{\partial^2 \psi}{\partial Y^2}-\left(\gamma^*+\frac{1}{4}\right)\psi=0 \quad (38)$$

Equation (38) is a two-dimensional homogeneous Helmholtz equation in the rectangular Cartesian system of coordinates, which may be solved by the separation of variables method. The boundary conditions are also similar to that of the case without vaporization:

$$\psi=\sum_n^{\infty}\frac{2\sin(\kappa_{\mathrm{n}}L)}{L\kappa_{\mathrm{n}}}\frac{\exp\left(-\sqrt{\kappa_{\mathrm{n}}{}^2+(\gamma^*+\frac{1}{4})}X\right)-\exp\left(\sqrt{\kappa_{\mathrm{n}}{}^2+(\gamma^*+\frac{1}{4})}(2l+X)\right)}{1-\exp\left(2l\sqrt{\kappa_{\mathrm{n}}^2+(\gamma^*+\frac{1}{4})}\right)}\cos\kappa_{\mathrm{n}}Y \quad (39)$$

Therefore, the triple flame temperature is obtained:

$$\Theta=\sum_n^{\infty}\exp\left(\frac{1}{2}X\right)\frac{2\sin(\kappa_{\mathrm{n}}L)}{L\kappa_{\mathrm{n}}}\times$$
$$\times\frac{\exp\left(-\sqrt{\kappa_{\mathrm{n}}{}^2+(\gamma^*+\frac{1}{4})}X\right)-\exp\left(\sqrt{\kappa_{\mathrm{n}}{}^2+(\gamma^*+\frac{1}{4})}(2l+X)\right)}{1-\exp\left(2l\sqrt{\kappa_{\mathrm{n}}^2+(\gamma^*+\frac{1}{4})}\right)}\cos\kappa_{\mathrm{n}}Y \quad (40)$$

Case 2. $V = 1$, $U = 1$: Eq. Eq. (34) becomes:

$$\frac{\partial \Theta}{\partial X}+\frac{\partial \Theta}{\partial Y}=\frac{\partial^2 \Theta}{\partial X^2}+\frac{\partial^2 \Theta}{\partial Y^2}+\lambda\Sigma(Z/Z_{\mathrm{s}},\Theta)\exp\left[-\beta(1-\Theta)\right]-\gamma\Theta^n Q_{\mathrm{v}} \tag{41}$$

Considering large activation energy, Eq. (41) becomes:

$$\frac{\partial \Theta}{\partial X}+\frac{\partial \Theta}{\partial Y}=\frac{\partial^2 \Theta}{\partial X^2}+\frac{\partial^2 \Theta}{\partial Y^2}-\gamma^*\Theta \tag{42}$$

Equation (42) is also a linear homogeneous partial differential equation, which is converted to Helmholtz differential equation by changing Θ to ψ by the substitution $\Theta(X,Y)=\exp(1/2(X+Y))\psi(X,Y)$, giving:

$$\frac{\partial^2 \psi}{\partial X^2}+\frac{\partial^2 \psi}{\partial Y^2}-(\gamma^*+\frac{1}{2})\psi=0 \tag{43}$$

Equation (43) is also a two-dimensional homogeneous Helmholtz equation in the rectangular Cartesian system of coordinates. However the boundary conditions here would become:

$$\begin{aligned}&\psi(-l,Y)=0\\&\psi(0,Y)\ \ =\exp(-Y/2)\\&\psi_{\mathrm{Y}}(X,0)\ =0\\&\psi(x,-L)=0\end{aligned}$$

Therefore, one obtains:

$$\psi=\sum_{n=1}^{\infty}\left(\begin{aligned}&\frac{\dfrac{\exp(-\frac{L}{2})\sin(\kappa_{\mathrm{n}}L)}{\kappa_{\mathrm{n}}}-\dfrac{3\exp(-\frac{L}{2})}{4\kappa_{\mathrm{n}}^2}\cos(\kappa_{\mathrm{n}}L)+\dfrac{3}{4\kappa_{\mathrm{n}}^2}}{\dfrac{L}{2}+\dfrac{\sin(\kappa_{\mathrm{n}}L)}{4\kappa_{\mathrm{n}}}}\\&\times\frac{\exp(-(\sqrt{\kappa_{\mathrm{n}}^2+\gamma^*+\frac{1}{2}})X)-\exp((\sqrt{\kappa_{\mathrm{n}}^2+\gamma^*+\frac{1}{2}})(2l+X))}{1-\exp(2l\sqrt{\kappa_{\mathrm{n}}^2+\gamma^*+\frac{1}{2}})}\cos\kappa_{\mathrm{n}}Y\end{aligned}\right) \tag{44}$$

Thus, Θ the triple flame temperature is obtained:

$$\Theta=\sum_{n=1}^{\infty}\exp(\frac{1}{2}(X+Y))\left(\begin{aligned}&\frac{\dfrac{\exp(-\frac{L}{2})\sin(\kappa_{\mathrm{n}}L)}{\kappa_{\mathrm{n}}}-\dfrac{3\exp(-\frac{L}{2})}{4\kappa_{\mathrm{n}}^2}\cos(\kappa_{\mathrm{n}}L)+\dfrac{3}{4\kappa_{\mathrm{n}}^2}}{\dfrac{L}{2}+\dfrac{\sin(\kappa_{\mathrm{n}}L)}{4\kappa_{\mathrm{n}}}}\\&\times\frac{\exp(-(\sqrt{\kappa_{\mathrm{n}}^2+\gamma^*+\frac{1}{2}})X)-\exp((\sqrt{\kappa_{\mathrm{n}}^2+\gamma^*+\frac{1}{2}})(2l+X))}{1-\exp(2l\sqrt{\kappa_{\mathrm{n}}^2+\gamma^*+\frac{1}{2}})}\cos\kappa_{\mathrm{n}}Y\end{aligned}\right) \tag{45}$$

RESULTS AND DISCUSSION

Some results may now be presented for variations of the dimensionless flame temperature *versus* the dimensionless coordinates. The three-dimensional diagram of the flame temperature for a non-vaporizing fuel stream *versus* the coordinates X and Y is shown in Fig. 2. The results of the flame contour are compared to experimental results,[11] which are displayed in Fig. 3.

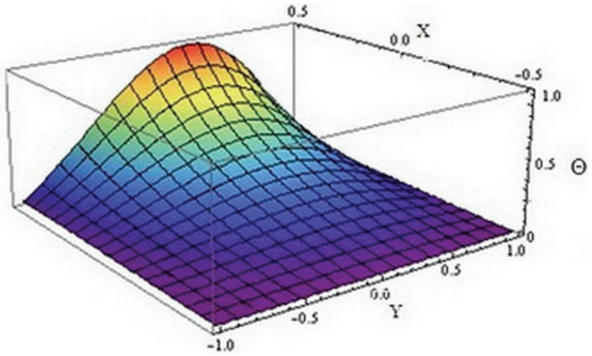

Fig. 2. Three-dimensional diagram of dimensionless flame temperature for non-vaporizing fuel stream *vs.* the dimensionless coordinates X and Y.

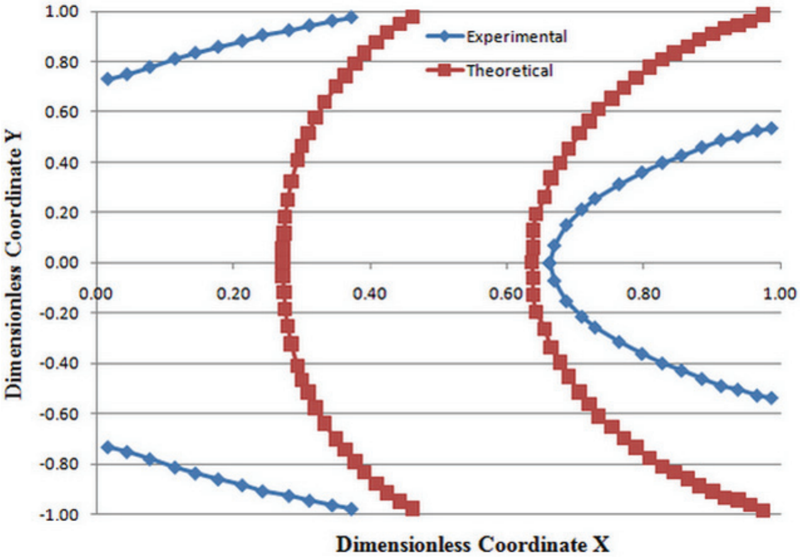

Fig. 3. Comparison of the theoretical and experimental results of the flame contour.

As can be observed in Fig. 3, the trend of flame contour for the theoretical solution presented in this paper is in good agreement with the experiments. In order to simplify the solution of the current governing differential equations, it was assumed that the location of the flame formation was at the origin of the Cartesian coordinate axis; this assumption is applied to the equation by the boundary conditions. While in reality the flame would be formed after mixing the fuel and oxidizer. Therefore the location of flame formation would be slightly shifted and displaced through the reactant stream propagation, namely in the positive *X*-direction (see Fig. 1b). As a result, referring to Fig. 3, it could be observed that for small values of *X* (very close to the *Y*-axis), the discrepancy between the theoretical and experimental results is quite significant, while it should be noticed that in spite of the discrepancy at the values of *X* close to unity due to the effects of the assumptions, in far upstream, the experimental results show more agreement with the theoretical results. Since in reality combustion is an unsteady phenomenon, flame propagation would be decreased in the places far from the stoichiometric line, while the steady state condition was studied in the presented work.

The variation of temperature along the *X*-axis is demonstrated in Fig. 4 for both sections of the non-vaporizing fuel stream and the volatile droplet stream. In this diagram, it may be seen that the temperature increases moving along the *X*-axis. In the case in which the fuel droplets vaporized into the gaseous phase, the curve of the temperature is located lower than in the case of the non-vaporizing fuel stream, because vaporization heat is given to the fuel droplets in order to convert them into the vapor phase. Therefore, the temperature has a lower value than the case of the non-vaporizing fuel. Moreover, the stream temperature with vaporization of the fuel droplets was studied under two fuel flow conditions; the former diagram (case 1) in which only the velocity parallel to the reactant flow

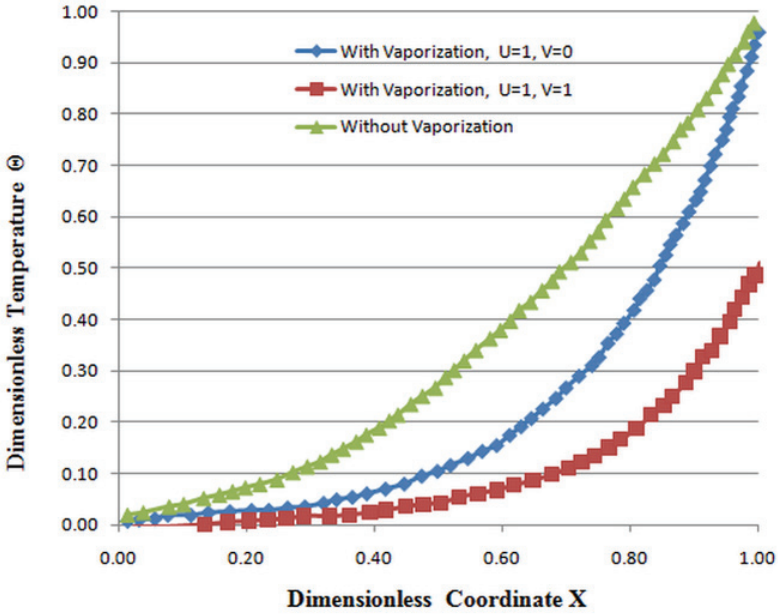

Fig. 4. Flame temperature *vs.* *X*-axis, comparison between non-vaporizing and volatile fuel streams; as well as the effects of the vertical velocity component of fuel flow.

(U) is considered with the vertical velocity being neglected and the latter one (case 2) in which the vertical velocity (V) was also considered. Therefore the effects of this additional term were studied. From Fig. 4, it can be seen that the inclusion of the vertical velocity in the energy equation affected a further shift to the right of the flame temperature along the X-axis.

The temperature variation along the Y-axis is illustrated in Fig. 5 in the same way as was the case for the X-axis. Here also, the effect of the additional term for the vertical velocity of the fuel stream was studied. As can be seen from Fig. 5, the flame temperature had its peak value at $Y = 0$, where the fuel and oxidizer were mixed in stoichiometric amounts, while when considering the velocity perpendicular to the flow path, the flame temperature peak value moved to the right and downwards. Thus, the extra momentum which is brought into the flow by considering the velocity perpendicular to the flow path causes a decrease in the maximum flame temperature and the location of the temperature peak is moved to the right.

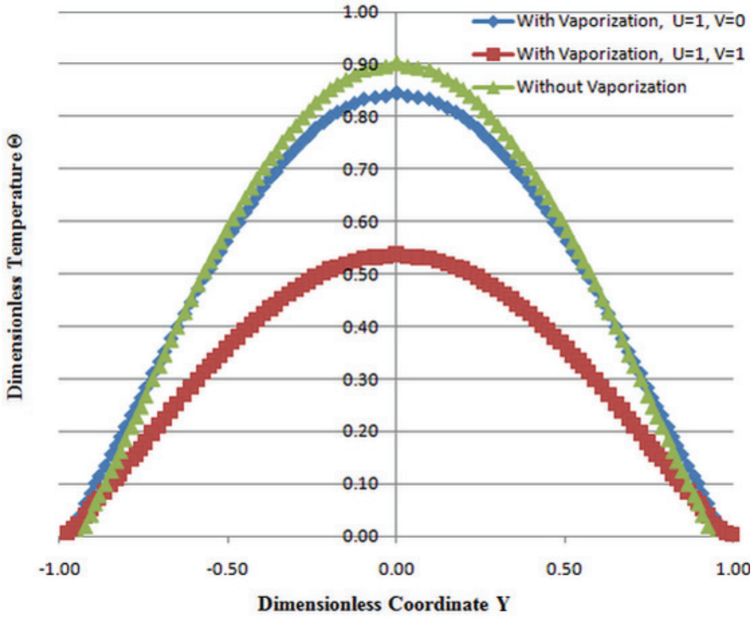

Fig. 5. Flame temperature *vs*. Y-axis, comparison between non-vaporizing and volatile fuel streams; as well as the effects of the vertical velocity component of fuel flow.

The flame temperature variations along the X- and Y-axis for particles of various radii are illustrated in Figs. 6 and 7, respectively. It can be observed that increasing the particle radius results in a decrease in the flame temperature. The smaller the particle, the higher would be the flame temperature due to the lower burning surface.

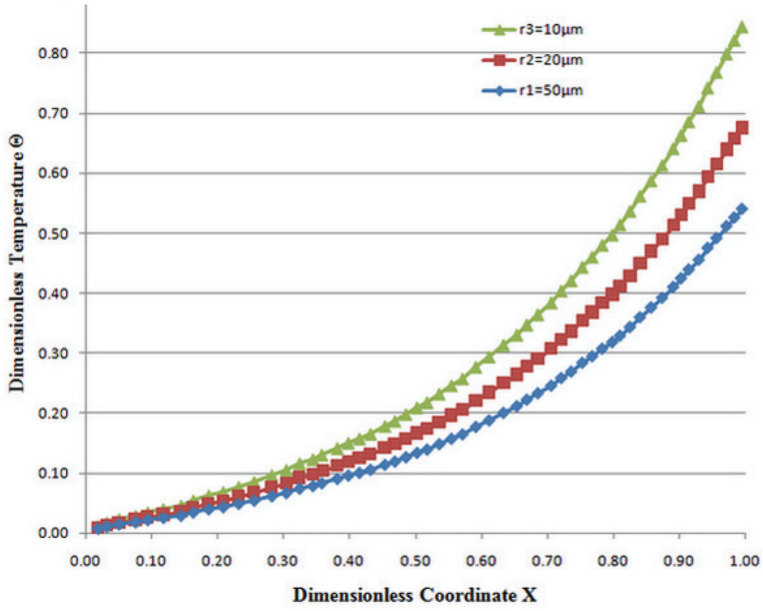

Fig. 6. Flame temperature *vs*. *X*-axis for various particle radii.

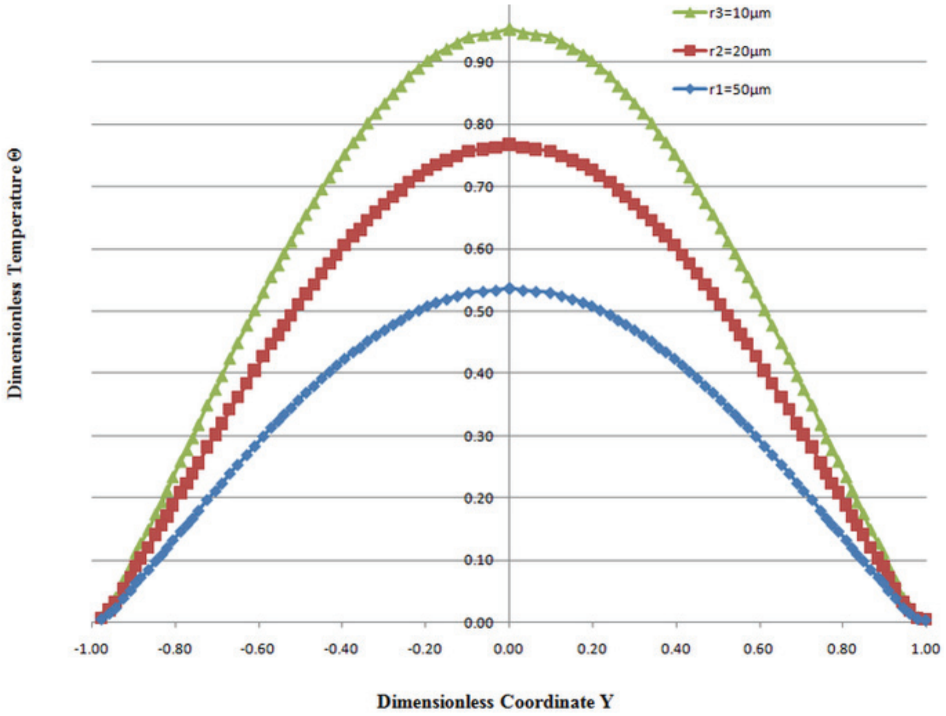

Fig. 7. Flame temperature *vs*. *Y*-axis for various particle radii.

The results shown are applicable to any triple flame configuration. According to the assumptions used in the present article, any volatile fuel particle could be considered in this study. The overall flame configurations are the same, because the methods within which the fuel and oxidizer are mixed and as well the governing equations are the same for different fuel droplets. The differences are related to some constant parameters in the equations, such as fuel density, the mixture fraction of the reactants, *etc*. Nevertheless the total schematic of the flame as shown in Fig. 1 is still valid. Therefore the presented results are not only applicable to a specific flame, but can also be applied to any triple flame configuration.

CONCLUSIONS

In this article, an analytical approach was developed for assessing the flame structure and combustion properties of a triple flame containing uniformly distributed volatile fuel droplet. The obtained results were compared to the results obtained for non-vaporizing fuel particles. Furthermore, the role of vaporization term was investigated in this research for two different approaches in which the stream velocity along the flow and perpendicular to the direction of the flow were considered. The calculated results were compared to the experimental data. When the vaporization term for the fuel droplets was included, it was observed that the temperature field of the triple flame was reduced compared to that for a non-vaporizing fuel stream because of the heat removed from the flow. In addition, by studying the temperature field with flow velocity effects along horizontal and vertical direction, it was demonstrated that the flame temperature was decreased due to the extra momentum brought into the flow comparing to the case in which only the horizontal velocity component was considered.

The calculation method used in this article is based on an analytical approach in which all the governing equations were derived according to the related energy equation in terms of temperature and the equations were written in the non-dimensional form by using dimensionless variables. In the analytical approach, no attention was paid to the analysis of the triple flame. However, experimental results were compared with the results of this study, and the terms of agreements and discrepancies are described in the discussion. Hence, the approach employed to follow the steps of combustion within a tripe flame is not a numerical method; however, there are many such methods, e.g., discretization of the equation within a finely meshed domain, which may be used to verify the results.

ИЗВОД

АНАЛИТИЧКО ИПИТИВАЊЕ ЕФЕКТА ИСПАРЉИВОСТИ НА ТРОСТРУКИ ПЛАМЕН СА ДВОДИМЕНЗИОНИМ КАПЉИЦАМА

MEHDI BIDABADI, GHAZAL BARARI и MILAD AZIMI

Combustion Research Laboratory, Department of Mechanical Engineering; Iran University of Science and Technology, Tehran, Iran

Испитивана је структура троструког пламена који пропагира у системима са сагоревањем и који садржи дистрибуиране честице испарљивог горива. Анализа је извршена за једностепену иреверзибилну реакцију са асимптотском границом, где је вредност Zeldovich-овог броја велика. Коришћењем јединичног Lewis-ог броја, постављен је математички модел и добијено је аналитичко решење за температуре у троструком пламену, Анализа је урађена у два дела. У првом делу је третирана неиспарљива струја горива, док је у другом делу узета у обзир испарљивост капљица горива. Претпостављено је да капљице горива испаравају и доприносе гасовитом гориву познате хемијске структуре, које се затим оксидише у гасовитој фази. Овде су разматрана два случаја. У првом случају, узима се у обзир само брзина паралелна са током реактанта, док се у другом случају разматра и вертикална брзина. Једначине енергетског биланса су решене и представљене су једначине температурног поља. Прво су приказани резултати за неиспарљиво гориво и упоређени са експериментима. Резултати температурног поља за испарљиво гориво су такође приказани у оквиру поређења горе поменутих случајева, што показује ефекте разматрања вертикалне компоненте брзине на температурно поље.

(Примљено 13. августа 2010, ревидирано10. јануара 2011)

REFERENCES

1. S. H. Chung, *Proc. Combust. Inst.* **31** (2007) 877
2. K. Bray, M. Champion, P. A. Libby, *Combust. Flame* **154** (2008) 181
3. M. Hirota, T. Yokomori, K. Yasuda, Y. Nagai, M. Mizomoto, G. Masuya, *Proc. Combust. Inst.* **31** (2007) 893
4. S. Ali, J. Daou, *Proc. Combust. Inst.* **31** (2007) 919
5. A. M. Briones, K. A. Suresh, R. K. Viswanath, *Combust. Flame* **153** (2008) 367
6. H. Guo, F. Liu, G. J. Smallwood, *Int. J. Therm. Sci.* **45** (2006) 586
7. G. I. Hong, J. H. Chen, *Combust. Flame* **126** (2001) 1384
8. P. N. Kioni, B. Rogg, K. N. Bray, A. Linan, *Combust. Flame* **95** (1993) 277
9. K. V. Dobrego, I. M. Kozlov, V. V. Vasiliev, J. P. Martin, P. Gillon, *Int. J. Heat Mass Transfer* **51** (2008) 1962
10. T. Shamim, *Int. J. Therm. Sci.* **45** (2006) 1213
11. R. Daou, J. Daou, J. Dold, *Proc. Combust. Inst.* **29** (2002) 1559
12. M. Bidabadi, Gh. Barari, M. Azimi, M. Mafi, *Int. Joint J. Conf. Eng. (IJJCE)* **1** (2009) 26
13. S. Ghosal, L. Vervisch, *J. Fluid Mech.* **415** (2000) 227
14. *Handbook of Linear Partial Differential Equations for Engineers and Scientists*, Ch. 7, Chapman & Hall, CRC, Boca Raton, FL, USA, 2002,
15. M. Bidabadi, A. Rahbari, *Combust. Explosion, Shock Waves* **45** (2009) 278.

Journal of the Serbian Chemical Society
JSCS-info@shd.org.rs • www.shd.org.rs/JSCS

J. Serb. Chem. Soc. 76 (11) 1583–1595 (2011)
JSCS–4231

UDC 544.032.72+669.73+669.3/.4:
504.45+504.73+504.53:543.421
Original scientific paper

Preconcentration and determination of heavy metals in water, sediment and biological samples

HAMID SHIRKHANLOO[1], HASSAN ZAVVAR MOUSAVI[2]*
and AHMAD ROUHOLLAHI[1]

[1]Department of Chemistry, Faculty of Science, K. N. Toosi University of Technology, Tehran, and [2]Chemistry Department, College of Sciences, Semnan University, Semnan, Iran

(Received 24 October 2010, revised 4 January 2011)

Abstract: In this study, a simple, sensitive and accurate column preconcentration method was developed for the determination of Cd, Cu and Pb ions in river water, urine and sediment samples by flame atomic absorption spectrometry. The procedure is based on the retention of the analytes on a mixed cellulose ester membrane (MCEM) column from buffered sample solutions and then their elution from the column with nitric acid. Several parameters, such as pH of the sample solution, volume of the sample and eluent and flow rates of the sample were evaluated. The effects of diverse ions on the preconcentration were also investigated. The recoveries were >95 %. The developed method was applied to the determination of trace metal ions in river water, urine and sediment samples, with satisfactory results. The 3δ detection limits for Cu, Pb and Cd were found to be 2, 3 and 0.2 μg dm^{-3}, respectively. The presented procedure was successfully applied for determination of the copper, lead and cadmium contents in real samples, *i.e.*, river water and biological samples.

Keywords: lead; copper; cadmium; mixed cellulose ester membrane; preconcentration.

INTRODUCTION

Heavy metals are defined as those metals and metalloids generally considered to be of sufficient distribution and abundance to be in some way environmentally or biologically significant as a toxic substance. Heavy metals may originate from various types of sources, such as mining and smelting ferrous ores, the surface finishing industry, energy and fuel production, fertilizer and pesticide industries and applications, metallurgy, the iron and steel industry, electroplating, electrolysis, electro-osmosis, leatherworking, photography, electric appliance manufacture, metal surface treatment, aerospace and atomic energy installation, *etc*. Thus, shortage of metal as a kind of resource is developing and metal also

---

* Corresponding author. E-mail: hzmousavi@semnan.ac.ir

doi: 10.2298/JSC101024139S

create serious environmental pollution, threatening human health and the ecosystem.[1–3]

Cadmium, copper and lead are three elements that are among the most hazardous to human health. Lead pollution in water systems has seriously influenced the quality of life, especially in developing country. Lead is accumulated in tissues and may cause serious health problems for humans and animals. This metal inhibits biosynthesis and affects the kidneys, brain cells and the permeability the liver membrane, thereby reducing some of their functions. It can be accumulated in the body and can promote disturbances such as nausea, vomiting, diarrhea, sweating and, in some cases, convulsions, coma and death.[4,5] Cadmium may cause renal injuries and may interfere with the renal regulation of the calcium and phosphate balance. Cadmium concentrations in urine reflect long term exposure and the quantity of cadmium stored in the body, particularly in the kidney and liver. With commencement of renal damage, excretion of Cd can increase markedly.[6,7]

Copper is an element essential for many biological systems and plays an important role in carbohydrate and lipid metabolism. In general, copper at nearly 40 $\mu g\ dm^{-3}$ is required for normal metabolism of many living organisms; however, in higher levels, it is considered to be toxic and severe oral intoxication will affect mainly the blood and kidneys.[8,9] Whenever toxic heavy metals are exposed to the natural ecosystem, accumulation of metal ions such as lead, cadmium and copper in the human body occurs through either direct intake or the food chain. Therefore, heavy metals should be prevented from reaching the natural environments because of their toxicity.

The determination of trace metals comprises one of the most important targets in analytical chemistry. This interest is also demonstrated in different areas, such as biology and medicine.[10] Various techniques have been applied for the determination of trace heavy metals in aqueous and biological samples. Flame atomic absorption spectrometry (FAAS) has been a very attractive technique for routine metal determinations, owing to its ease of operation, its low acquisition and operating costs compared with inductively coupled plasma optical emission spectrometry (ICP–OES).[11]

Direct instrumental analysis of these samples is difficult because of complex formation and significance of the matrices, which invariably influence normal instrumental analysis. In addition, some metals are present at low concentrations, which are near to or below the limit of detection of the instrument. Moreover, the low level of trace elements in real samples is not compatible with the detection limit of AAS. Preconcentration can solve the above two problems and lead to simplified heavy metal determination. There are many methods of preconcentration, including cloud point extraction,[12–14] coprecipitation,[15–17] cathodic adsorptive stripping voltammetry,[18] ICP–OES,[19,20] microextraction,[21] ion exchange,[22] inductively coupled plasma mass spectrometry,[23] liquid–liquid extraction,[24] electrothermal atomic absorption spectrophotometery[25] and solid phase extraction.[26–28]

Among the various preconcentration methods, solid-phase extraction (SPE) is one of the most effective multi-element preconcentration methods because of its simplicity, rapidity and ability to attain a high concentration factor. In addition SPE provides for the removal of potentially interfering matrices.

Various materials, including amberlite (XAD) resins,[29–32] activated carbon,[32–35] modified silica gel,[36–38] alumina,[39,40] and synthetic zeolites[41] have been widely used for the preconcentration and separation of trace metal ions from various matrices.

The purpose of the present study was to demonstrate the feasibility of using mixed cellulose ester membrane as a solid-phase extractant for the preconcentration of lead, copper and cadmium found at trace level in water and biological samples. In the procedure, the analytes were retained on a short mixed cellulose ester filter column from a buffered sample solution and then eluted from the column with nitric acid. In the development of the procedure, several parameters relevant to the retention and elution of the analytes were examined.

EXPERIMENTAL

Materials

All the reagents used were of analytical reagent grade. Doubly-distilled water (DW) and high purity reagents were used for the preparations of all the standard and sample solutions. Standard stock solutions containing 1000 mg dm^{-3} analyte were prepared from nitrate salts of Cd(II), Cu(II) and Pb(II) in 1 % of HNO_3 in 1-L calibrated flasks (Merck, Darmstadt, Germany, atomic absorption grade). Ammonium chloride buffer solution (0.2 mol dm^{-3}) was prepared by adding an appropriate amount of ammonia to ammonium chloride solution (Merck) to prepare a solution of pH 8. The mixed cellulose ester membrane was purchased from Sartorius, No. 10401706 (USA). A GBC atomic absorption spectrophotometer (AA-932, Dandenong, Victoria, Australia) equipped with a single-element hollow cathode lamp and an air––acetylene burner were used for the determination of the metal ions. All instrumental settings were those recommended in the manufacturer's manual book. A Metrohm E-744 model pH meter (Herisau, Switzerland) with a glass electrode was employed for measuring pH values of the aqueous phases. The preconcentration system consisted of cartridge tube with cellulose ester membrane (100 mm height, 25 mm internal diameter) connected to a vacuum system. The instrumental and extraction conditions are listed in Table I.

TABLE I. The instrumental settings for the flame atomic absorption spectrometer

Parameter	Lead	Copper	Cadmium
Wavelength, nm	217	324.8	228.8
Lamp current, mA	5	3	3
Spectral bandwidth, nm	1	0.5	0.5
Air flow rate, dm^3 min^{-1}	8	8	8
Acetylene flow rate, dm^3 min^{-1}	2	1.5	2

Characteristics of the adsorbent material

The microstructure and surface morphology of the adsorbent was characterized by a Phillips PW3710 field emission scanning electron microscope (SEM) at an accelerating voltage of 15.0 kV. The SEM image of the MCEM, showing the highly porous morphology of adsorbent with nanosized pores (200 nm), is presented in Fig. 1.

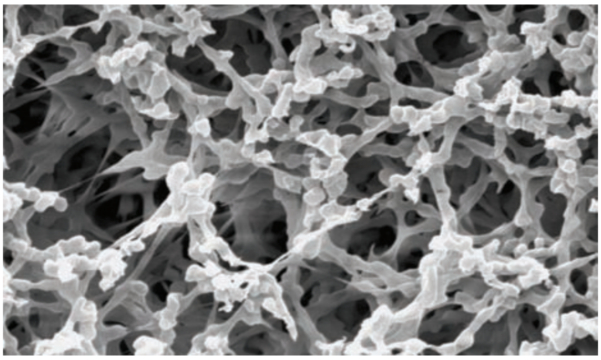

Fig. 1. An SEM image of mixed cellulose ester membrane, 4500×.

General procedure

A cartridge tube (100 mm length and 38 mm i.d) with mixed cellulose ester membrane (0.83 mm thickness and 36 mm i.d) was used as a preconcentration column. An aliquot of the sample solution (25 mL) containing 10–100, 12–350 and 0.8–35 μg dm^{-3} of Cu, Pb and Cd, respectively, were passed through the column at a flow rate of 1.0 ml min^{-1}. Then, the metals retained on the column were completely dissolved in 2 mL of HNO_3 (1.5 mol dm^{-3}). The concentration of metals in the final solution was determined by FAAS. A blank solution was also run under the same analytical conditions without the addition of Cu, Pb and Cd. A fresh cartridge tube with mixed cellulose ester membrane was used for each experimental run.

RESULTS AND DISCUSSION

Nowadays, membrane filtration is one of the important enrichment techniques for trace heavy metal ions. In membrane filtration, the collection of traces metal ions is performed very quickly by filtration under suction with the aid of a vacuum aspirator.[42,43] Initial experiments showed that MCEM has a tendency to retain lead, copper and cadmium. Hence, a column containing MCEM adsorbent was chosen for the preconcentration of lead, copper and cadmium and their subsequent determination by flame atomic absorption spectrometry. In order to obtain the best performance for the flow system, the effects of various chemicals and instrumental variables on the preconcentration and determination of the metal ions were studied and optimized using the one-at-a-time optimization method. Therefore, the various analytical parameters, such as pH, sample volume, amount of sorbent, flow rate and the matrix effect were investigated and optimized.

Effect of the pH

The pH value of a sample solution is one of the most important variables controlling the adsorption of the metal ions on the column. Therefore in order to determine the optimum pH, the effect of pH in the range 4–9 on the retention by the column was investigated. The effect of pH on the retention of Cu, Pb and Cd on the MCEM column is shown in Fig. 2, from which it can be seen that a pH value of 8 found to be the optimum for the quantitative extraction of the metal ions and the metals recovery was about 99 %. Therefore, pH 8.0 was selected for the all subsequent experiments.

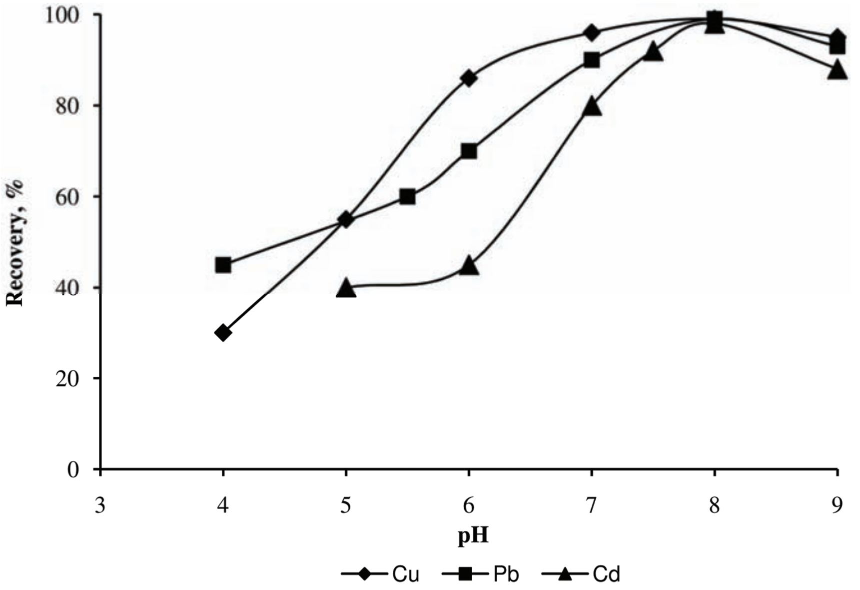

Fig. 2. Effect of pH on retention of metal ions by MCEM column. Conditions: copper, lead and cadmium concentration: 25 µg dm^{-3}; sample volume: 50 mL; flow rate: 1 mL min^{-1}.

Sample flow rate

The sample flow rate through the column is a very important parameter, since this is one of the steps that control the analysis time.[44] The influence of the sample flow rate on the preconcentration efficiency was tested at flow rates of 5.0–60 mL min^{-1}. A flow rate in the range of 5.0–10 mL min^{-1} had no significant effect on the recoveries of the investigated elements. In addition, it was found that analytical signal decreased slightly on increasing the sample flow rate to above 10 mL min^{-1} because of incomplete retention of the metal ions on the column. Therefore, a sample flow rate of 10 mL min^{-1} was selected for further studies (Fig. 3).

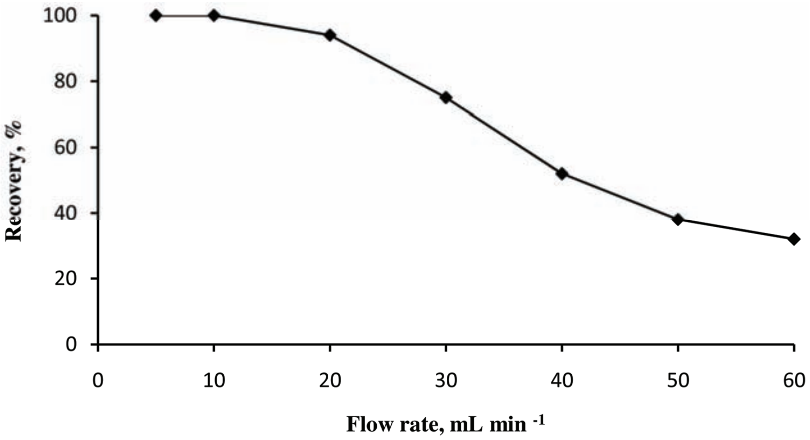

Fig. 3. Influence of flow rate on retention of metal ions by MCEM column. Conditions: copper, lead and cadmium concentration: 25 µg dm^{-3}; sample volume: 50 mL; pH 8.

Influence of sample volume

In order to explore the possibility of enriching low concentrations of the analytes from large sample volume, the effect of the volume of the sample solution on the metal sorption was studied by passing 25–400 mL volumes through the column. In this work, the amounts of analyte added were constant. The results are shown in Fig. 4. The adsorption of the metal ions by MCEM was not affected by the sample volume below 200 mL. Above this volume, the percent sorption of the analytes decreased. In the present study, sample solution volume of 200 mL of was adopted for the preconcentration of the investigated ions from synthetic water samples; the adsorbed metals can be eluted with 2 mL of HNO_3 and an enrichment factor of 100 was thus achieved by this technique (Fig. 4).

Effect of eluent volume

The effect of eluent volume on the desorption of the analytes was studied by keeping the eluent concentration constant at 0.1 mol dm^{-3} and varying it volumes from 0.5 to 3.0 mL. The experimental results indicated that with 2.0 mL HNO_3, quantitative recoveries (>98 %) for the target analytes could be obtained. Therefore, 2.0 mL of eluent was selected for the subsequent experiments.

Adsorption capacity

In order to successfully represent the dynamic adsorptive behavior, it is important to have a satisfactory description of the equation state between the two phases composing the adsorption system. Several isotherm models are available. In this study, the Langmuir adsorption isotherm was employed. The Langmuir model assumes uniform energies of adsorption onto the surface and no transmigration of the adsorbate in the plane of the surface. The Langmuir Equation may be written as:

$$\frac{c_e}{q_e} = \frac{1}{bQ_{max}} + \frac{c_e}{Q_{max}} \tag{1}$$

where c_e is the equilibrium concentration (mg dm^{-3}), q_e is the amount adsorbed at surface equilibrium (mg g^{-1}) and Q_{max} and b are Langmuir constants related to the adsorption capacity and the energy of adsorption, respectively. It is clear from Table II and Fig. 5 that the Langmuir model provided a good fit throughout the concentration range. The applicability of the isotherm models and the high values of the correlation coefficients (R^2 = 0.978, 0989 and 0.998, respectively) for Cu, Pb and Cd, suggest favorable and monolayer adsorption. The values of Q_{max} as determined from the Langmuir plots are 24, 17 and 16 mg g^{-1} for Cu, Pb and Cd, respectively. According to the results, the maximum capacity of the adsorbent under column conditions, due to the shorter contact time, is slightly lower than under batch conditions, which is apparently quite expected. The values of the constants of the Langmuir isotherm model are given in Table II.

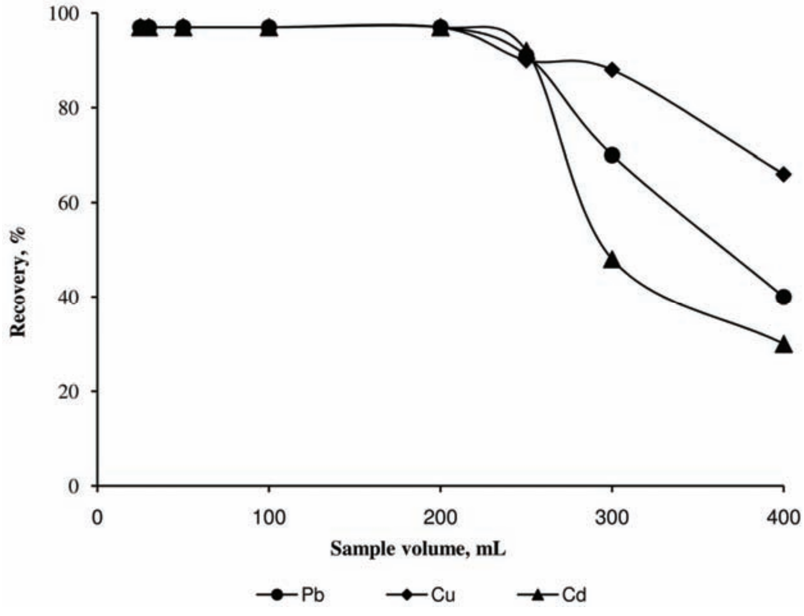

Fig. 4. Influence of sample volumes on the recovery of metal ions. Conditions: copper, lead and cadmium concentration: 25 µg dm^{-3}; flow rate: 1 mL min^{-1}; pH 8.

Interference studies

In order to assess the effects of commonly co-existing ions, which could interfere with the determination of Cu, Cd and Pb, several analytes were tested at the concentration levels at which they may occur in the sample concerned. The results are given in Table III. The tolerance limit is defined as the ion concentration causing a relative error smaller than ±4 % related to the preconcentration and determination of the analyte ions. The ions normally present in water did not interfere under the employed experimental conditions. In addition, some of the transition metals at mg dm^{-3} levels did not interfere with the recoveries of the analyte ions. These results show that the proposed preconcentration/determination method could be applied to highly saline samples and the samples that contain some of the transition metals given in Table III at mg dm^{-3} levels.

TABLE II. The Langmuir isotherm model constants

Langmuir parameter	Cu	Pb	Cd
$Q_{\max}$ / mg g^{-1}	24	17	16
b / mg^{-1} L^{-2}	0.178	0.053	0.062
R^2	0.997	0.989	0.998

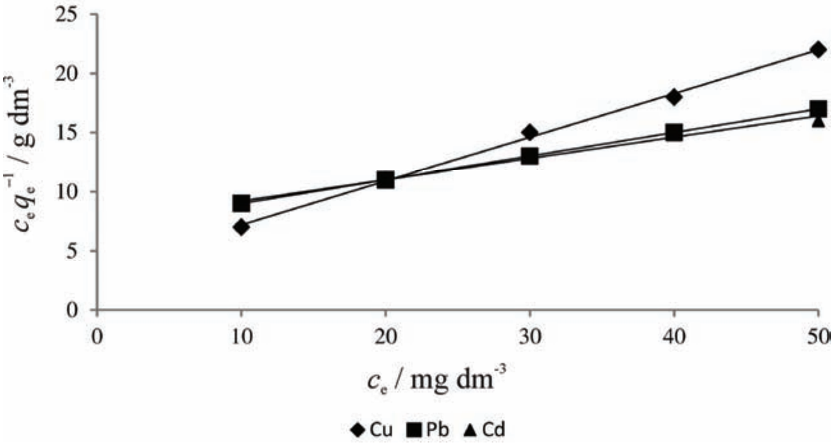

Fig. 5. Langmuir plots for adsorption of metal ions on MCEM.

TABLE III. Tolerance limits of interfering ions in the determination of 50 µg dm^{-3} of Cu, Pb and Cd

Ion	Metal to interferent ratio (w/w)		
	Cu	Pb	Cd
Na^+	1/5000	1/5000	1/5000
K^+	1/10000	1/10000	1/10000
Mg^{2+}	1/2000	1/2000	1/2000
Cl^-	1/2000	1/2000	1/2000
CO_3^{2-}	1/3000	1/3000	1/3000
Ni^{2+}	1/1000	1/1000	1/1000
V^{3+}	1/1000	1/1000	1/1000
Pb^{2+}	1/2000	–	1/2000

TABLE III. Continued

Ion	Metal to interferent ratio (w/w)		
	Cu	Pb	Cd
Mn^{2+}	1/1000	1/1000	1/1000
Cr^{3+}	1/1000	1/1000	1/1000
Ca^{2+}	1/2000	1/2000	1/2000
Al^{3+}	1/2000	1/2000	1/2000
Cd^{2+}	1/2000	1/2000	–
Zn^{2+}	1/2000	1/2000	1/2000
Fe^{3+}	1/2000	1/2000	1/2000
Cu^{2+}	–	1/2000	1/2000
Ba^{2+}	1/1000	1/1000	1/1000
Ag^{+}	1/1000	1/1000	1/1000

Statistical evaluation of the method

The limits of detection (*LOD*) of the proposed method for the determination of the investigated elements were studied under optimal experimental conditions by applying the procedure for blank solutions. The detection limits of the investigated elements based on three times the standard deviations of the blank ($k = 3$, $N = 10$) were 2 μg dm^{-3} for Cu(II), 3 μg dm^{-3} for Pb(II) and 0.2 μg dm^{-3} for Cd(II). The values of the limit of quantification (*LOQ*) were obtained as 7, 8 and 0.6 μg dm^{-3} for Cu, Pb and Cd, respectively ($S/N = 10$). The reproducibility of the presented procedure was evaluated by a model solution containing heavy metal ions ($N = 6$). The relative standard deviations (*RSD*) of these determinations were below 4.7 %.

The calibration curves for analyte ions were drawn after setting various parameters of FAAS, including wavelength, slit width, lamp current, at the optimum level. The optimum concentration ranges and regression equations for analytes are given in Table IV. The statistical calculations are based on the average of triplicate readings for a standard solution of the analyte ions.

TABLE IV. Analytical characteristics of the calibration curves of the analytes

Analyte	Correlation coefficient	Linear range, μg dm^{-3}	*RSD* / %
Cu	0.9995	10.0–100	3.2
Pb	0.9997	12.0–350	4.3
Cd	0.9998	0.8–35	1.8

Addition/recovery tests

Tests of addition/recovery in the experiments for analyte ions were performed for river water samples. The results are given in Table V. Good agreement was obtained between the added and measured analyte amounts. The recovery values for copper, cadmium and lead were in the range of 92–105 %. These values are quantitative and show that the presented method can be applied for the separation–preconcentration of analyte ions in real samples and the results indicate the applicability of the developed procedure for the determination of cadmium, copper and lead free of interference.

TABLE V. Application of the presented procedure to the analysis of a river water sample from Tehran City, Iran

Analyte	Concentration, μg dm^{-3}		Recovery, %
	Added	Found[a]	
Cu	–	40.0±0.5	–
	30	68.2±0.2	94
	40	81.0±0.6	102
	50	88.0±0.8	96
Pb		125±1.0	
	100	227±2.0	102
	150	273±1.5	99
	200	331±2.1	103
Cd		12.0±0.3	
	10	21.2±0.6	92
	15	26.5±0.5	97
	20	33.0±0.9	105

[a] Average of three determinations ± *SD*

Accuracy of the method

In order to evaluate the accuracy of the proposed preconcentration method, the analytes were determined in certified standard reference material (RM 8704 Buffalo River sediment). The sediment sample was dissolved and the column preconcentration procedure was applied to the sediment solution. The results obtained from the analysis of the certified reference material are depicted in Table VI, from which it can be seen that the achieved relative error values (%) were lower than 5%, meaning that the described method has good accuracy. The results obtained from the proposed method were in a good agreement with the certified values for Pb, Cd and Cu. In addition, the accuracy of the proposed procedure was also checked by analysis of urine samples by electrothermal atomic absorption spectrometry (ET–AAS). There was no significant difference at the 95 % confidence limit between the results obtained by proposed method and ET–AAS (see Table VII).

Comparison with other preconcentration studies

A comparison of the presented procedure with other preconcentration systems for the determination of cadmium, copper and lead can be seen in Table VIII. Analytical features, such as enrichment factor and detection limits, of the proposed method are comparable to those of other methods described in the literature.

TABLE VI. The levels of analyte ions in the reference material ($N = 6$)

Element	Content, mg kg^{-1}		*RSD* / %	Relative error, %
	Certified value	Observed value[a]		
Cu	98.6	97.2±1.40	2.1	–1.4
Pb	161	154±2.20	1.9	–4.3
Cd	3.5	3.38±0.09	0.5	–3.4

[a]Mean of six determinations at the 95 % confidence limit

TABLE VII. Determination of Cu, Pb and Cd in a urine samples

Element	Concentration, μg dm^{-3}		Relative error, %
	Present method[a]	ET–AAS method	
Cu	58.4±0.75	61.3±0.25	–4.7
Pb	81.4±0.57	85.3±0.51	–4.5
Cd	1.20±0.21	1.22±0.15	–1.6

[a]Mean of six determinations at the 95 % confidence limit

TABLE VIII. Comparison of the proposed method with previously reported methods

Elements	Enrichment factor	*LOD* / μg dm^{-3}	Reference
Cu, Pb	20, 20	1.1, 6.1	45
Cu, Cd	35, 38	1.8, 1.6	46
Cu, Pb	100, 100	0.54, 4.5	27
Pb, Cd	19.6, 15.1	4.6, 0.74	6
Pb, Cu, Cd	60, 60, 60	0.02, 3.1, 0.9	42
Pb, Cu, Cd	20, 20, 20	22.5, 1.0, 1.1	47
Pb, Cu, Cd	100, 100, 100	2.0, 3.0, 0.2	Present work

CONCLUSIONS

The developed procedure is very simple, sensitive and shows high tolerance to interference ions. Due to its good analytical characteristics, such as detection limit, enrichment factor and precision, the method is suitable for trace element analysis. In addition, no modification or functionalization of the employed adsorbent is required. The recoveries of the studied analytes were nearly quantitative. The accuracy of the results was verified by analyzing a certified reference material and spiked water samples. The recoveries for these elements were very satisfactory, which evidence for the reliability of the proposed method in the analysis of real samples.

Acknowledgments. The authors are grateful for the financial support provided by K. N. Toosi University of Technology and Semnan University Scientific Research Foundation, Iran.

ИЗВОД

ПРЕДКОНЦЕНТРИСАЊЕ И ОДРЕЂИВАЊЕ ТЕШКИХ МЕТАЛА У ВОДИ, СЕДИМЕНТУ И БИОЛОШКИМ УЗОРЦИМА

HAMID SHIRKHANLOO[1], HASSAN ZAVVAR MOUSAVI[2] и AHMAD ROUHOLLAHI[1]

[1]*Department of Chemistry, Faculty of Science, K. N. Toosi University of Technology, Tehran Chemistry*
и [2]*Department, College of Sciences, Semnan University, Semnan, Iran*

У овом раду развијена је осетљива и прецизна метода за колонску предконцентрацију при одређивању јона Cd, Cu и Pb у узорцима речне воде, урина и седимента пламеном атомском апсорпционом спектрометријом. Овај поступак је заснован на ретенцији аналита на колони од мембране естра мешане целулозе (MCEM) из пуферованог раствора узорка и њиховог елуирања из колоне азотном киселином. Проучен је утицај неколико параметара, као што су pH раствора узорка, запремине узорка и елуента и брзине протока узорка. Испитани су и утицаји разних јона на преконцентрацију. Принос аналитичког поступка је увек био >95 %. Овај метод је примењен на одређивање трагова металних јона у узорцима речне воде, урина и седимента, са задовољавајућим резултатима. Границе детекције 3δ за Cu, Pb и Cd су биле 2, 3, односно 0,2 µg dm^{-3}. Изложени поступак је успешно примењен за одређивање бакра, олова и кадмијума у стварним узорцима као што су речна вода и биолошки узорци.

(Примљено 24. октобра 2010, ревидирано 4. јануара 2011)

REFERENCES

1. E. Melek, M. Tuzen, M. Soylak, *Anal. Chim. Acta* **578** (2006) 213
2. J. L. Wang, C. Chen, *Biotechnol Adv*. **24** (2006) 427
3. M. J. Yonone-Lioy, P. J. Lioy, *J. Exposure Sci. Environ. Epidemiol*. **16** (2006) 397
4. T. A. Maranhao, D. L. G. Borges, M. A. M. S. da Veiga, A. J. Curtius, *Spectrochim. Acta* **60** (2005) 667
5. R. K. Sharma, M. Agrawal, F. M. Marshall, *Food Chem. Toxicol.* **47** (2009) 583.
6. E. L. Silva, P. S. Roldan, *J. Hazard. Mater*. **161** (2009) 142
7. W. Torjussen, H. Zachariasen, I. Andersen, *J. Environ. Monit*. **5** (2003) 198
8. H. B. Tabrizi, *J. Hazard. Mater*. **139** (2007) 260
9. V. A. Lemos, G. S. Novaes, A. L. de Carvalho, E. M. Gama, A. G. Santos, *Environ. Monit. Assess*. **148** (2009) 245
10. E. L. da Silva, A. O. Martins, A. Valentini, V. T. Favere, E. Carasek, *Talanta* **64** (2004) 181
11. E. L. Silva, P. S. Roldan, M. F. Giné, *J. Hazard. Mater*. **171** (2009) 1133
12. M. Ghaedi, A. Shokrollahi, K. Niknam, E. Niknam, A. Najibi, M. Soylak, *J. Hazard. Mater*. **168** (2009) 1022
13. D. Citak, M. Tuzen, *Food Chem. Toxicol*. **48** (2010) 1399
14. C. A. Sahin, I. Tokgoz, S. Bektas, *J. Hazard. Mater*. **181** (2010) 359
15. M. Tuzen, D. Citak, M. Soylak, *J. Hazard. Mater.* **158** (2008) 137
16. T. Oymak, S. Tokalıoglu, V. Yılmaz, S. Kartal, D. Aydın, *Food Chem*. **113** (2009) 1314
17. D. Citak, M. Tuzen, M. Soylak, *Food Chem. Toxicol*. **47** (2009) 2302
18. A. A. Ensafi, T. Khayamian, A. Benvidi, E. Mirmomtaz, *Anal. Chim. Acta* **561** (2006) 225
19. B. Feist, B. Mikula, K. Pytlakowska, B. Puzio, F. Buhl, *J. Hazard. Mater*. **152** (2008) 1122

20. A. L. Escudero, S. Cerutti, R. A . Olsinaa, J. A. Saloniaa, J. A. Gasquez, *J. Hazard. Mater*. **183** (2010) 218
21. C. A. Sahin, I. Tokgoz, *Anal. Chim. Acta* **667** (2010) 83
22. H. Filik, B. D. Ozturk, M. Dogutan, G. Gumus, R. Apak, *Talanta* **44** (1997) 877
23. A. P. Packer, M. F. Giné, C. E. S. Miranda, B. F. Reis, *J. Anal. At. Spectrom*. **12** (1997) 563
24. S. V. Mahamuni, P. P. Wadgaonkar, M. A. Anuse, *J. Serb. Chem. Soc*. **75** (2010) 1099
25. H. I. Afridi, T. G. Kazi, M. B. Arain, G. H. Kazi, M. K. Jamali, *J. AOAC Int.* **90** (2007) 470
26. T. Madrakian, M. A. Zolfigol, F. Aboulghazi, *J. Serb. Chem. Soc*. **75** (2010) 669
27. N. Pourreza, R. Hoveizavi, *Spectrochim. Acta* **59** (2004) 515
28. Z. Todorović, P. Polić, T. Sabo, M. Cakić, *J. Serb. Chem. Soc*. **67** (2002) 879
29. M. Soylak, M. Tuzen, *J. Hazard. Mater*. **137** (2006) 1496
30. Z. Fang, J. Ruzicka, E. H. Hansen, *Anal. Chim. Acta* **164** (1984) 23
31. E. J. Dos Santos, A. B. Herrmann, A. S. Ribeiro, A. J. Curtius, *Talanta* **65** (2005) 593
32. V. A. Lemos, E. S. Santos, E. M. Gama, *Sep. Purif. Technol*. **56** (2007) 212
33. S. Cerutti, M. F. Silva, J. A. Gasquez, R. A. Olsina, L. D. Martinez, *Spectrochim. Acta* **58** (2003) 43
34. M. Ghaedi, F. Ahmadi, M. Soylak, *Ann. Chim*. **97** (2007) 277
35. S. Cerutti, S. Moyano, J. A. Gásquez, J. Stripeikis, R. A. Olsina, L. D. Martinez, *Spectrochim. Acta* **58** (2003) 2015
36. F. Xie, X. Lin, X. Wu, Z. Xie, *Talanta* **74** (2008) 836
37. G. Göktürk, M. Delzendeh, M. Volkan, *Spectrochim. Acta* **55** (2000) 1063
38. V. A. Lemos, L. S. G. Teixeira, M. A. Bezerra, A. C. S. Costa, J. T. Castro, L. A. M. Cardoso, D. S. de Jesus, E. S. Santos, P. X. Baliza, L. N. Santos, *Appl. Spectrosc. Rev*. **43** (2008) 303
39. A. M. Haji Shabani, S. Dadfarnia, Z. Dehghani, *Talanta* **79** (2009) 1066
40. M. Ezoddina, F. Shemirani, Kh. Abdi, M. Khosravi Saghezchi, M. R. Jamali, *J. Hazard. Mater*. **178** (2010) 900
41. Y. P. de Pena, W. Lopez, J. L. Burguera, M. Burguera, M. Gallignani, R. Brunetto, P. Carrero, C. Rondon, F. Imbert, *Anal. Chim. Acta* **403** (2000) 249
42. U. Divrikli, A. A. Kartal, M. Soylak, L. Elci, *J. Hazard. Mater*. **145** (2007) 459
43. M. Soylak, U. Divrikli, L. Elci, M. Dogan, *Talanta* **56** (2002) 565
44. Y. Li, B. Hu, Z. Jiang, *Anal. Chim. Acta* **576** (2006) 207
45. E. Matoso, L. T. Kubota, S. Cadore, *Talanta* **60** (2003) 1105
46. M. Ghaedi, B. Karami, Sh. Ehsani, F. Marahel, M. Soylak, *J. Hazard. Mater*. **172** (2009) 802
47. W. Ngeontae, W. Aeungmaitrepirom, T. Tuntulani, *Talanta* **71** (2007) 1075.